AD-A016 853

EXPERIMENTAL INVESTIGATION OF A CIRCULATION CONTROLLED SHROUDED PROPELLER

Richard E. Walters, et al

West Virginia University

Prepared for:

Office of Naval Research

February 1974

DISTRIBUTED BY:

NTIS

National Technical Information Service
U. S. DEPARTMENT OF COMMERCE

WEST VIRGINIA UNIVERSITY
College of Engineering

316106

Aerospace
Engineering
TR-39

AD A016853

EXPERIMENTAL INVESTIGATION OF A CIRCULATION CONTROLLED SHROUDED PROPELLER

BY

Richard E. Walters and Jeffrey C. Ashworth

February, 1974

Prepared Under Contract
N00014-68-A-0512

for

Vehicle Technology, Code 211
Office of Naval Research
Arlington, Virginia 22217
(NR 215-163)

DDC
RECEIVED
NOV 10 1975
A

Reproduction in whole or in part is permitted for any purpose of the United States Government

Approved for public release; distribution unlimited

Department of Aerospace Engineering
West Virginia University
Morgantown, West Virginia 26506

Reproduced by
NATIONAL TECHNICAL
INFORMATION SERVICE
US Department of Commerce
Springfield, VA. 22151

Unclassified
Security Classification

DOCUMENT CONTROL DATA - R & D

(Security classification of title, body of abstract and indexing annotation must be entered when the overall report is classified)

1. ORIGINATING ACTIVITY (Corporate author)
West Virginia University
Department of Aerospace Engineering
Morgantown, West Virginia 26506

2a. REPORT SECURITY CLASSIFICATION
Unclassified

2b. GROUP

3. REPORT TITLE
Experimental Investigation of a Circulation Controlled Shrouded Propeller

4. DESCRIPTIVE NOTES (Type of report and inclusive dates)
Scientific

5. AUTHOR(S) (First name, middle initial, last name)
Richard E. Walters and Jeffrey C. Ashworth

6. REPORT DATE	7a. TOTAL NO. OF PAGES	7b. NO. OF REFS
February, 1974	113	10

8a. CONTRACT OR GRANT NO	9a. ORIGINATOR'S REPORT NUMBER(S)
N00014-68-A-0512	
b. PROJECT NO NR 215-163	Aerospace Engineering TR-39
c. Project Navy V/STOL Aerodynamics	9b. OTHER REPORT NO(S) (Any other numbers that may be assigned this report) -
d.	

10. DISTRIBUTION STATEMENT
Approved for Public Release; distribution unlimited.

11. SUPPLEMENTARY NOTES	12. SPONSORING MILITARY ACTIVITY
-	Office of Naval Research Vehicle Technology, Code 211 Arlington, Virginia 22217

13. ABSTRACT

A preliminary experimental investigation was made on a 14.18 inch inside diameter, ten inch long, symmetrical airfoil shaped shroud equipped with blowing slots on a blunt semicircular trailing edge. The purpose of the investigation was to determine the effect of circulation control on the thrust of the shroud-propeller combination. Static tests were performed at three propeller blade pitch angles, three propeller speeds and three levels of inside slot blowing rates. Data recorded consisted of the propeller thrust and torque, shroud static pressures, total pressure in front of the inside struts, and total pressure at the blowing slot. Static pressure data was reduced to coefficient form and integrated to obtain thrust and normal force coefficients. This was converted to lb_f and compared with the propeller thrust. The drag on the inside support struts was approximated using drag coefficient data for the particular airfoil section use. With no blowing, the combined propeller and shroud thrust was about double that of the propeller in free air, which is in good agreement with conventional sharp trailing edge shroud tests. With blowing on the inside slot of the shroud the propeller thrust increased, but the shroud thrust decreased due to low pressure over the rounded trailing edge. Total thrust decreased for the combination with blowing, but increased propeller disk loading improved the performance. It was concluded that a modified shape for the trailing edge might result in significant performance increases, and should be investigated. Testing should also be conducted to evaluate effects at forward flight velocities.

DD FORM 1 NOV 65 1473 (PAGE 1)
S/N 0101-807-6801

Unclassified
Security Classification

14 KEY WORDS	LINK A		LINK B		LINK C	
	ROLE	WT	ROLE	WT	ROLE	WT
Shrouded Propeller Circulation Control Experimental Aerodynamics External Diffusion						

WEST VIRGINIA UNIVERSITY
College of Engineering

Aerospace
Engineering
TR-39

EXPERIMENTAL INVESTIGATION OF A CIRCULATION CONTROLLED SHROUDED PROPELLER

by

Richard E. Walters and Jeffrey C. Ashworth

February, 1974

Prepared Under Contract
N00014-68-A-0512

for

Vehicle Technology, Code 211
Office of Naval Research
Arlington, Virginia 22217
(NR 215-163)

Reproduction in whole or in part is permitted for
any purpose of the United States Government

Approved for public release; distribution unlimited

Department of Aerospace Engineering
West Virginia University
Morgantown, West Virginia 26506

ib

ABSTRACT

A preliminary experimental investigation was made on a 14.18 inch inside diameter, ten inch long, symmetrical airfoil shaped shroud equipped with blowing slots on a blunt semicircular trailing edge. The purpose of the investigation was to determine the effect of circulation control on the thrust of the shroud-propeller combination.

Static tests were performed at three propeller blade pitch angles, three propeller speeds and three levels of inside slot blowing rates. Data recorded consisted of the propeller thrust and torque, shroud static pressures, total pressure in front of the inside struts, and total pressure at the blowing slot.

Static pressure data was reduced to coefficient form and integrated to obtain thrust and normal force coefficients. This was converted to lb_f and compared with the propeller thrust. The drag on the inside support struts was approximated using drag coefficient data for the particular airfoil section used.

With no blowing, the combined propeller and shroud thrust was about double that of the propeller in free air, which is in good agreement with conventional sharp trailing edge shroud tests. With blowing on the inside slot of the shroud the propeller thrust increased, but the shroud thrust decreased due to low pressure over the rounded trailing edge. Total thrust decreased for the combination with blowing, but increased propeller disk loading improved the performance. It was concluded that a modified shape for the trailing edge might result in significant performance increases, and should be investigated. Testing should also be conducted to evaluate effects at forward flight velocities.

ACKNOWLEDGMENTS

A portion of this report represents work done by the second author toward the graduate MSAE degree. The first author was the thesis advisor, and conceived and initiated the project.

The authors would like to acknowledge and express gratitude to the following people for their contributions to this project:

Dr. John Loth, for his helpful suggestions;

The second author's wife, Rebecca Susan, for her typing and encouragement throughout the course of investigation;

Mr. Thomas A. Csencsitz, for his assistance in developing the data reduction program;

Mr. Joel Bowlby, for his assistance in constructing the test model and air supply system.

This research project was sponsored by The Aeronautics Branch of the Office of Naval Research; Mr. Tom L. Wilson was Contract Monitor for the Navy V/STOL Aerodynamics Contract N00014-68-A-0512.

TABLE OF CONTENTS

	Page
TITLE PAGE	i
ABSTRACT	ii
ACKNOWLEDGMENTS	iii
TABLE OF CONTENTS	iv
LIST OF FIGURES	vii
SYMBOLS	ix
INTRODUCTION	1
APPARATUS	4
Shroud	4
Design	4
Construction	6
Propeller	7
Motor and Nacelle	7
Support Struts	8
Test Stand	8
Blowing Air Supply System	8
Compressor and Storage Tank	9
Line with Regulators and Valves	9
Flowmeter	9
Distribution Tank	10
Total Pressure Taps in Line	10
Pitot Calibration Probe	11
Manometer System	11
Motor Power Supply	11
RPM Indicator	11
Strain Amplifier and Recorder Unit	12

TABLE OF CONTENTS (CONTINUED)

Page

Thermometer 12

PRELIMINARY INVESTIGATIONS 13

Strain Gage Calibration 13

Temperature Influence 14

Slot Total Pressure Distribution 14

Line Total Pressure 15

RPM Calibration 15

Drag on Inside Struts 15

Tuft Tests 16

Symmetrical Flow Test 17

EXPERIMENTAL PROCEDURE AND DATA REDUCTION 18

General Procedure 18

Data Reduction 19

Thrust and Inward Force Coefficients 19
Total Forces of the Shroud-Propeller System . . . 20
Drag on Inside Struts 21
Blowing Momentum Coefficient 22
Brake Horsepower 23

RESULTS 24

Propeller Thrust 24

Pressure Distributions 24

Shroud Forces 26

Strut Drag 27

Propeller Torque 27

Free-Air Propeller Thrust 27

TABLE OF CONTENTS (CONTINUED)

	Page
Slot Horsepower	28
Comparison with Previous Work	28
CONCLUSIONS	29
REFERENCES	31
APPENDIX A - FIGURES	33
APPENDIX B - TABLES	95
DISTRIBUTION LIST	101

LIST OF FIGURES

No.	Title	Page
1	Efficiency of Shrouded Propeller Systems.	34
2	Effect of Circulation Control on Air Flow	35
3	Front and Cut Away Side View of Entire Shroud and Supports.	36
4a	Cross Section of Shroud Airfoil Section at Top. .	37
4b	Cross Section of Shroud and Support Screws. . . .	38
4c	Cross Section of Shroud and Connection Screws . .	38
5	Pressure Tap Locations.	39
6	Test Stand.	40
7	Air Supply System	41
8	Distribution Tank	42
9a	Front View of the Shroud.	43
9b	Side View of the Shroud	44
9c	Back View of the Shroud	45
9d	Testing Equipment	46
10	Motor Calibration Equipment	47
11	Calibration Graph for Thrust.	48
12	Calibration Graph for Torque.	49
13	Slot Total Pressure Survey, C_μ = 0.012.	50
14	Slot Total Pressure Survey, C_μ = 0.045.	51
15	Calibration Graph for Motor RPM	52
16-18	Shroud Thrust Coefficient	53-55
19-27	Thrust Versus Brake Horsepower.	56-64

LIST OF FIGURES (CONTINUED)

No.	Title	Page
28-54	Pressure Coefficient Versus Vertical Ordinate. .	66-91
55-57	Pressure Coefficient Versus Chordwise Ordinate .	92-94

SYMBOLS

English Letters

a	Speed of sound, ft/sec
A	Effective planform area of shroud, πcd, ft
BHP	Brake horsepower
c	Chord length of shroud airfoil section, ft
C_D	Drag coefficient
C_F	Normal sectional force coefficient
C_p	Pressure coefficient
C_T	Chordwise sectional force coefficient
C	Blowing momentum coefficient
d	Diameter at shroud chord, ft
D	Drag, lb_f
F	Normal force, lb_f
g	Acceleration of gravity, ft/sec^2
KE	Kinetic energy per unit volume per unit time, $ft\text{-}lb_m/sec$
$\dot{m}$	Mass flow rate per unit span of shroud, slugs/ft-sec
M	Mach number
MF	Mass flow rate, lb_m/sec
N	Revolutions per minute, rpm
p	Static pressure, lb_f/ft^2
p_t	Total pressure, lb_f/ft^2
q	Dynamic pressure, lb_f/ft^2
S	Wetted area of inside strut, ft^2
SP	Shroud effective span length, πd, ft

T	Thrust, lb_f
Tq	Torque, $ft\text{-}lb_f$
t	Temperature, °R
t_t	Total temperature, °R
V	Velocity, ft/sec
X	Chordwise coordinate, ft
Y	Vertical coordinate, ft (positive outward)

Greek Letters

θ	Propeller blade pitch angle, degrees, at 3/4 radius
ρ	Density, slugs/ft^3
η	Propulsive efficiency
γ	Ratio of specific heats, 1.4 for air

Subscripts

$( )_f$	Free-air condition
$( )_j$	Blowing jet values
$( )_n$	Number of pressure tap
$( )_s$	Values at inside strut
$( )_\infty$	Freestream conditions

INTRODUCTION

In recent years, an urgent need for more effective V/STOL aircraft has been realized. The space available for take-off and landing of both commercial and military aircraft has necessarily become smaller. This need for more efficient V/STOL aircraft has brought about research into the use of shrouded propellers as high thrust producing devices. However, these high thrust producers are limited to low speed operation. The shroud design, therefore, has proven to be a limiting factor in the effectiveness of the aircraft (Reference 1).

The shape of the shroud can be designed so that the shroud-propeller combination is capable of producing nearly twice the static thrust per horsepower as a free-air propeller of the same diameter. However, this shroud is only useful at very low speeds. Another shroud can be designed to permit a finite loading to be maintained at the tips of the propeller blades when the aircraft is operating at higher speeds (Reference 2). The efficiency of this design is quite low at take-off and landing speeds (Reference 3). The efficiency of the different designs is shown in Figure 1. Unsuccessful attempts have been made to design an efficient shroud with variable shape which can operate in a large speed range. These unsuccessful attempts have lead to this investigation of a circulation controlled shroud.

It has been found experimentally that blowing high energy air into the boundary layer near the trailing edge of an airfoil alters the velocity profile of the air about the entire airfoil. Applying this principle to a circular shroud influences the air flow around

and through the shroud. Therefore, blowing high energy air from different slots around the trailing edge of the shroud will change the velocity and pressure at the propeller as well as the pressure distribution about the shroud surface. Blowing slots can then be used to replace the variable geometry requirement of a shroud used in a large speed range. The circulation control effect is shown in Figure 2.

The purpose of this investigation is to study the effects of circulation control on a 2 inch thick, 10 inch chord length, symmetrical airfoil shroud around a 14 inch diameter propeller (Figure 3). The shroud trailing edge is a semicircle with a blowing slot on top and bottom.(Figure 4). The tests were performed at static conditions with the shroud-propeller combination mounted on a test stand. Figures 9a, b, c show the shroud on the test stand. The inside blowing slot was used and the increase in thrust of the system, compared to a nonblowing system, was investigated.

The investigation was conducted by setting the blowing momentum coefficient of the high energy air through the slot and varying the blade pitch angle and the angular velocity of the propeller. The thrust of the propeller and of the shroud were measured separately and combined to obtain the system total thrust. This total thrust was compared at different conditions of blade pitch angle, propeller speed and blowing momentum coefficient. The results of this test show the effect of circulation control at each different disk loading.

Wind tunnel tests of this model should show an efficiency increase of the shroud-propeller combination over the free-air propeller when

operating at most speed ranges. The effect of a variable area shroud is achieved using circulation control. This quality makes this system feasible for application to both military and commercial aircraft.

APPARATUS

Shroud

Design

The design of the shroud began in January, 1972. At that time, a small 1.5 horsepower motor equipped with a 4-blade, 14 inch diameter propeller was available. Therefore, the shroud design began with this dimension criteria. Since it was found in Reference 3 that the efficiency of a propeller-shroud combination is inversely proportional to the tip clearance, the inside diameter of the shroud at the propeller location was made as small as possible. The tip clearance was designed to be 0.09 inches to allow for some vibration of the propeller. This spacing was found to be adequate by static testing of the motor-propeller combination. The minimum inside diameter of 14.18 inches was then used as a beginning design criteria for the entire shroud shape.

It has been found from previous experiments, described in Reference 1, that the minimum inside diameter of the shroud should be located at the position where the propeller is mounted and that this position should be approximately 30% c from the leading edge. Since the effective camber of the shroud airfoil section would be changed by blowing on different slots, the actual airfoil section was chosen to be symmetrical. The first inch of the airfoil section, or the leading edge section, is a NACA 0021 airfoil. From 1 inch back from the leading edge to the maximum thickness of 2 inches at 30% c the surface dimensions were smoothly drawn. The remainder of the

surface was also smoothly drawn back to the necessary thickness at the trailing edge. The shape is shown in Figure 5.

The thickness of the trailing edge section was determined by the blowing slot configuration. It has been found in past experimental work (Reference 4) that a rounded trailing edge yields close to optimum results when circulation control using blowing slots is applied. Therefore, the trailing edge section is equipped with a ring (Figure 4a) that is adjusted into the shroud so that air can be blown over the top or bottom through slots between the ring and shroud surface. The shroud surface provides the outside slot boundary while the ring provides the inside boundary.

Past experimental investigation (Reference 5) has shown that the ratio of rounded trailing edge radius to chord length should be approximately 2.75% for good circulation control. The same investigation yielded an optimum slot thickness to rounded trailing edge radius ratio of approximately 2.75%. Therefore, the rounded edge radius is 0.225 inches and the slot thickness is 0.0075 inches.

The chord length was designed to allow a gradual increase of pressure over the 30% c to trailing edge section. The chord is 10 inches which will allow effective operation at higher Mach numbers while not adversely affecting low Mach number operation.

The stagnation point will be shifted around the leading edge by blowing from different slots. Therefore, the static pressure taps in this critical measurement area are tightly spaced. The spacing is shown in Figure 5. The 32 taps are symmetrically located about the airfoil section. The taps are also closely spaced in the location

of the propeller and on the trailing edge semicircle. Two rows of 32 taps each are located on the sides of the shroud 180° apart (Figure 3).

Construction

When the construction phase started, it was found that the facilities in the Aerospace Engineering Shop would not allow such a large model to be made of aluminum. It was suggested by the shop technician that the shroud be made of Snowite Body Filler and molded to the correct exterior shape. A plaster mold was constructed for the front part of the shroud. Pressure taps were inserted into the mold and the front half of the shroud was constructed. This front section is 4.962 inches long and is shown in Figure 4a.

It was found after the construction of the front section that the weight of the body filler was too great to be mounted securely. Therefore, the rear section was redesigned to be machined from aluminum. This work was done by Romisch Manufacturing Company. The back section, without the rounded trailing edge, is 4.812 inches long (Figure 4a). The front and back sections are connected by 12 screws (Figure 4c). A slot was cut into the back section to provide an air chamber for the blowing slots.

The air chamber is shown in Figure 4b. The screws which hold the semicircular trailing edge ring in place pass through the air chamber and into the aluminum front of the chamber. Since these screws were over 3.5 inches long and only 1/8 inch diameter, a spacer ring was needed near the middle of the screw length to insure a rigidly mounted trailing edge ring and thus a uniform blowing slot

size. Therefore, the back air chamber was made 1/16 inch smaller in thickness than the outer chamber to hold the spacer ring in place. The spacer ring was held tight against the chamber division by placing tubes around the support screws between the spacer ring and the trailing edge ring. Holes were drilled in the spacer ring to allow air to flow into the outer chamber. The outer air chamber was machined to a 0.5651 inch width. This would allow the 0.55 inch diameter trailing edge ring to be inserted into the end of the outer air chamber and leave a 0.0075 inch blowing slot on both sides.

Propeller

The propeller is a highly twisted 4-bladed, 14 inch diameter model. The blade is a Hamilton Standard design (H.S. report No. 1829) using a NACA 16 series airfoil with a constant chord length of 1.25 inches. The blades are fiberglass with aluminum reinforcement. The pitch angle of any blade can be changed individually by taking apart the propeller hub.

Motor and Nacelle

The propeller is driven by a 1.5 horsepower, 3 phase induction motor. The motor has a rating of 11,200 RPM at 400 hertz, 220 volts. The two main bearings of the motor are equipped with thermistors in order to monitor the temperature build-up.

Two yokes, one at each end of the motor, affix the motor to the inner nacelle. These yokes are instrumented with strain gage bridges which detect thrust, torque, pitching moment and normal force on the motor. Thrust and torque were the only variables recorded for this investigation.

An inner and outer nacelle encircle the motor. The inner nacelle is 3 3/8 inches in diameter and 9 inches in length. An outer nacelle 1/4 inch thick encasing the inner nacelle provides the thickness to hold the threads for the support rods.

Support Struts

The motor nacelle was fastened to the shroud inner surface by 1/4 inch diameter rods equipped with turnbuckles. A pair of these rods was located at 4 points, 90 degrees apart, about the nacelle. Wooden struts, which can be separated along the chord line to allow turnbuckle adjustment, were placed around each pair of support rods (Figure 3). These struts were designed from a NACA 0018 symmetrical airfoil section with a 4.75 inch chord length, 0.856 inch thickness and 6 inch length.

The aluminum outer struts encase the 1 inch air pipe and the pressure tap tubing from the shroud outer surface to the endplates on the test stand. These struts are designed from a NACA 0024 symmetrical airfoil section. The length of the strut is 7 inches while the thickness and chord length are 1.44 and 6 inches respectively.

Test Stand

The test stand, shown in Figure 6, holds the model so that the flow through the shroud is horizontal. Two horizontal support beams hold the endplates of the outer struts. The 1 inch diameter air pipes which provide the structural support as well as the air for the blowing slots are fastened to each endplate.

Blowing Air Supply System

A diagram of the blowing air supply system is shown in Figure 7. The system is a composite of 5 parts: compressor and storage tank;

flowmeter; distribution tank; air line with valves and regulators; and, total pressure taps in the air line.

Compressor and Storage Tank

The compressor and storage tank were part of a supersonic blowdown wind tunnel installation manufactured by Worthington Corporation. The compressor is capable of 104.2 cfm displacement at 175 psi discharge pressure. The storage tank has an internal volume of 380 cubic feet and could withstand a maximum internal pressure of 200 psig. In order to protect the supply line components, the automatic shutoff valve was set at 175 psig. During a test using maximum mass flow, the pressure was depleted to approximately 140 psig.

Line with Regulators and Valves

The air line consists of standard 1 inch gas pipe. Regulators and valves were used on the line to regulate the amount of air flow through the flowmeter and the distribution tank. The maximum inlet and outlet pressure of the regulators was 150 psig and 55 psig respectively. A T-joint was placed in the line to divide the air flow to pass through both the flowmeter and the distribution tank.

Flowmeter

The air flow from one side of the T-joint passed through a pressure gauge; a gauge-valve combination; and then through a flowmeter. The meter is a Series 12 Certified Flowmeter manufactured by Cox Instruments. This instrument has a capacity of 85 SCFM at 100 psia inlet pressure and has a maximum operating inlet pressure of 160 psia. The accuracy of this flowmeter is $\pm$ 1%.

Distribution Tank

The air flow from the other side of the T-joint flows through a gauge-valve combination and then into a distribution tank. It was found, during preliminary calculations, that the flowmeter range 0-85 SCFM was not adequate for measuring the large amount of mass flow required for this investigation. Therefore, a distribution tank was constructed. The inside dimensions are shown in Figure 8. This tank receives the air directly from the line as well as the air that passes through the flowmeter. The pipe attached directly to the line passes into the tank and has three holes of 11/32 inch in diameter to allow the air to flow into the bottom section of the tank. The line which passes through the flowmeter has one hole of the same diameter. When the gauge between the T-joint and the tank and the gauge between the flowmeter and the tank record the same pressure, then the mass flow recorded by the flowmeter is 1/4 the total mass flow leaving the bottom section of the tank and proceeding to the shroud.

Total Pressure Taps in Line

Two 1 inch air pipes extend from the bottom of the distribution tank to the shroud top and bottom support struts. Since the air flow through each of these lines was to remain the same, a total pressure tap and a valve were placed in each line just upstream of where the air passes into the struts. The pressure in each line was regulated by the valves and both were recorded on a water manometer. When the total pressures were kept equal, it was assumed that the mass flow in the lines was equal.

Pitot Calibration Probe

A pitot tube was used to survey the total pressure distribution at the blowing slot around the tailing edge. A 0.032 inch outside diameter pressure tap tube was flattened to a wedge shape on the end with an opening of 0.003 x 0.030 inches so that it could be inserted into the blowing slot from outside the airfoil. The tubing was connected to a mercury manometer. Two graphs of the inches of mercury versus slot position in degrees are shown in Figures 13 and 14.

Another pitot tube of 0.060 inches outside diameter tubing was used to record the total pressure in front of the inside support struts. This tubing was attached to a water manometer. The pressure reading was used to compute the drag on the inside struts.

Manometer System

A water manometer bank was used to record the static pressure from the taps located on the shroud surface. The range of water level was 0-40 inches. Fifty tubes are located across the bank and only 32 were used.

Motor Power Supply

The power to the motor was regulated using a variable frequency control console. The voltage control has a range of 0-220 volts and the frequency control can be varied from 0-400 hz. A 5 KVA variable frequency generator of a motor-generator set provides the frequency variation. This power supply controlled the RPM setting of the motor.

RPM Indicator

A small generator is attached to the rear of the motor. This generator has an output of volts per RPM which is used to determine

the rotor speed. It is connected to a Digitec precision digital voltmeter made by United Systems Corporation. A calibration of volts per RPM was made using a Strobotac electronic stroboscope made by General Radio Company. The calibration is shown in Figure 15.

Strain Amplifier and Recorder Unit

The strain gages mounted on the motor yoke to record thrust and torque were connected to two Brush Bridge Amplifiers made by Clevite Corporation. The sensitivity of these amplifiers ranges from 5 to 100% load for full scale deflection.

The amplifiers were connected to a Clevite Brush Mark 280 Recorder which has a sensitivity of 0.5 to 100 millivolts per division. Each division was 0.2 centimeter. A calibration of this instrument was made and the graphs of thrust and torque versus centimeter deflection are shown in Figures 11 and 12.

Thermometer

Previous investigations on the motor show that as the operating time increases, the temperature increases dramatically. This temperature increase influences the thrust and torque readings. Thermistors are located inside the motor bearings to monitor this temperature. These thermistors are connected to a Digitec Digital Thermistor Thermometer produced by United Systems Corporation. This thermometer scale reads in degrees Centigrade.

PRELIMINARY INVESTIGATIONS

Strain Gage Calibration

Two separate, strain gage full-bridges are located on the rear yoke of the motor nacelle. These two bridges measure thrust and torque. The signal from each bridge is passed through an amplifier and then goes on to a recorder. In order to read the thrust and torque from the recorder a ratio of pounds to centimeter deflection must be calibrated.

The calibration equipment is shown in Figure 10. Since the motor was mounted in the shroud, a system of nearly frictionless pulleys was used to provide the force in the proper direction. The thrust and torque were calibrated independently and the propeller was removed from the motor for both tests.

To calibrate the thrust, a nut was placed on the threads on the front part of the motor shaft. A string was tied behind the nut and stretched straight out from the motor and down over a pulley. Weights from one to six pounds were placed on the string. The pen on the recorder was set at zero deflection with no weight on the string and then 6 pounds were placed on the string. The sensitivity of the strain gage bridge amplifier and the recorder was varied until a maximum centimeter deflection was obtained. The weights were then applied one at a time from 0 to 6 pounds, and then removed one at a time. The centimeter deflection was recorded in each case. A graph of pounds thrust versus centimeter deflection is shown in Figure 11.

A calibrating bar, 3/4 inch in diameter and 13 1/2 inches in length, was affixed to the shaft in order to calibrate the torque. Since the torque bar needed to be turned in the same direction that the rotor turns, a system of two pulleys was used. The first was placed inside the shroud near the end of the torque bar. The second was placed straight out, horizontally from the first. The string was attached to the bar 5 1/2 inches away from the motor shaft. The procedure was the same as that for calibrating the thrust. The weight was then multiplied by 0.458 foot to give the torque in ft-lb_f. The calibration graph for torque is shown in Figure 12.

Temperature Influence

It was found during preliminary investigations that only a few seconds after the motor speed had become constant, the thrust began to drift. This was due to the temperature rise expanding the material and therefore disturbing the strain gage signal. To account for this heating effect, the thrust and torque recordings were taken as soon as the motor RPM stabilized. This would insure accurate data.

Slot Total Pressure Distribution

Since it was not known if the blowing around the slot was uniform, a total pressure survey was taken. The previously described total pressure probe was used with a mercury manometer. The investigation began at the top of the shroud just beneath the top outside support strut and proceeded clockwise. A pressure recording was made every 22.5 degrees. A graph was made of the total pressure verses slot location for both the blowing momentum coefficients used. These graphs are shown in Figures 13 and 14.

Line Total Pressure

In order to have symmetry around the blowing slot, the air flow coming into the top and bottom of the inside air chamber must be equal. This was controlled by regulating the air flow into the top and bottom outside support struts. Pressure tap tubes were placed in the air line pointing into the flow. These are located in each line just before the flow goes into the support struts. The two tubes were connected to a water manometer. When the flow was turned on, the pressure regulating valves at these positions were adjusted until the two water heights were equal.

RPM Calibration

Due to possible losses in the connection lines, the volts per RPM were calibrated. This was done using an electronic stroboscope. The propeller speed was regulated so that the digital voltmeter recorded a particular voltage and the stroboscope light frequency was varied until the propeller blades seemed motionless. This was repeated for several voltage settings. The frequency was then recorded as the motor RPM. Erasable marks were placed on the blades to insure that the four blades would not be out of phase by 90, 180 or 270 degrees. The actual volts per RPM were then plotted and are shown in Figure 15.

Drag on Inside Struts

The total thrust of the shroud-propeller combination could not be determined until the drag on the inside support struts was determined. Since the inside struts are NACA 0018 airfoil sections, the drag could be determined on each strut separately. The velocity in front of the strut was required.

Since the struts are located behind the propeller, the spanwise velocity was not constant. A total pressure probe was constructed from 0.060 outside diameter pressure tap tubing. This probe was placed in the airflow 1 inch upstream of the strut. Four different spanwise locations were chosen and the total pressure upstream of each location was recorded on a water manometer. The swirl around the struts due to flow angularity from the propeller could not be measured since pressure taps were not installed in the struts.

Tuft Tests

In order to acquire a better knowledge of how the flow would be affected by the change in blowing coefficient and propeller speed, tufts were placed on the shroud and one of the inside support struts. Five yarn tufts were placed in a line on the inside surface of the shroud. The most forward tuft was 2 inches behind the propeller and the most aft tuft was 1/2 inch in front of the blowing slot. Two tufts were placed on each side of one of the inside support struts. Lines drawn in a chordwise direction through these tufts would divide the strut into three equal spanwise sections. Tufts were also placed in the wake behind the motor-shroud combination. The tufts were attached 1 1/2 inches apart to a small rod which was positioned across the wake approximately 8 inches behind the trailing edge of the shroud. The tuft reaction was noted for three different settings of blowing coefficient and propeller speed.

It was found, as expected, that an increase in blowing coefficient increased the diameter of the wake by approximately 1 1/2 inches and 3 inches for C_μ equal to 0.012 and 0.045 respectively. The increase

in blowing momentum had some stabilizing effect on the flow near the inside surface of the shroud, however, this was very slight except at the higher blowing coefficient. The highest blowing coefficient also caused more turbulence on the surface of the inside support strut. No flow separation was detected at any condition investigated.

The increase in propeller speed caused an increase in the turbulence on the inside of the shroud surface and the sides of the struts. The wake diameter was also expanded slightly by the increased propeller speed.

At both values of C_μ, a strong Coanda effect was present, and the wall jet flow from the slot extended around the trailing edge well past 90 degrees. This wall jet flow remained at all propeller speeds.

Symmetrical Flow Test

A row of static pressure taps are positioned from front to back of the shroud at two locations 180 degrees apart. To determine if the flow around the shroud was symmetrical, a test was run and the height of the manometer tubes connected to the taps on the left side of the shroud were recorded. Another test, under the same conditions, was performed and the height of the manometer tubes connected to the taps on the right side of the shroud were recorded. The manometer data from the two sides was compared. It was found that the data had no detectable differences. Therefore, the flow around the shroud was symmetrical.

EXPERIMENTAL PROCEDURE AND DATA REDUCTION

General Procedure

The outside diameter of this shroud prevents the acquisition of accurate data from a wind tunnel test in the West Virginia University, 32 x 45 inch, subsonic wind tunnel. The clearance between the shroud surface and the tunnel wall would be only approximately 7 inches. Since at low speeds, this model will expand the radius of the wake, the wall effects would be very great. Therefore, static tests were performed with the shroud mounted on a test stand, with the outside slot closed with clay and only the inside slot being used.

Tests were performed on the model at various blowing momentum coefficients, propeller blade pitch angles and motor speeds. Nine runs were made at each blowing momentum coefficient of 0, 0.012 and 0.045. At each blowing momentum coefficient the propeller blade pitch angle was changed three times from 8 degrees to 10 degrees and then 12 degrees. At each blade pitch angle the motor speed was changed from 3,010 revolutions per minute to 4,400 and then 6,900. During each test, the thrust, torque, and manometer height for each of the static pressure taps on the shroud surface were recorded. The atmospheric pressure and temperature were recorded each time. The total pressures just forward of the inside support struts were also recorded. The propeller was also tested outside the shroud to determine the free-air values. The data is listed in Table III. This data was sufficient to calculate the shroud thrust, propeller thrust, drag on the strut, and blowing momentum coefficient.

Data Reduction

Thrust and Inward Force Coefficients

Since the investigation was carried out under static conditions, the freestream velocity was zero. When the thrust and inward force coefficients are calculated, a dynamic pressure, q_∞, is required. Therefore, a dynamic pressure of 3 inches of water was assumed. This assumption did not affect the actual thrust and inward force in pounds because it is cancelled out of the final equation.

With the static pressure known at each tap location, a pressure coefficient can be found using

$$C_p = \frac{p_n - p_\infty}{q_\infty} \quad , \tag{1}$$

where

$$q = 1/2 \rho_\infty V_\infty^2 \quad (q_\infty \text{ assumed} = 3 \text{ in. water}). \tag{2}$$

A pressure coefficient was found at each tap location and graphs of these coefficients versus vertical and chordwise ordinate are shown in Figures 28 through 57. To obtain the static pressure in lb_f/ft^2 from inches of water, the equation

$$p(\text{inches water}) \times 5.209 = p(lb_f/ft^2) \tag{3}$$

was used (Reference 6).

After these pressure coefficients were found, the chordwise sectional coefficient, C_T, and the normal sectional coefficient, C_F, were calculated using the expressions

$$C_T = \oint C_p \, d(Y/c) \quad , \tag{4}$$

and

$$C_F = \oint C_p \, d(X/c) \quad . \tag{5}$$

These expressions neglect the divergence factor in the geometrically exact expressions for local projected surface areas, but only a small percentage error would result due to the large shroud mean radius. The pressure coefficients were numerically integrated by the trapezoidal rule using a Hewlett Packard Model 9810A Calculator and Plotter. The results of C_T and C_F are listed in Table IV. The thrust coefficient versus motor horsepower is plotted on the graphs shown in Figures 16 through 18. Shroud friction drag was neglected.

Total Forces of the Shroud-Propeller System

When the thrust and normal or inward force coefficients are known, the thrust and inward force in lb_f can be found by using

$$T = C_T \, q_\infty A \tag{6}$$

$$F = C_F \, q_\infty A \tag{7}$$

found in Reference 7. The area, A, was found by multiplying the chord length, c, by the effective span (circumference) of the shroud, πd.

The thrust and torque in lb_f and $ft\text{-}lb_f$ respectively were taken from the graphs of thrust and torque versus centimeter deflection shown in Figures 11 and 12. Since the thrust and torque recorded during the tests were for x2 millivolts per division less sensitivity scale than the calibration sensitivity setting, the results from the graphs were divided by 2. This division gave an accurate result in lb_f for the thrust and $ft\text{-}lb_f$ for the torque.

The total thrust of the shroud-propeller combination could now be obtained by adding the shroud thrust and the propeller thrust. The values of shroud thrust and propeller thrust versus motor horsepower are shown in Figures 19 through 27. The total thrust produced by the shroud-propeller combination is also plotted on these graphs. Figures 19-21 also contain

a plot of the free-air propeller thrust. Thrust from the blowing slot was neglected.

Drag on Inside Strut

A total thrust of the model is not complete unless the drag on the inside support struts is included. Since these struts are NACA 63_3-018 symmetrical airfoils, the drag coefficient at zero angle of attack can be found in Reference 8. The expression

$$D_s = C_{D_s} q_s S_s \tag{8}$$

where

$$q_s = 1/2 \rho_s V_s \tag{9}$$

can be used to calculate the drag on each strut. The dynamic pressure at the strut, q_s, can be obtained using

$$p_{static} + q_s = p_{total_s} \tag{10}$$

Since the velocity was not spanwise constant on the struts, the strut was divided into four spanwise sections and a total pressure was measured for each section. These measured values were checked by using the momentum equation to calculate the propeller thrust, and good agreement with the measured propeller thrust resulted. (This indicated propeller swirl was small.) The static pressure was recorded from the tap on the shroud surface near the front of the strut. The total pressures and static pressures were recorded for the three motor speed settings. A dynamic pressure and planform area were calculated for each spanwise section at each motor speed. These were used to obtain a drag force for each section. The drag forces in lb_f were then added to obtain a total drag force for each strut. Since there are four inside struts, the total drag for one strut was multiplied by 4. This calibration produced a value for the drag force in lb_f at each motor speed setting. These drag values are listed in Table IV.

Blowing Momentum Coefficient

The blowing momentum coefficient is represented by

$$C_\mu = \frac{\dot{m} V_j}{q_\infty c} \tag{11}$$

This coefficient is defined as the ratio of the momentum per unit time issuing from the blowing slot to the product of the freestream dynamic pressure and the shroud airfoil chord length. The freestream dynamic pressure was again calculated using a static pressure of 3 inches of water. This assumption made the blowing momentum coefficient lower than actual but was necessary for non-dimensionalization. This coefficient was used only as a reference.

Since the total and static pressure at the slot were known, the Mach number of the jet was calculated using the isentropic equation

$$M_j = \left\{ \left[\frac{2}{\gamma - 1} \right] \left[\left(\frac{p_{t_j}}{p_j} \right)^{\frac{\gamma - 1}{\gamma}} - 1 \right] \right\}^{1/2} \tag{12}$$

The static temperature of the jet was calculated from the isentropic equation

$$\frac{T_{t_j}}{T_j} = 1 + \frac{\gamma - 1}{2} M_j \tag{13}$$

The speed of sound of air in the jet was found from

$$a_j = 49.015 \sqrt{T_j (^\circ R)} \tag{14}$$

The jet velocity could then be found using

$$V_j = M_j a_j \tag{15}$$

The volume flow rate, in SCFM, was obtained directly from the flowmeter. The flowmeter scale is in standard cubic feet per minute when the entrance pressure to the flowmeter is kept at 100 psig. This entrance pressure was maintained through the investigation. The mass flow rate per unit span was then found using

$$\dot{m} = \left[\frac{SCFM}{60} \times \rho\right] / SP \tag{16}$$

Brake Horsepower

In order to compare the efficiency of the shroud-propeller combination, the brake horsepower was calculated for the propeller mounted in free-air as well as in the shroud. The equation used to make these calculations was

$$BHP = \frac{2\pi(N)(Tq)}{33,000} \tag{17}$$

In order to establish the actual efficiency of any circulation control system employing blowing, the power of the blowing slot must be determined. The power required to provide the blowing air is a design factor in an actual aircraft model. The power at the slot can be found from the kinetic energy equation

$$KE = \frac{1}{2} \frac{MF}{g} V_j^2 \tag{18}$$

The horsepower at the slot is found by using the expression

$$BHP = \frac{KE}{550} \tag{19}$$

The horsepower required to operate the motor plus that quantity required to provide the blowing is the total required to operate this system. This power requirement is <u>not</u> included in the results shown in graphical form, but is listed in Table IV.

RESULTS

Propeller Thrust

The thrust produced by the propeller was dependent on all three of the variable conditions of blade pitch angle, blowing momentum coefficient and rotational speed. This is illustrated by the propeller thrust data in Table IV. The propeller thrust always increased with an increase in propeller speed. The propeller thrust also went up, in almost every case, as the blade pitch angle was increased. The only exceptions were at the lower speed setting, and these few decreases were not substantial. The thrust produced by the propeller also went up as the blowing momentum coefficient was increased. This was as expected. The maximum propeller thrust of 3.025 lb_f was found at the maximum blade pitch angle, rotational speed and blowing momentum coefficient. The propeller thrust versus brake horsepower is plotted at the different blade pitch angles and blowing momentum coefficients and can be found in Figures 19-27.

Pressure Distributions

The pressure coefficient distributions are plotted against tap vertical ordinate in Figures 28-54. Figures 55-57 are plots of pressure coefficient versus chordwise ordinate for each C_μ at the maximum motor speed and blade pitch angle. Only 31 tap locations are noted on the graphs since the tap located in the outside slot was filled when that slot was filled. It can be seen from these graphs, that the pressure was quite low around the blunt nose of the shroud. The inner surface was at a lower pressure than the outer surface due to the air being pulled through the propeller. A sharp gradient in the chordwise

ordinate curve is observed between tap locations 25 and 26. This was caused by the propeller being located at tap 26. The pressure distribution is observed to be affected by all three variables in the investigation.

The blade pitch angle caused a slight increase in velocity through the propeller. This increased velocity around the shroud produced a small drop in the pressure coefficients on the inside surface and around the nose of the shroud. This decrease, however, was small when it was compared to the decrease caused by the propeller speed increase.

As the propeller speed was increased the pressure coefficients decreased. The propeller speed had a significant effect on the pressure distribution at every blowing momentum coefficient setting.

At zero blowing momentum coefficient, the pressure coefficients were zero for the taps near the trailing edge of the shroud. An increase in the blowing caused a high velocity region on the semi-circular trailing edge. Therefore, a substantial decrease in the pressure coefficients in this region was noted. As the blowing momentum coefficient increased, the pressure coefficients at the trailing edge decreased. This effect on the data was caused by the high energy air being blown from the slot in a direction tangential to the semicircular trailing edge. The effect of the high energy air injection was noticeable, not only at the slot location, but around the entire semicircular trailing edge. This is due to the Coanda effect discussed in Reference 9. The recovery in pressure coefficient around the outer quarter of the semicircular section is caused by mass entrainment and viscous dissipation.

Shroud Forces

The chordwise and normal force coefficients produced on the shroud by the flow of air were found by integrating the pressure coefficients around the shroud. To check the accuracy of the force coefficient data, a planimeter was used on several of the graphs. The differences in values obtained by integration and the planimeter were less than 4%. The normal force coefficient, which has a direction inward toward the motor, was calculated in order to examine the magnitude of this force coefficient. This shroud blowing slot configuration could be changed so that the normal force produced on both sides of the shroud would point in the same direction. Therefore, a lift could be produced by the shroud for STOL application. The results in Table IV indicate that this force coefficient is of a higher magnitude than the thrust coefficient.

The chordwise or thrust coefficient is plotted against brake horsepower in Figures 16-18. This coefficient was used to calculate the thrust of the shroud shown in Figures 19-27. These figures illustrate that the thrust is very much dependent on the blowing momentum coefficient. The shroud thrust force at zero blowing momentum coefficient and blade pitch angle equal to 8 degrees was nearly the same as the thrust produced by the propeller. As the blade pitch angle was increased, the shroud thrust became greater than the propeller thrust. The value of θ had more effect on the shroud thrust than on the propeller thrust. When the blowing was increased, the low pressure region on the trailing edge of the shroud caused the shroud thrust to decrease. At the higher blowing momentum coefficient, the thrust force was

actually negative, or a drag force, due to this very low pressure region. The increase in propeller speed also caused the shroud thrust to increase.

Strut Drag

The drag on the four inside struts is listed in Table IV. This quantity of 0.0136 for the maximum velocity through the shroud was found to be quite small when compared to the propeller + shroud thrust. This amount of force was subtracted from the propeller + shroud thrust to obtain the total thrust of the system. This total thrust of the system is listed in Table IV and also plotted versus horsepower in Figures 19-27. Slot flow thrust and shroud friction drag are neglected.

Propeller Torque

The torque in ft-lb_f on the propeller was calculated and is listed in Table IV. This quantity was found in order to obtain the propeller brake horsepower. The horsepower was calculated for the propeller both inside the shroud and in the free-air condition.

Free-Air Propeller Thrust

In order to evaluate the efficiency of the shroud-propeller system, a comparison of this system to a non-shrouded system must be made. The thrust and brake horsepower were calculated for the propeller operating in a free-air condition. These values were obtained for three values of blade pitch angle and speed and are listed in Table IV. The propeller thrust in free-air is plotted versus the brake horsepower in free-air in Figures 19-21. The free-air propeller thrust was greater than the shrouded propeller thrust, but much less than the total thrust produced by the shrouded propeller system. This result was expected. Theoretically,

the presences of the shroud substantially reduces the slipstream contraction of the propeller, thus increasing the mass flow through the propeller disk. However, past experimental data has shown that the shrouded propeller generally produces less thrust than the free-air propeller (Reference 1).

Slot Horsepower

The horsepower required to provide the blowing air at each C_{μ} setting was calculated and is listed in Table IV. These horsepower values of 0.080 and 0.226, for C_{μ} equal to 0.012 and 0.045 respectively, were nearly equivalent to the horsepower required by the motor at 3,030 and 4,400 revolutions per minute. The power required to operate the total system was therefore not excessive.

Comparison with Previous Work

Since there is no knowledge of any previous work on circulation controlled shrouds, a comparison was not applicable. However, a comparison of the thrust produced by the shroud with no blowing to general shrouded-propeller data was made. References 1 and 10 indicate that at various propeller speed ranges, the thrust produced by the shroud can be greater than the propeller thrust. This was the case when the circulation controlled shroud was tested at zero blowing momentum coefficient.

CONCLUSIONS

Several important conclusions can be drawn from the results noted in the previous section. These conclusions were based upon the effect produced on the shroud and propeller thrust by changing the three variables; blade pitch angle, propeller speed, and blowing momentum coefficient. The conclusions listed below are the most significant concerning this investigation:

1) The circulation controlled shroud did produce the effect of a cambered shroud.

2) The efficiency of the shroud with no blowing applied was quite high, and on the order of that produced by sharp edged shrouds. The shroud thrust was generally higher than the thrust produced by the propeller

3) The efficiency of the shroud as a thrust producer decreased as the blowing was increased. This was caused by the low pressure region at the trailing edge of the shroud.

4) The increase in blowing momentum coefficient caused an increase in the thrust produced by the propeller.

5) The increase in propeller thrust was not sufficient to balance the decrease in shroud thrust. Therefore, the total thrust decreased with an increase in blowing.

6) The variation of the blade pitch angle was found to be of very little significance in changing the propeller thrust. However, the shroud thrust was increased substantially at the higher blade pitch angle settings.

7) The increased propeller speed caused an increase in shroud and propeller thrust.

8) The drag on the inside support struts was not significant in reducing the thrust of the shroud-propeller combination.

9) The free-air propeller thrust was greater than the shrouded propeller thrust.

10) The horsepower required to operate the propeller and the blowing slot was sufficiently low to assume that this system could be employed on an actual aircraft.

11) Changes in the geometry of the trailing edge downstream of the slot should be considered, to decrease the magnitude of the low pressures resulting with blowing. The mixing of the slot flow and the propeller flow was apparently not optimized, and should be studied in detail.

It can be seen from these conclusions that further investigations performed on this system are required in order to determine the overall efficiency. The model should be mounted in a large subsonic wind tunnel. The increase in freestream velocity should cause an efficiency increase of this circulation controlled shroud. Blowing from the outer slot at high freestream speed ranges should also be investigated.

REFERENCES

1. Black, Donald M., Wainauski, Harry S., and Rohrbach, Carl, "Shrouded Propellers-A Comprehensive Performance Study", AIAA Paper No. 68-994, presented at the AIAA 5th Annual Meeting and Technical Display, Philadelphia, Pa., October 21-24, 1968.
2. McCormick, Barnes W., Jr., Aerodynamics of V/STOL Flight, Academic Press, New York, 1967, pp. 231-245.
3. Lazareff, M., "Aerodynamics of Shrouded Propellers, The Aerodynamics of V/STOL Aircraft, North Atlantic Treaty Organization Advisory Group for Aerospace Research and Development, presented at a Lecture Series held at von Karman Institute, Rhode-Saint-Genese, Belgium, May 13-17, 1968, pp. 239-272.
4. Walters, Richard E., Myer, Danny P., and Holt, Daniel J., Circulation Control by Steady and Pulsed Blowing for a Cambered Elliptical Airfoil, Technical Report 32, Department of Aerospace Engineering, West Virginia University, July 1972, (AD 751045).
5. Loth, J. L., "Some Aspects of STOL Aircraft Aerodynamics," SAE Paper No. 730328, presented at the SAE Business Aircraft Meeting, Wichita, Kansas, April 3-6, 1973.
6. Pope, Alan and Harper, John J., Low-Speed Wind Tunnel Testing, John Wiley and Sons, Inc., New York, 1966, p. 454.
7. Kuethe, A. M. and Schetzer, J. D., Foundations of Aerodynamics, John Wiley and Sons, Inc., New York, 1967, p. 110.
8. Abbott, Ira H. and Doenhoff, Albert E., Theory of Wing Sections, Dover Publications, Inc., New York, 1959, p. 533.

9. Ambrosiani, Jack P., and Ness, Nathan, Analysis of a Circulation Controlled Elliptical Airfoil, Technical Report 30, Department of Aerospace Engineering, West Virginia University, April 197i, pp. 3-4.

10. Conference on V/STOL and STOL Aircraft, held at Ames Research Center, Moffett Field, California, NASA SP-116, National Aeronautics and Space Administration, Washington, D.C., 1966, pp. 106-113.

APPENDIX A

FIGURES

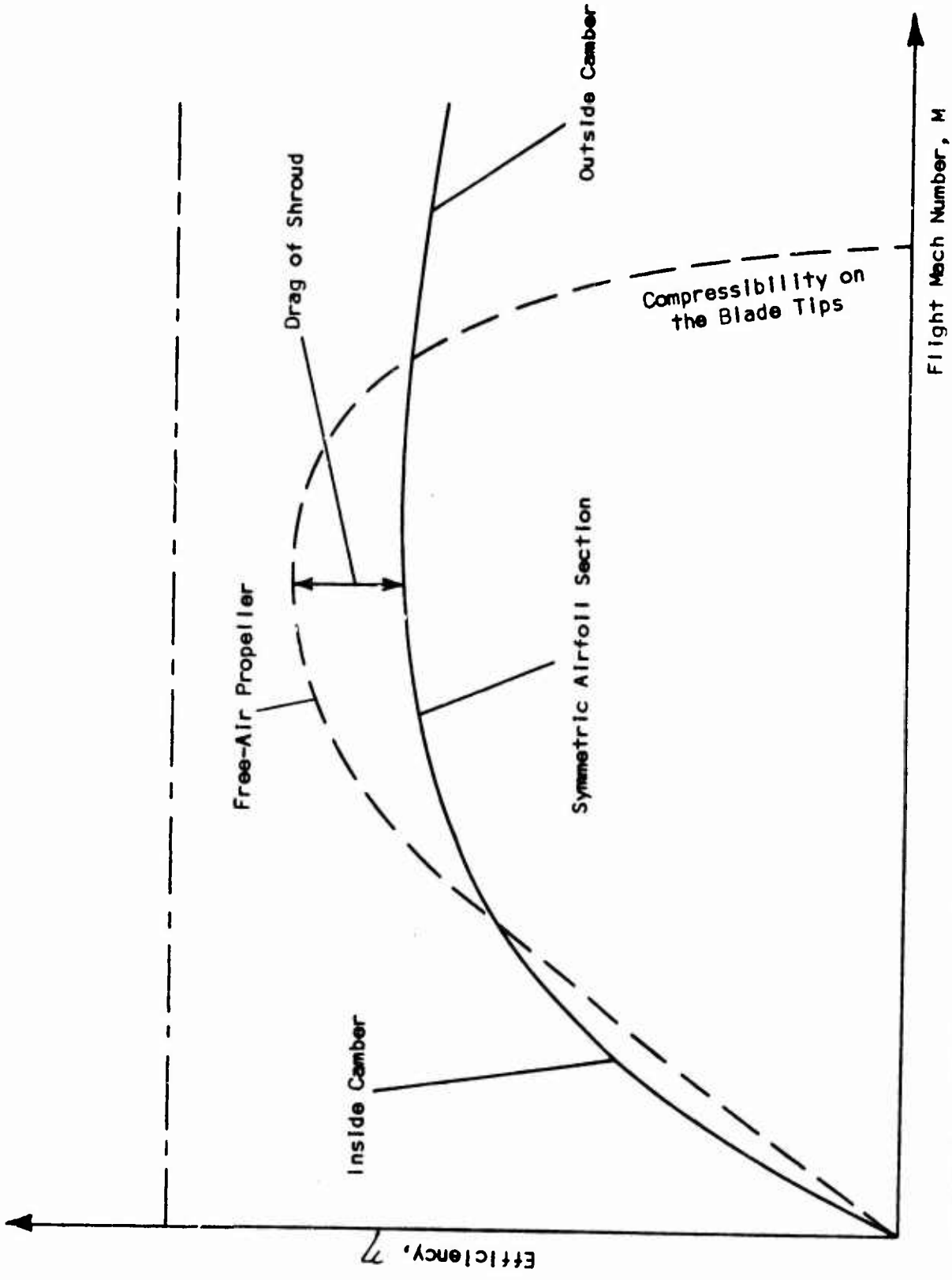

FIGURE 1. Efficiency of Shrouded Propeller Systems

Blowing from inside slot expands the wake at low speeds

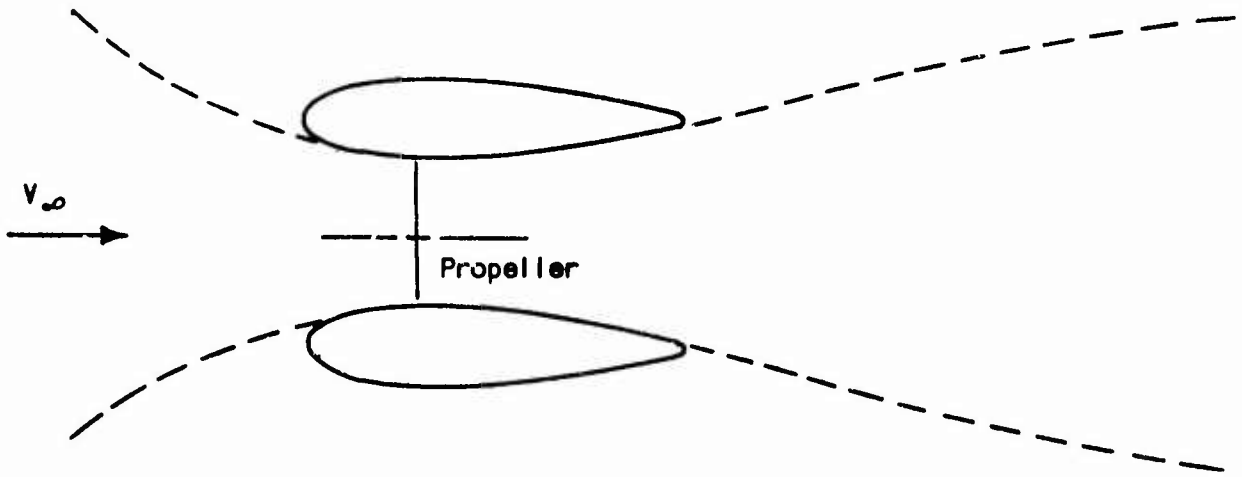

Blowing from outside slot contracts the wake at high speeds

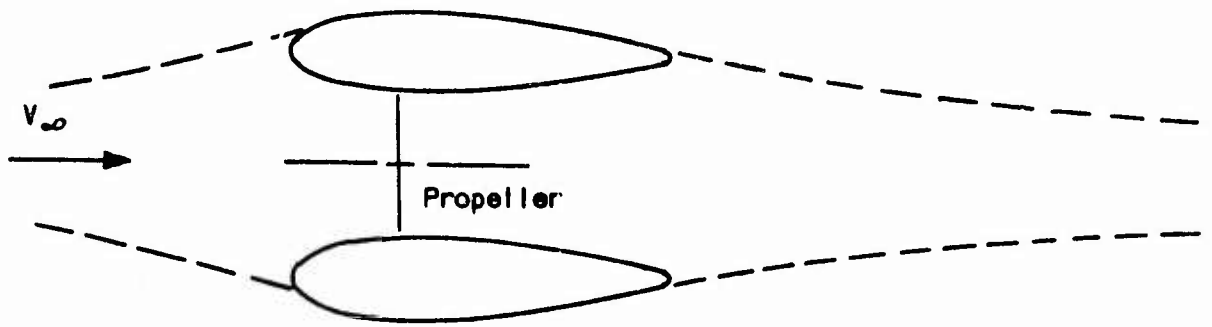

FIGURE 2. Effect of Circulation Control on Air Flow

1/8 Scale
All Dimensions in Inches

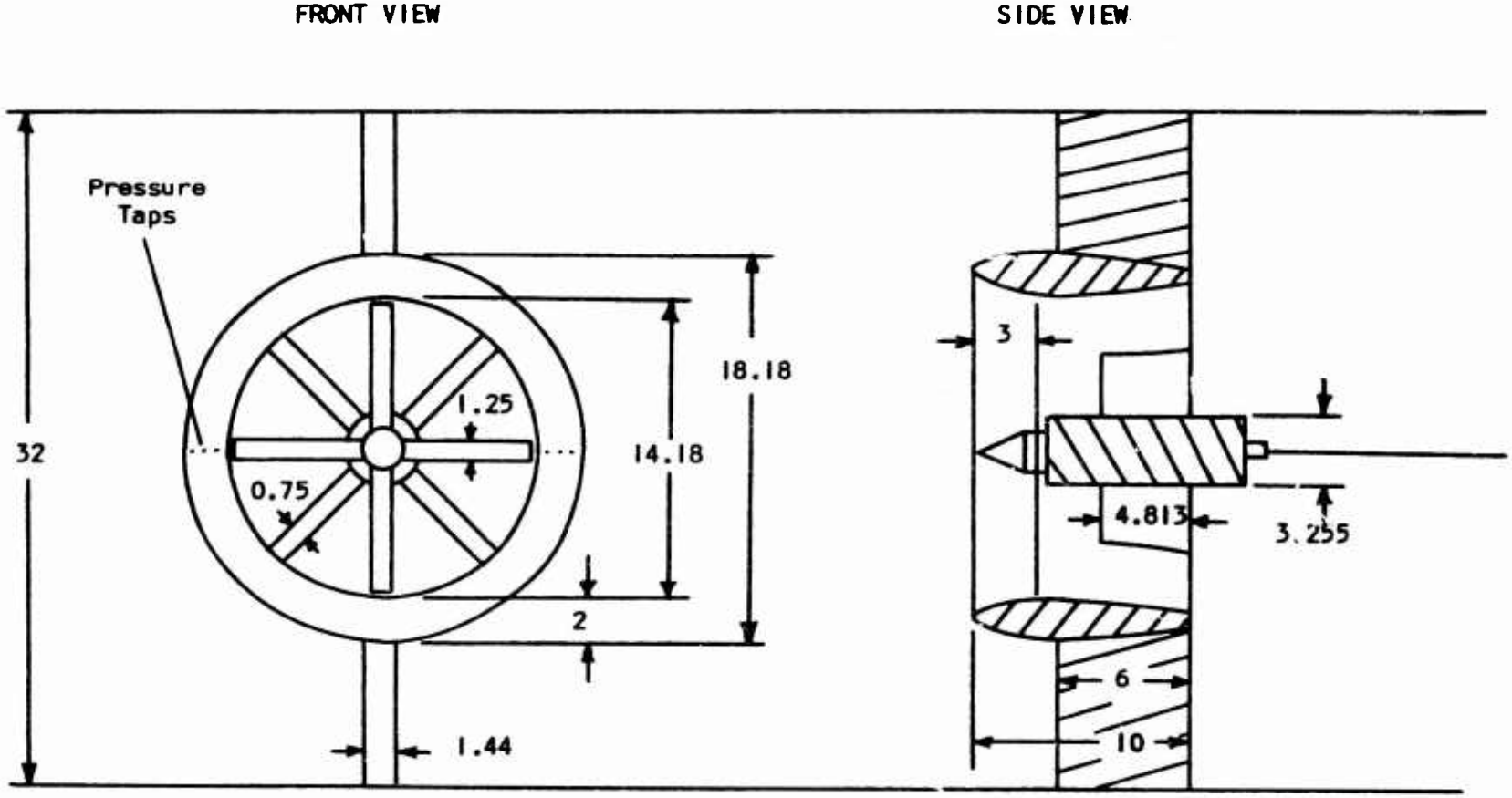

FIGURE 3. Front and Cutaway Side View of Entire Shroud and Supports

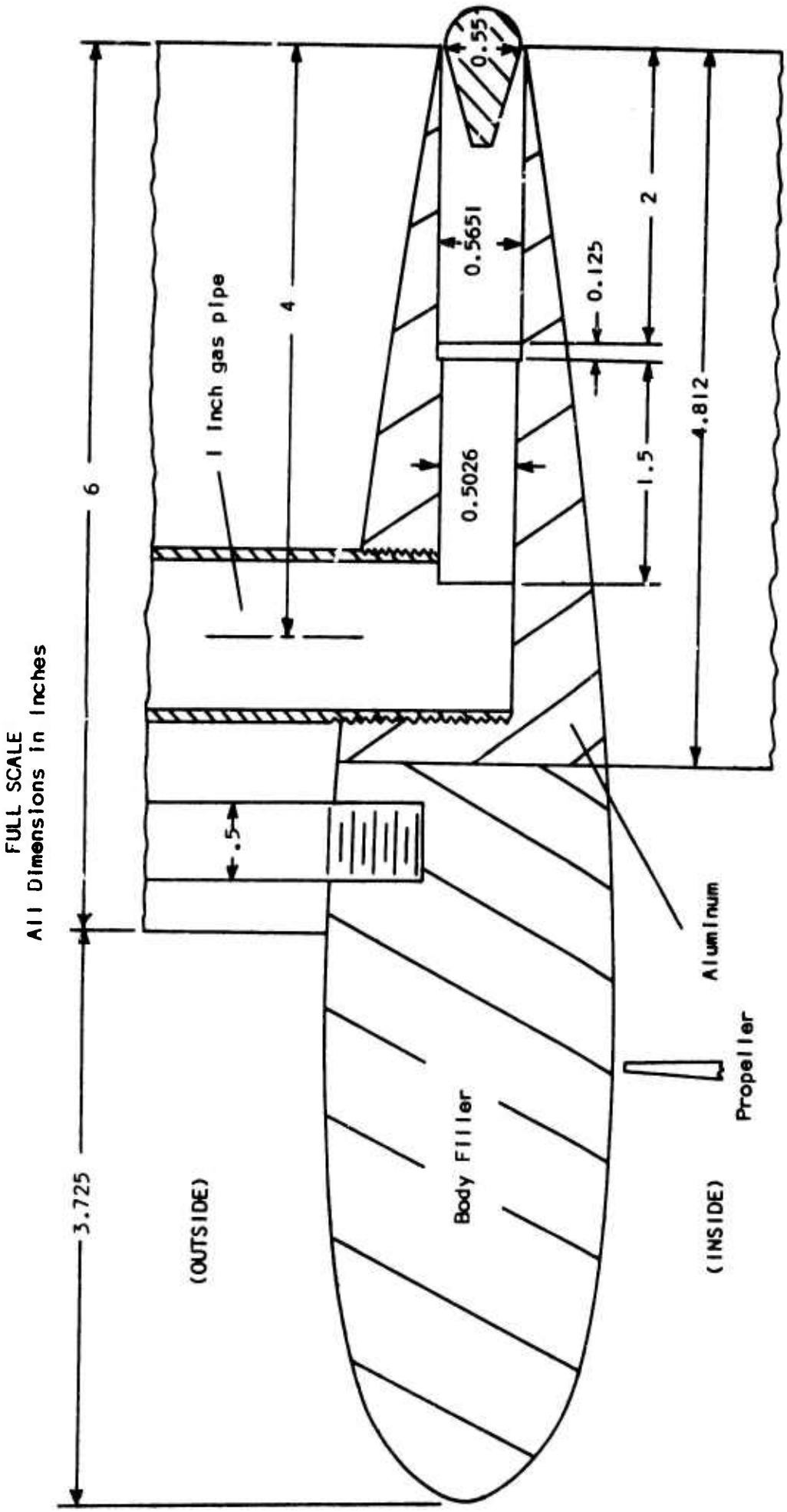

FIGURE 4a. Cross Section of Shroud Airfoil Section at Top

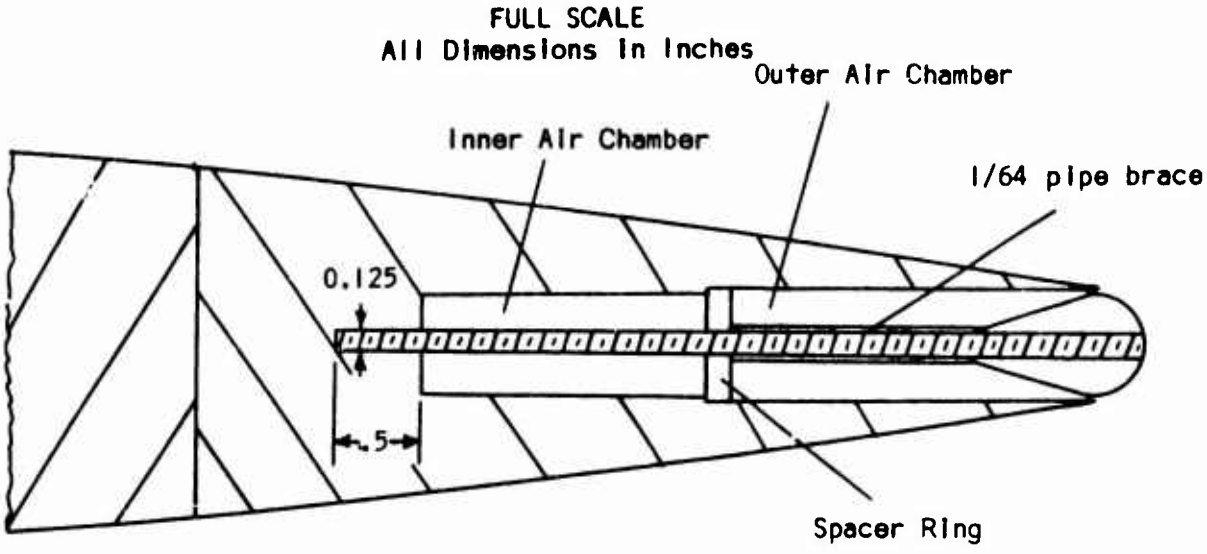

FIGURE 4b. Cross Section of Shroud and Support Screws

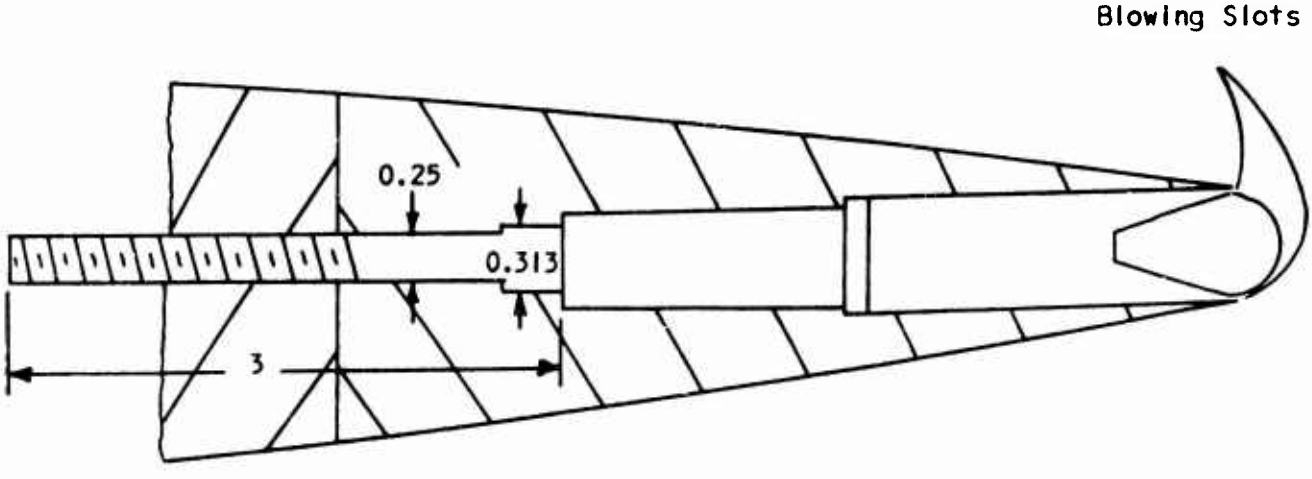

FIGURE 4c. Cross Section of Shroud and Connection Screws

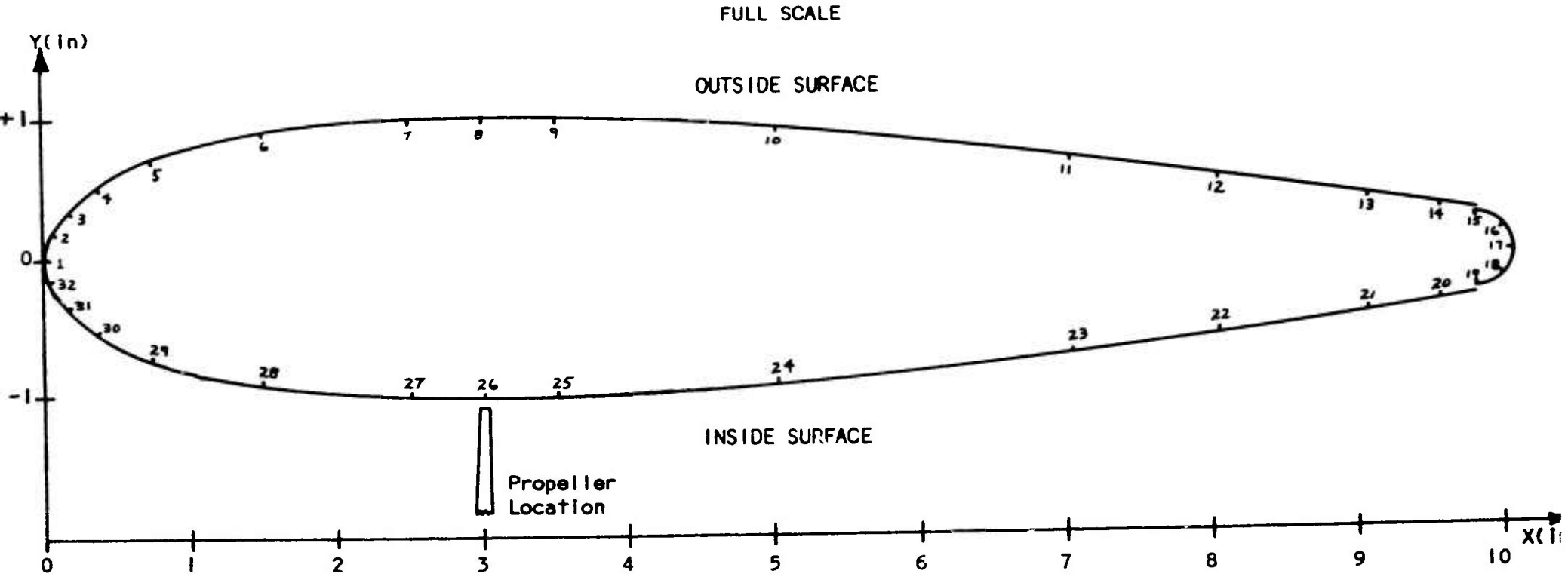

FIGURE 5. Pressure Tap Locations

All Dimensions In Feet
Scale: 1/2 inch = 1 foot

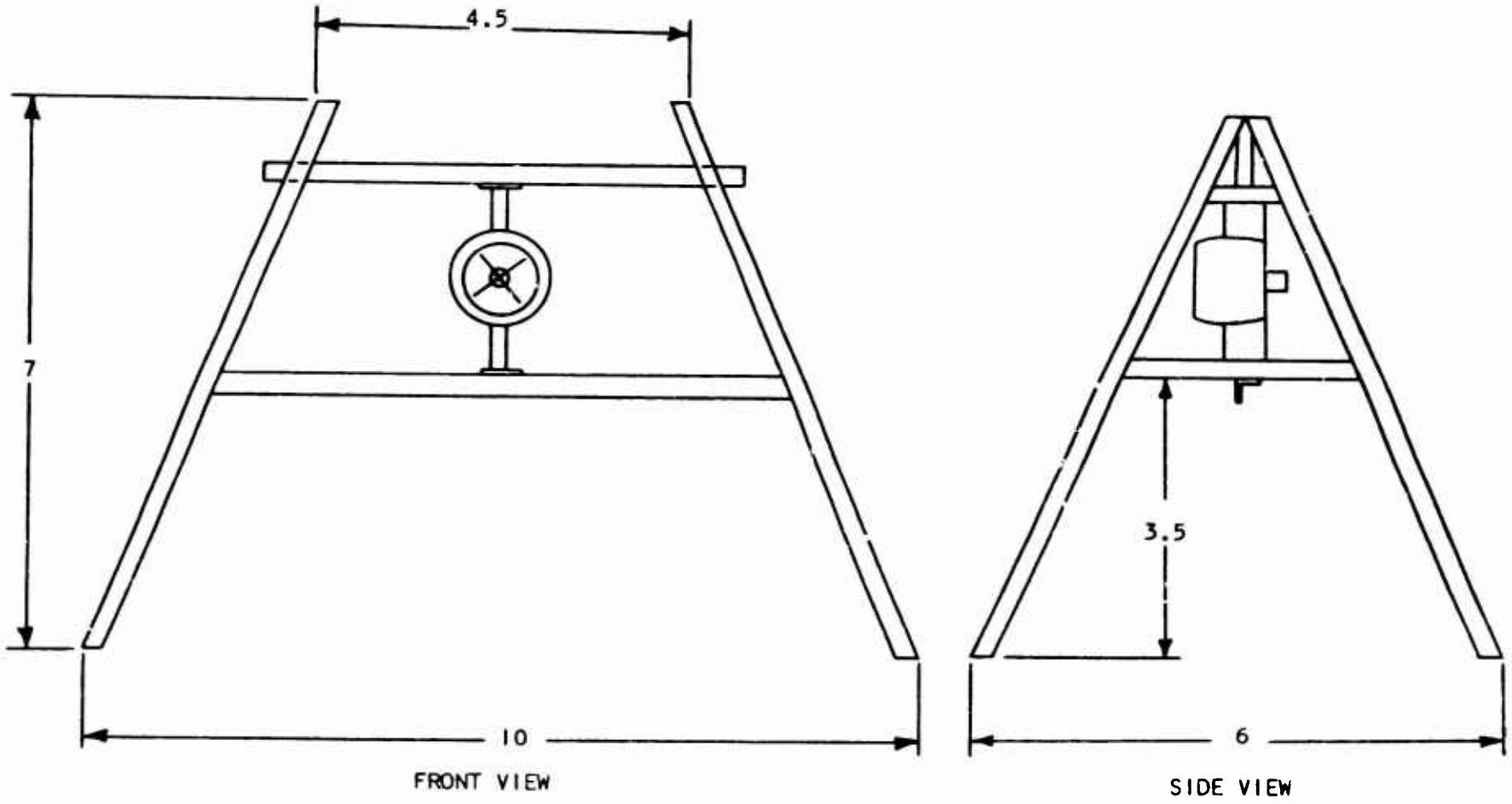

FIGURE 6. Test Stand

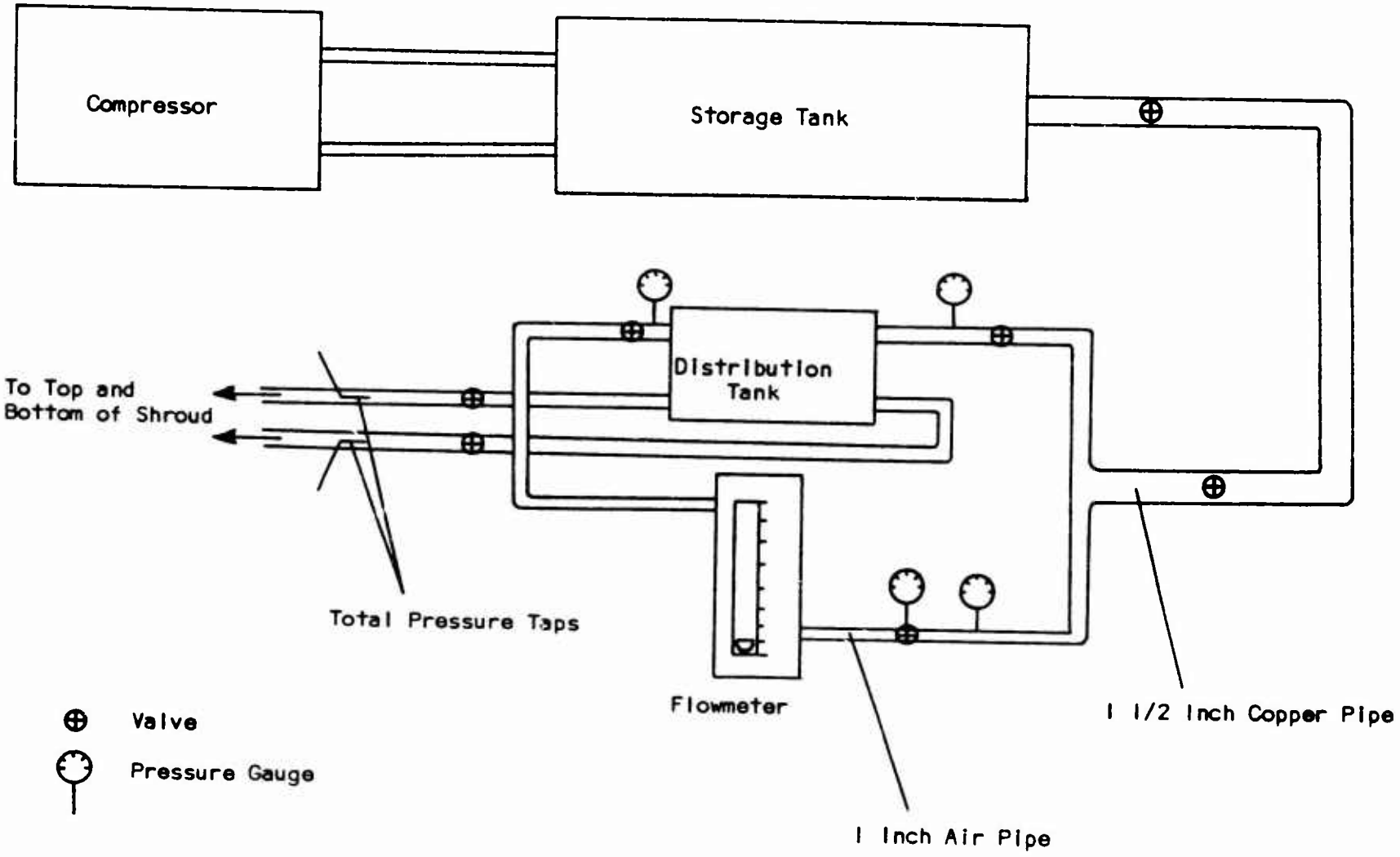

FIGURE 7. Air Supply System

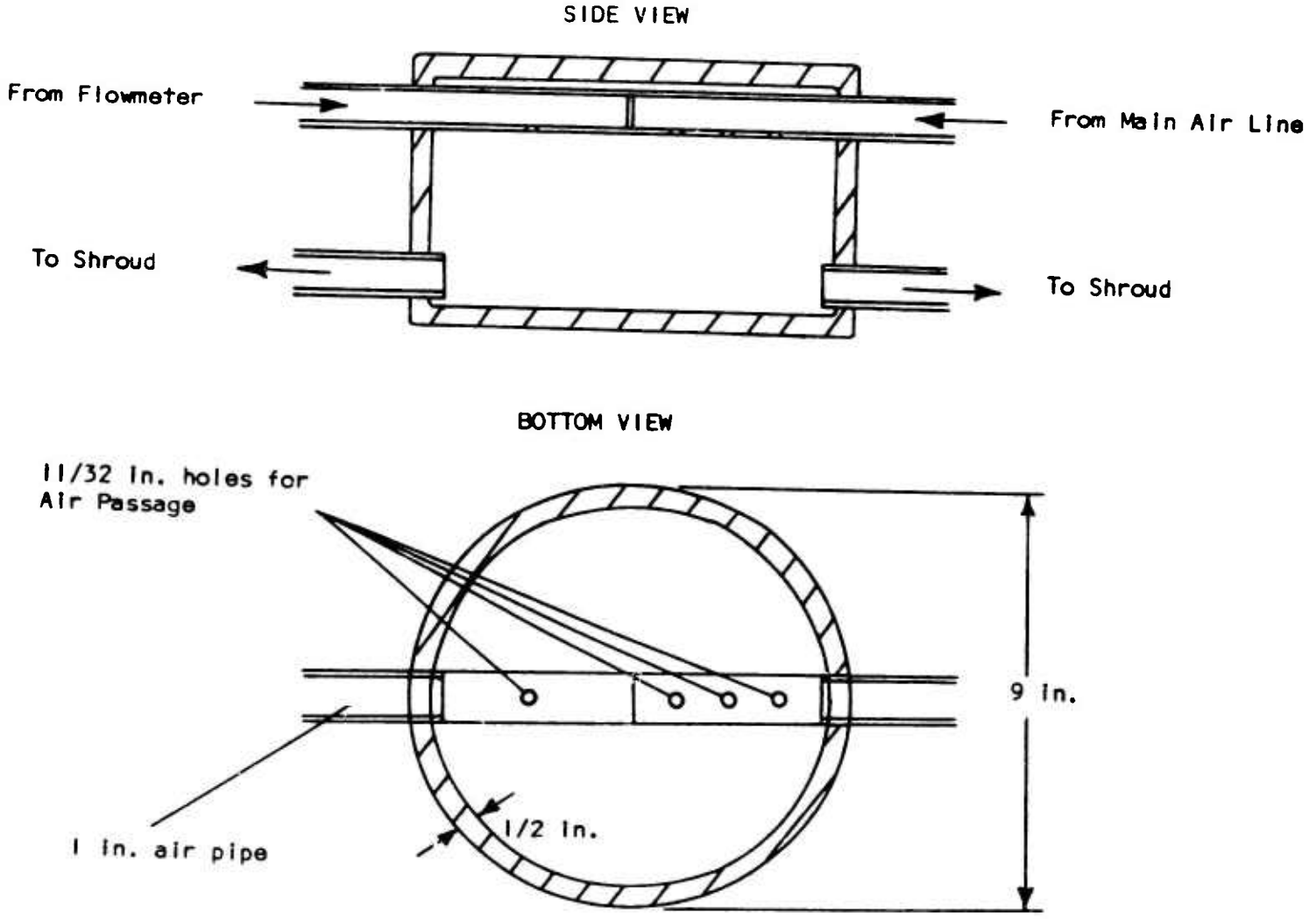

FIGURE 8. Distribution Tank

FIGURE 9a. Front View of Shroud

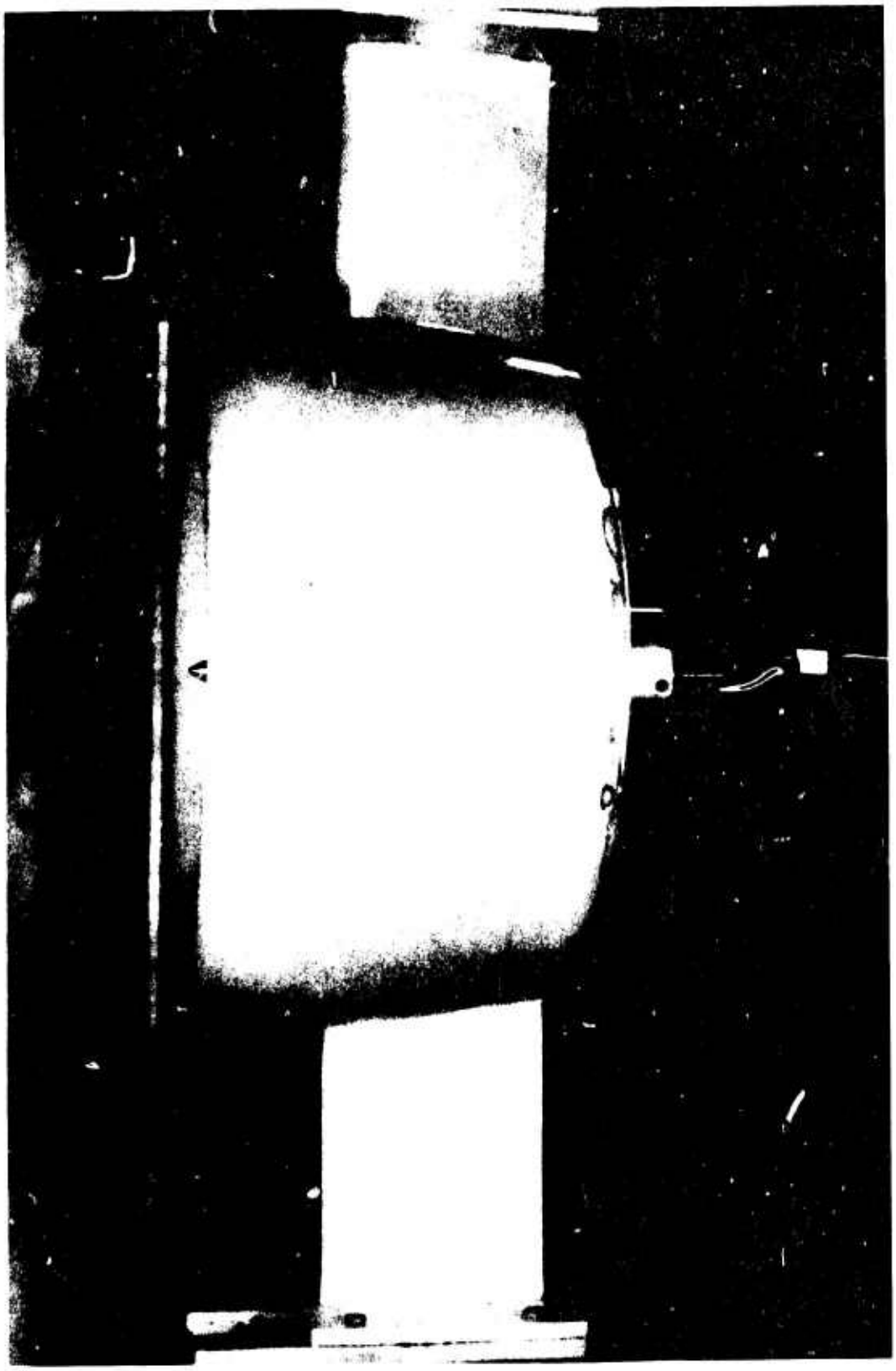

FIGURE 9b. Side View of Shroud

FIGURE 9c. Back View of Shroud

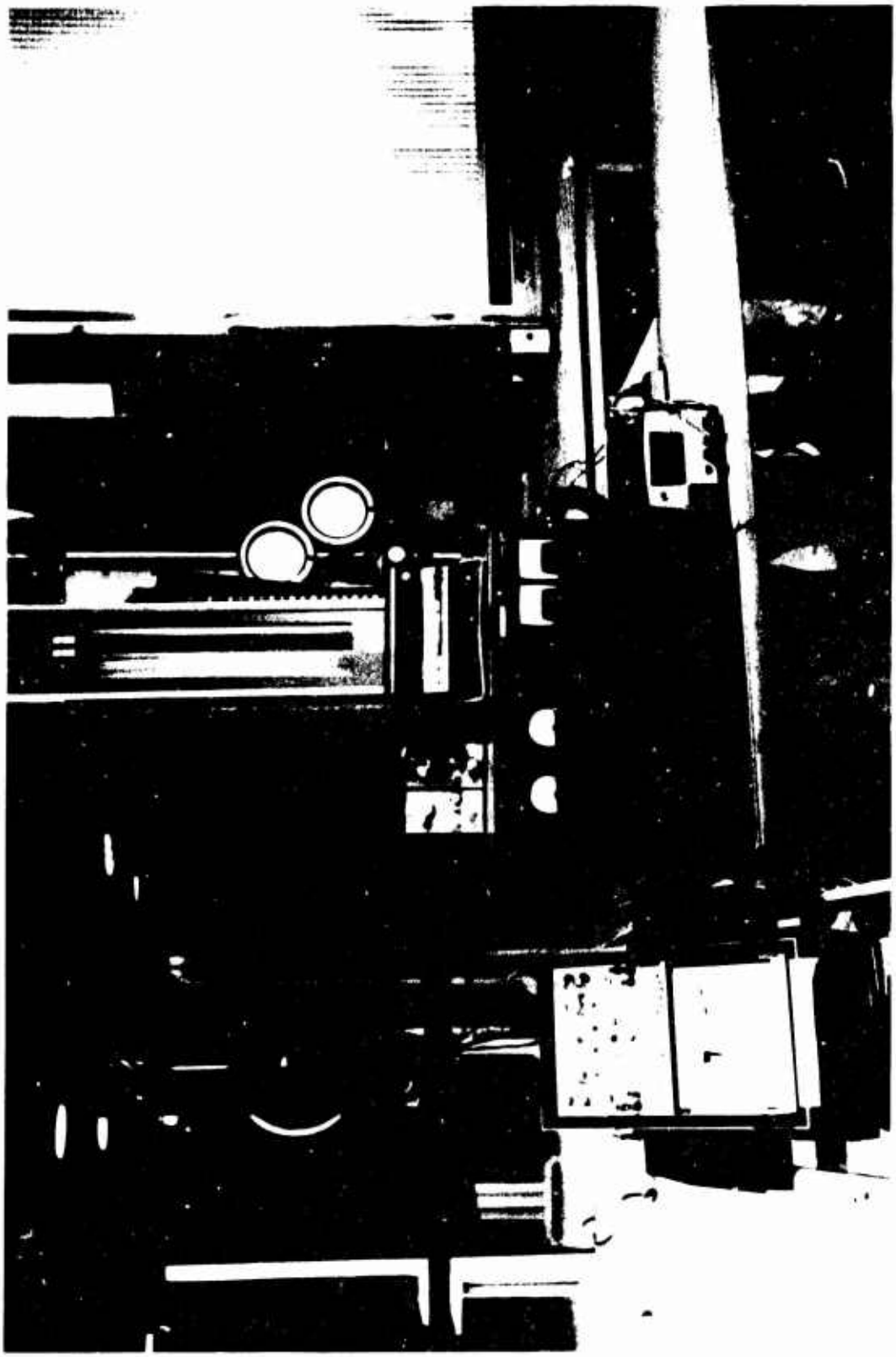

FIGURE 9d. Testing Equipment

THRUST CALIBRATION

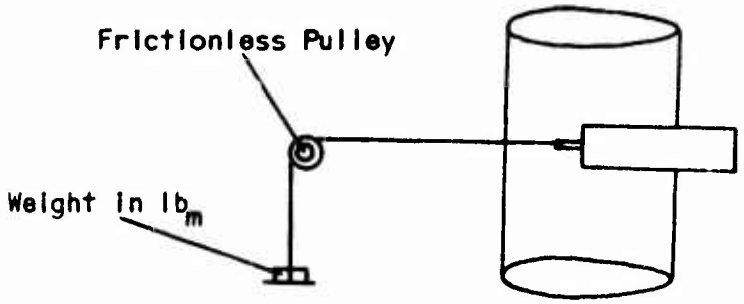

TORQUE CALIBRATION

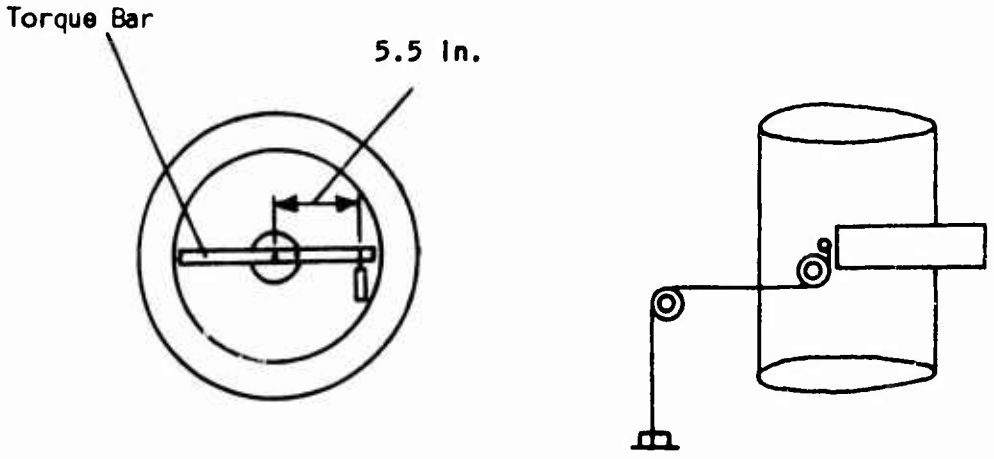

FIGURE 10. Motor Calibration Equipment

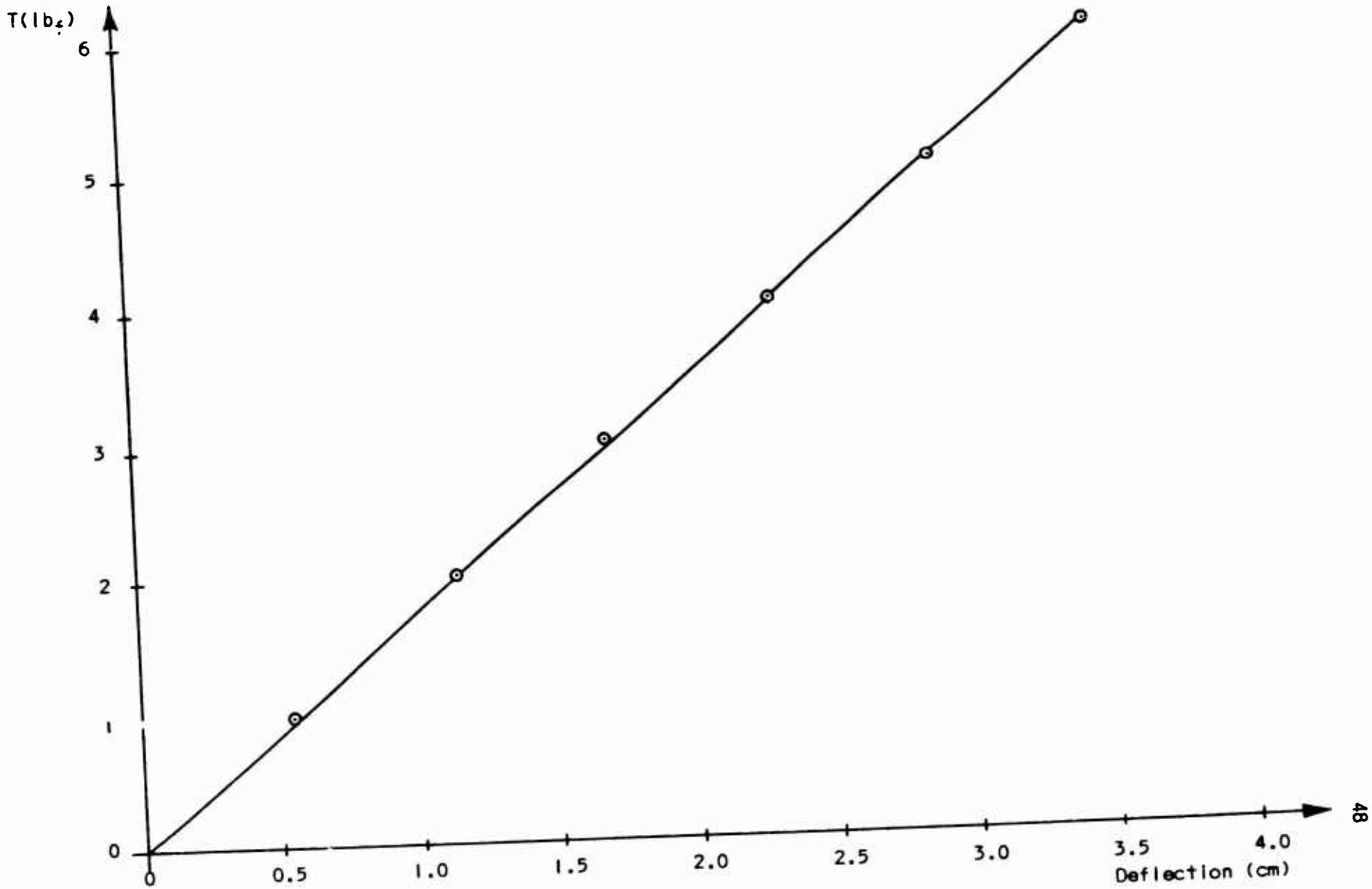

FIGURE 11. Calibration Graph for Thrust

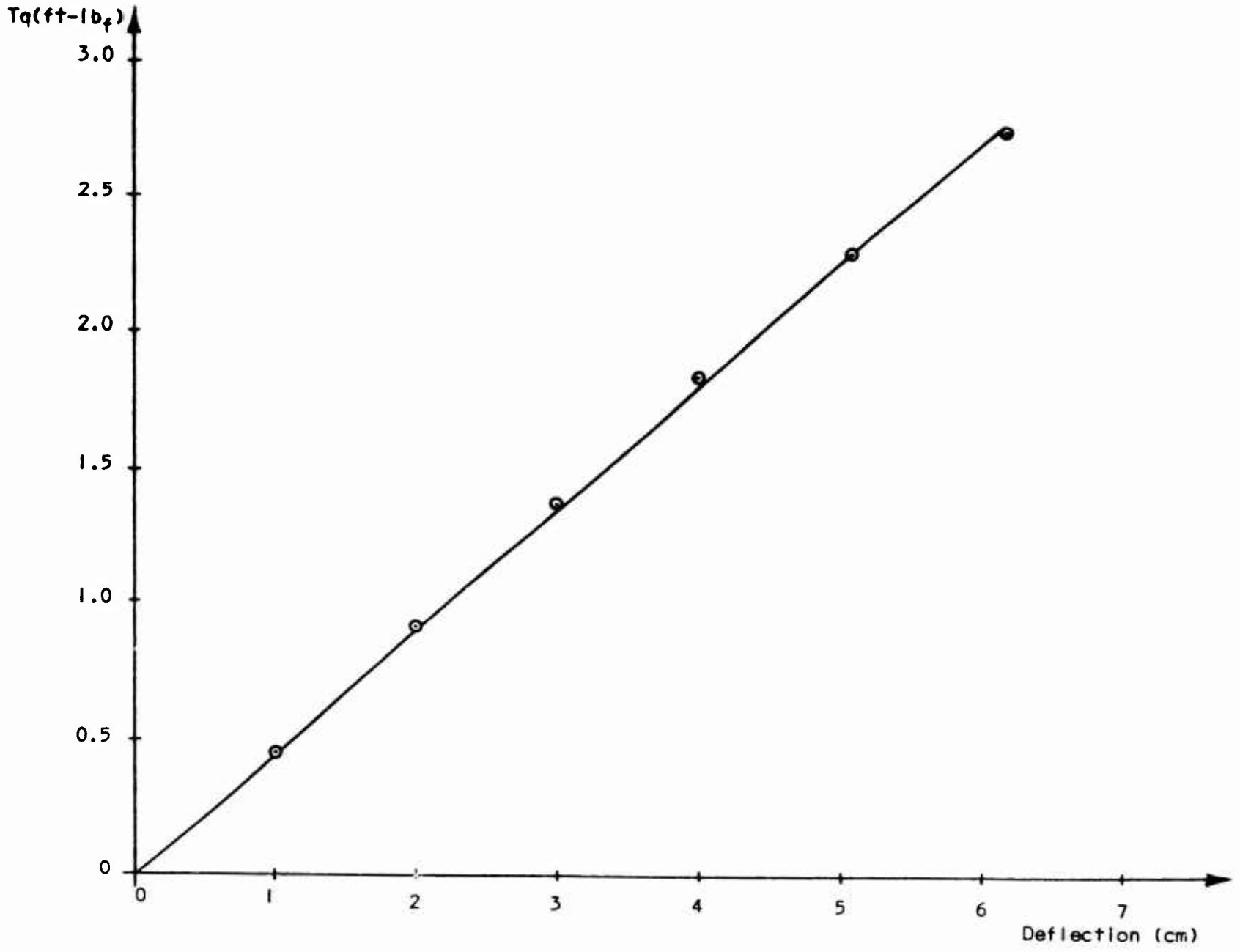

FIGURE 12. Calibration Graph for Torque

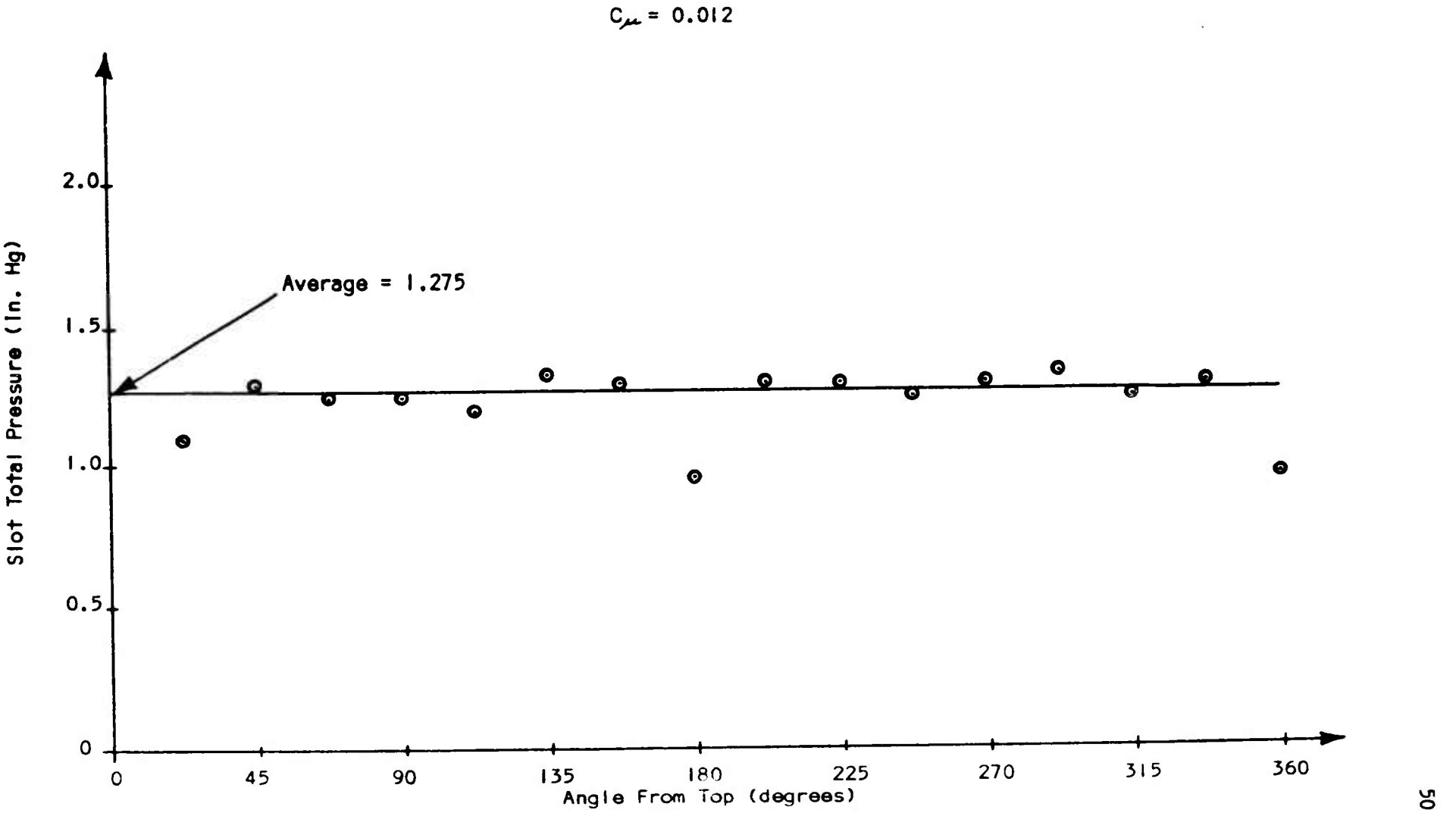

FIGURE 13. Slot Total Pressure Survey

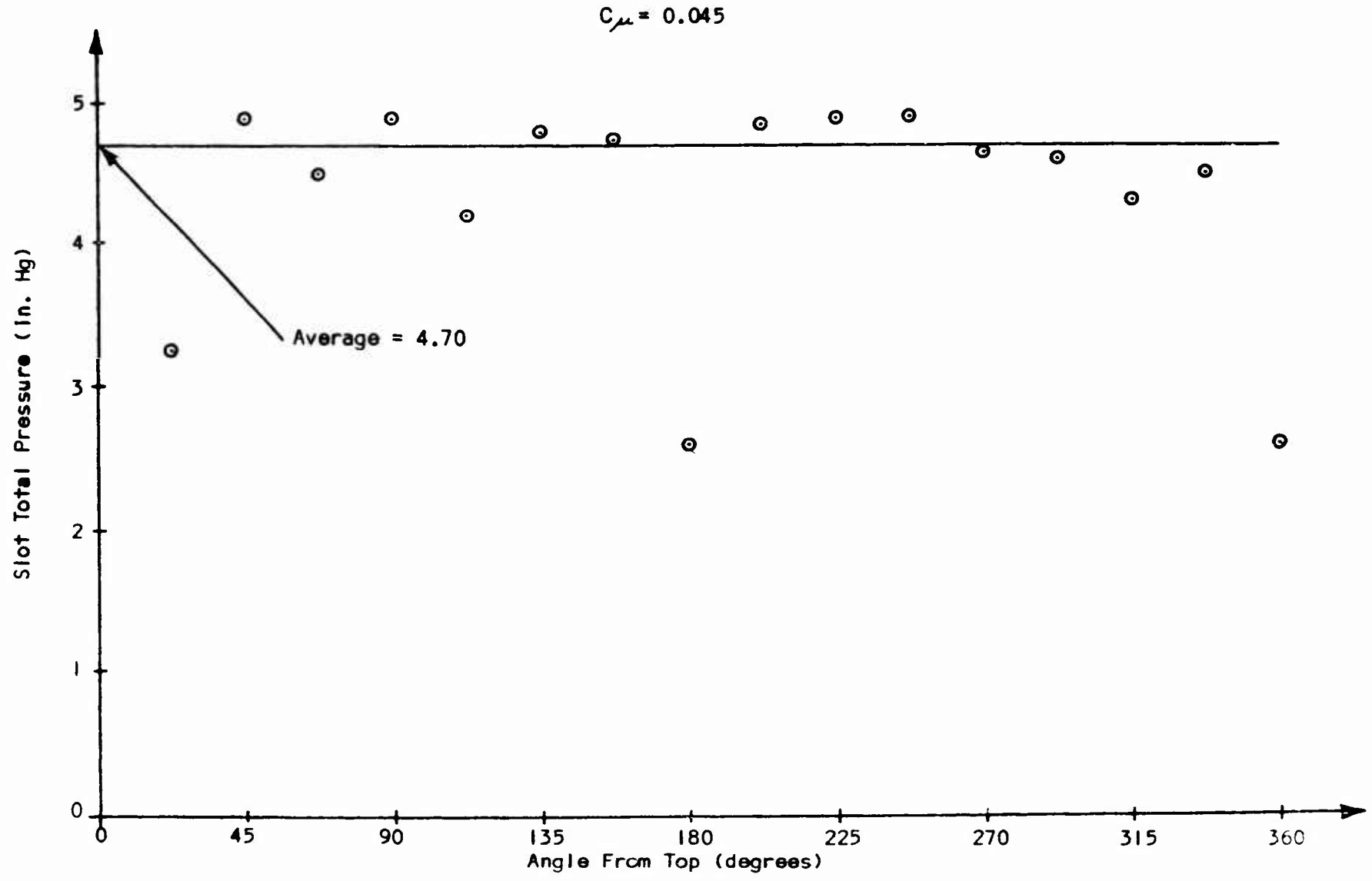

FIGURE 14. Slot Total Pressure Survey

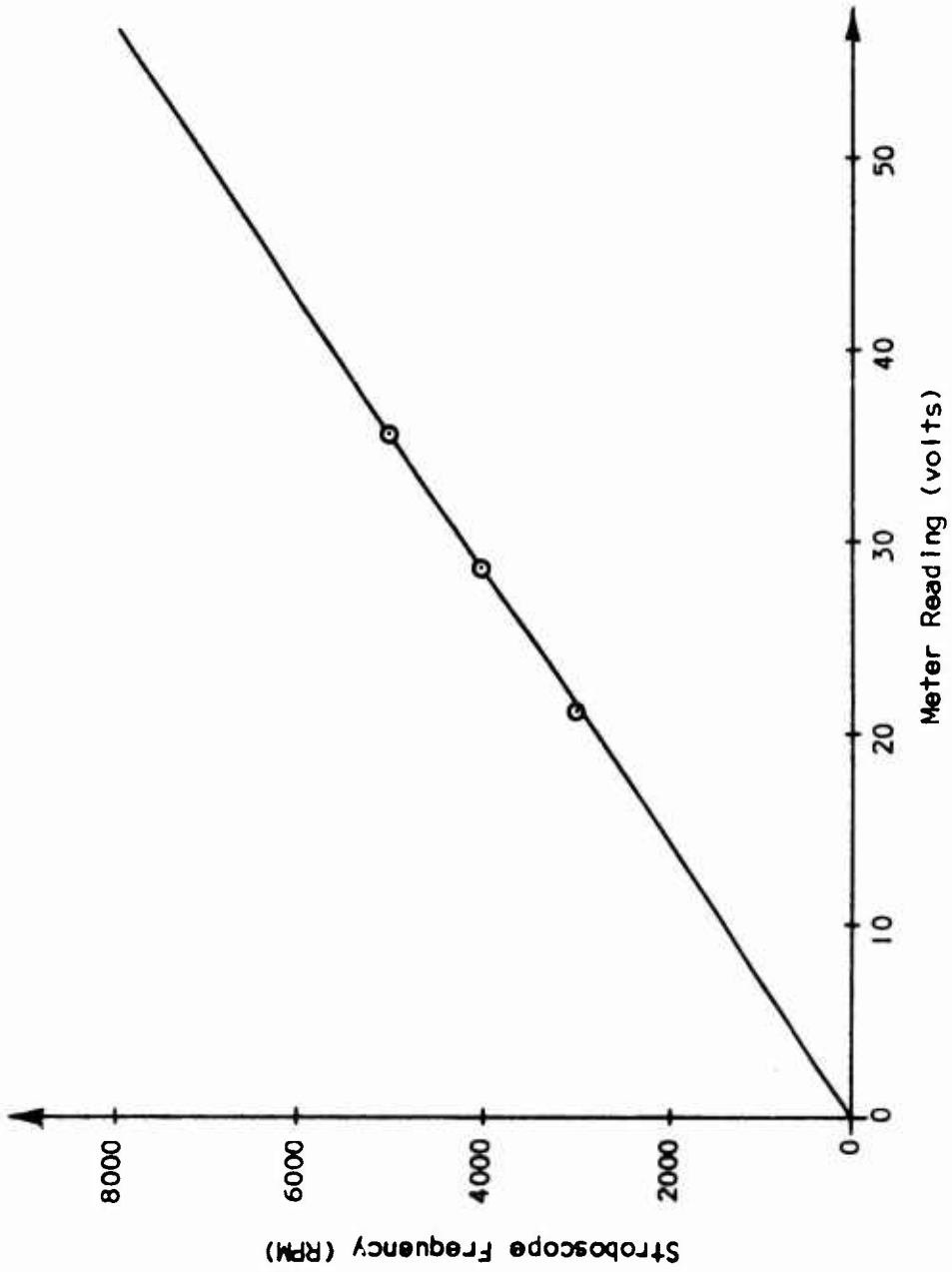

FIGURE 15. Calibration Graph for Motor RPM

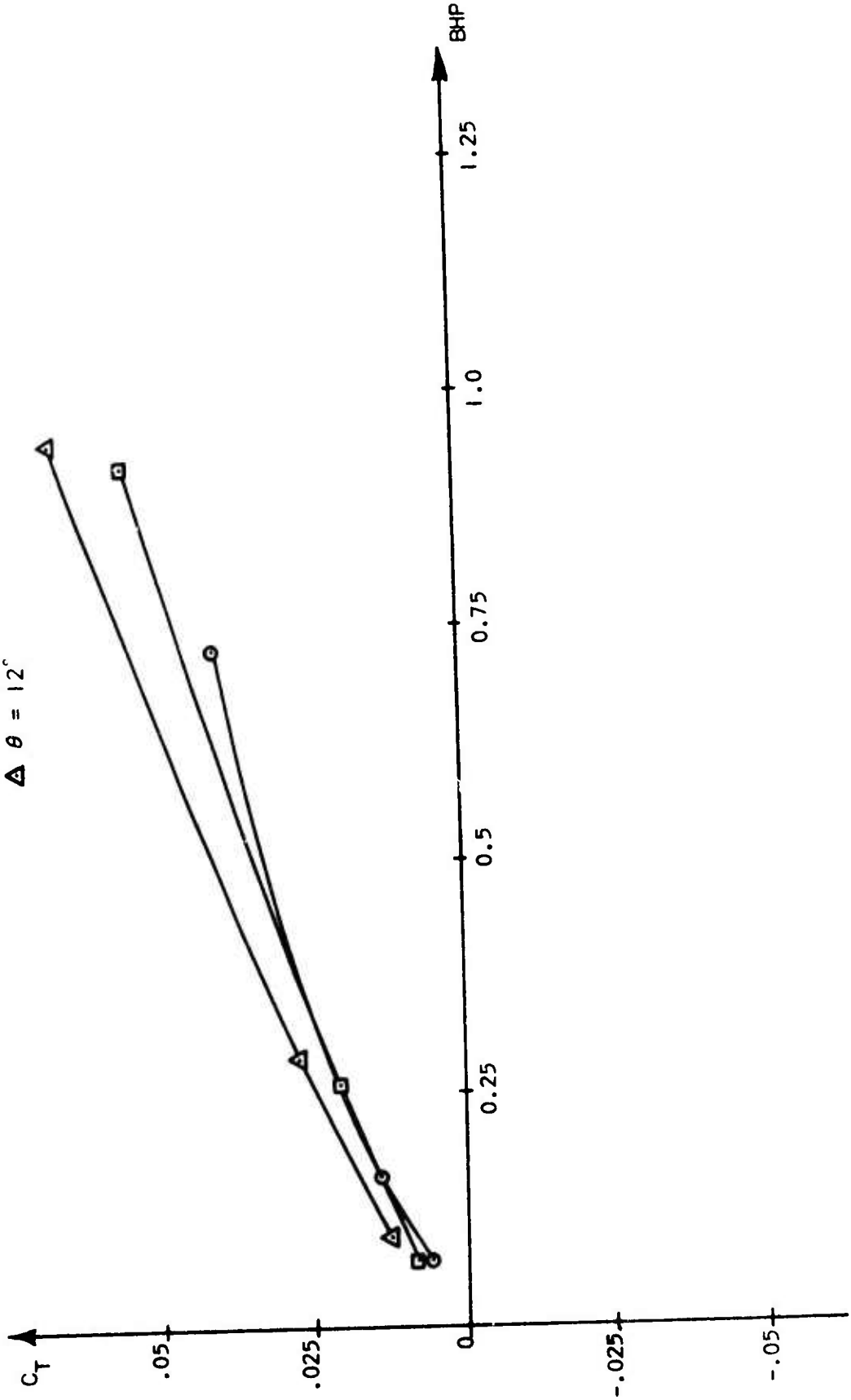

FIGURE 16. Shroud Thrust Coefficient

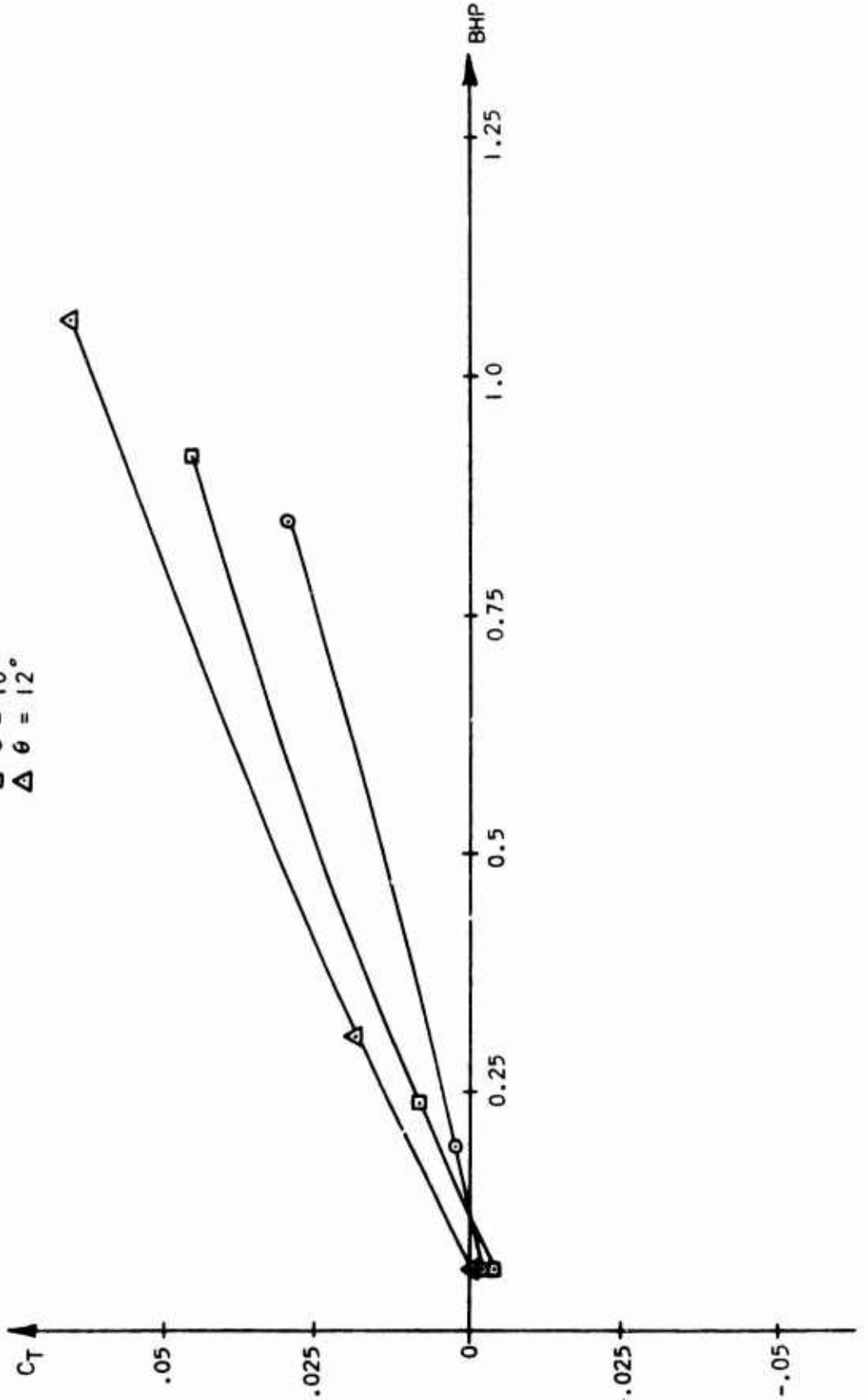

FIGURE 17. Shroud Thrust Coefficient

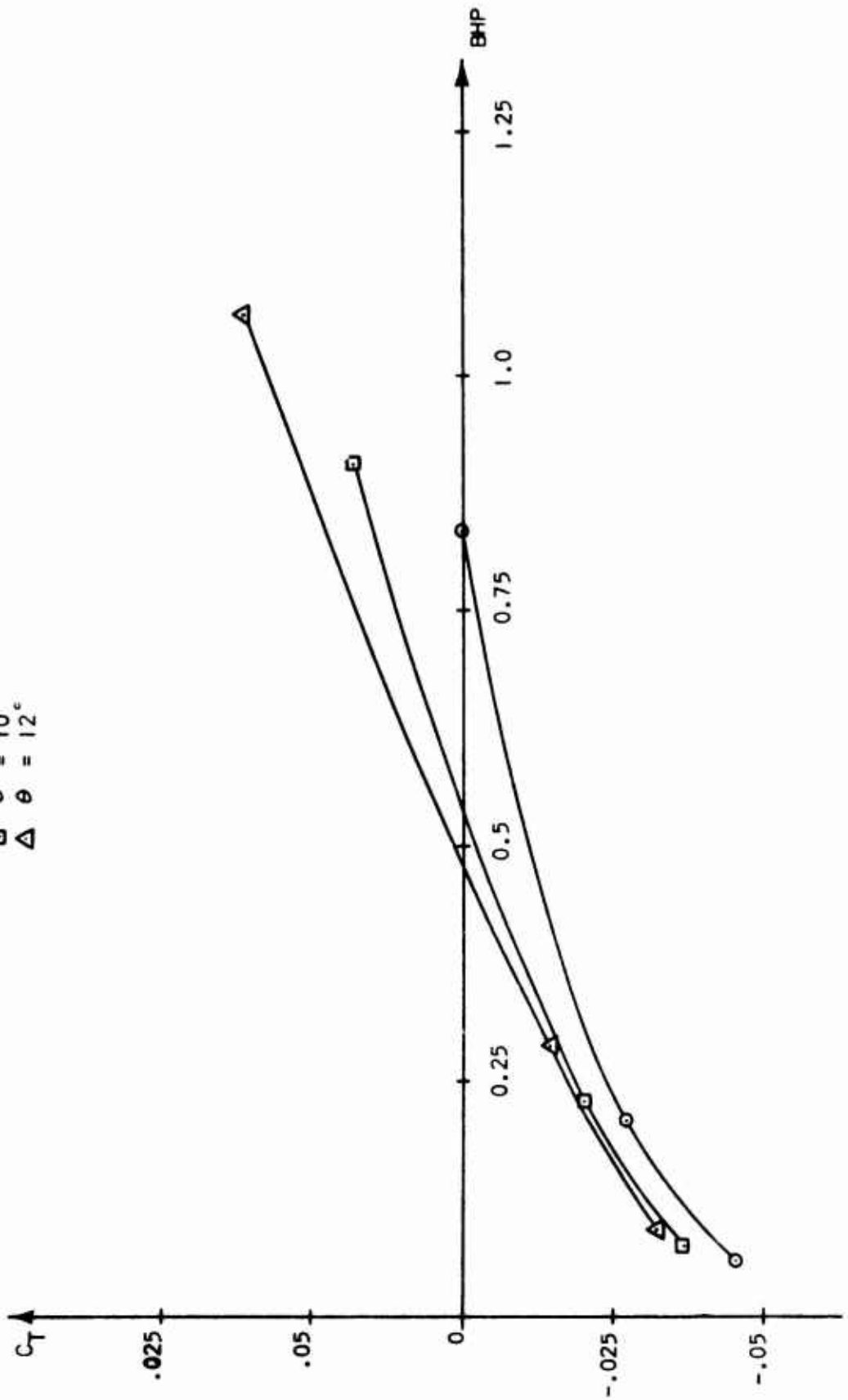

FIGURE 18. Shroud Thrust Coefficient

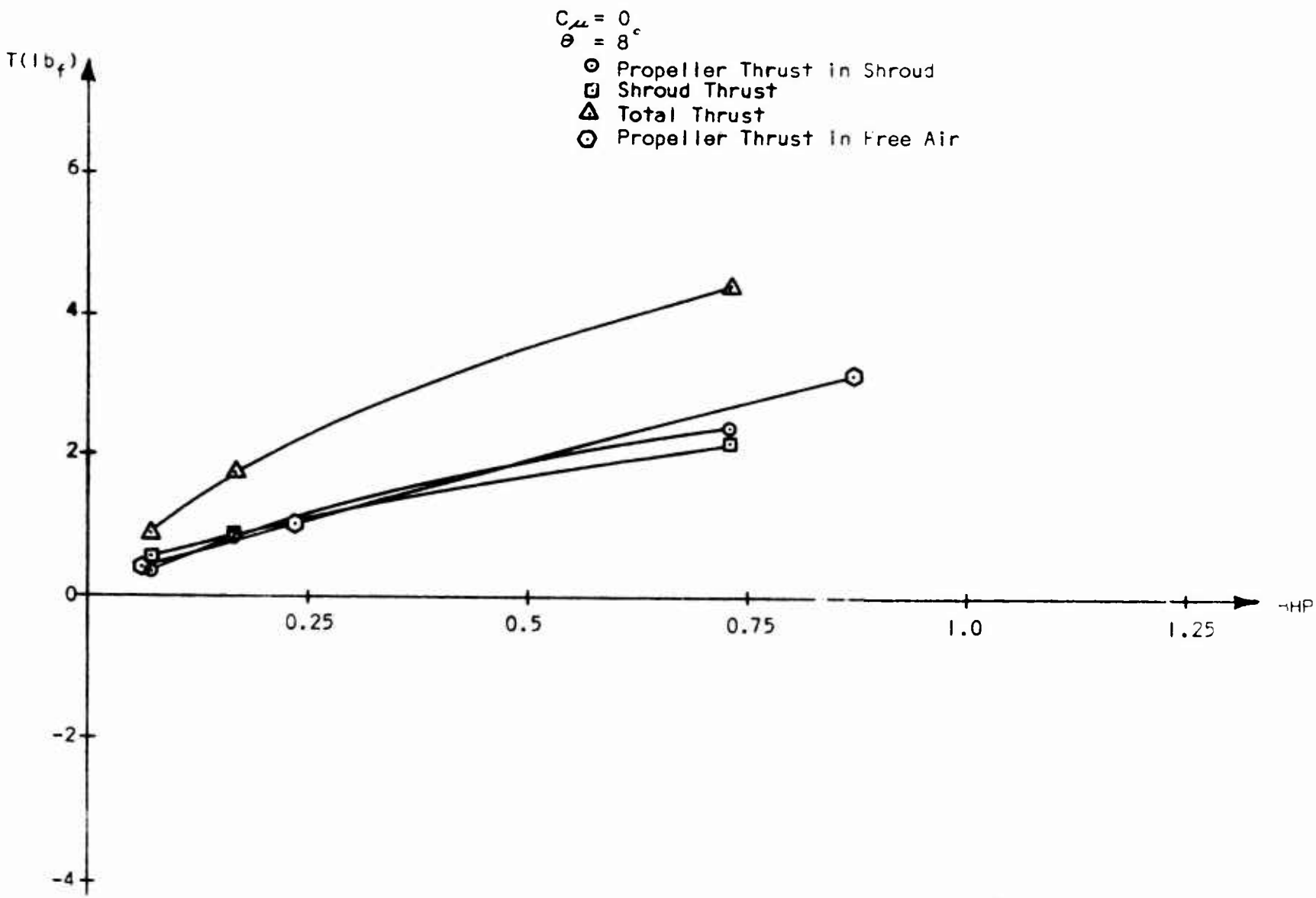

FIGURE 19. [illegible]st Versus Brake Horsepower

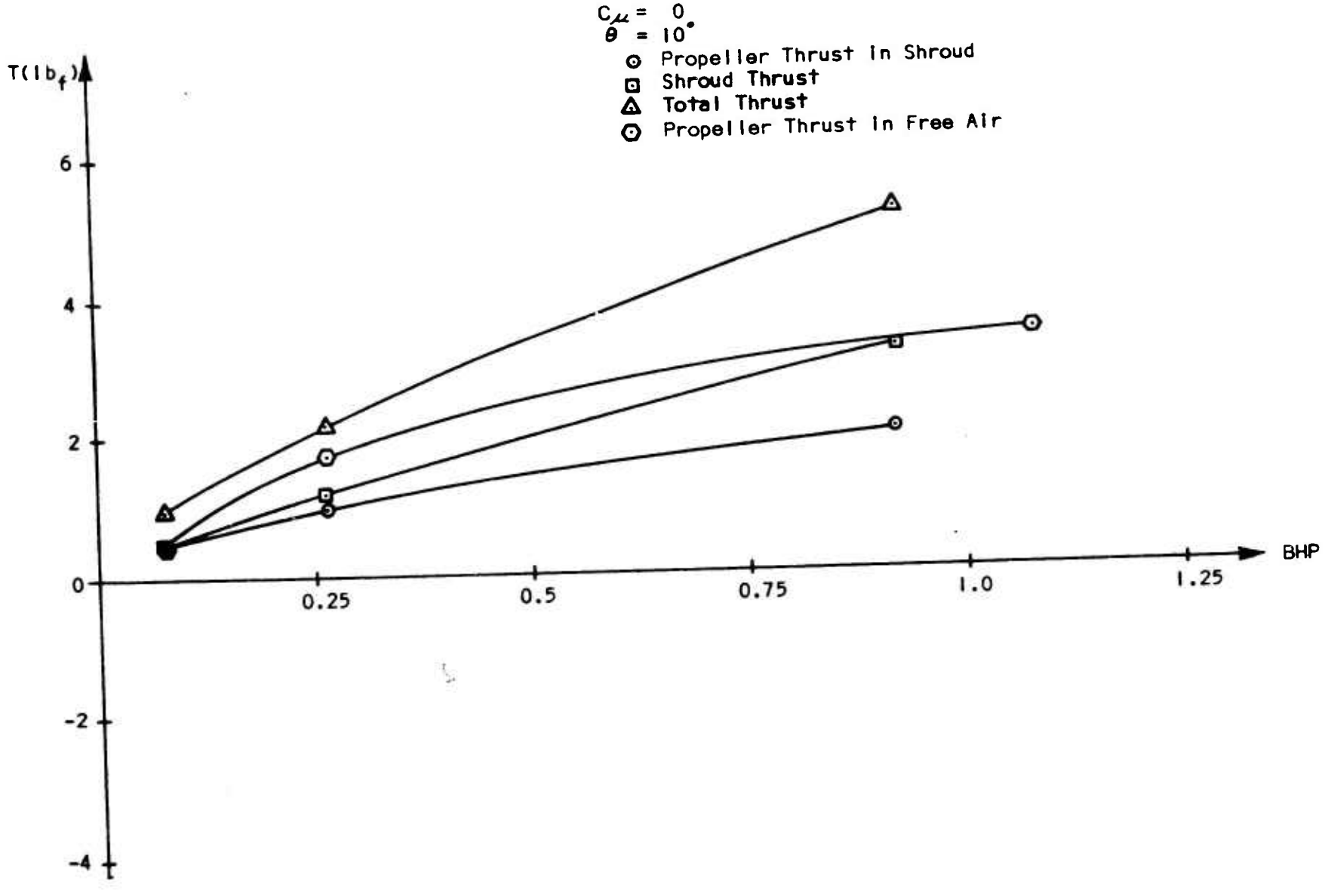

FIGURE 20. Thrust Versus Brake Horsepower

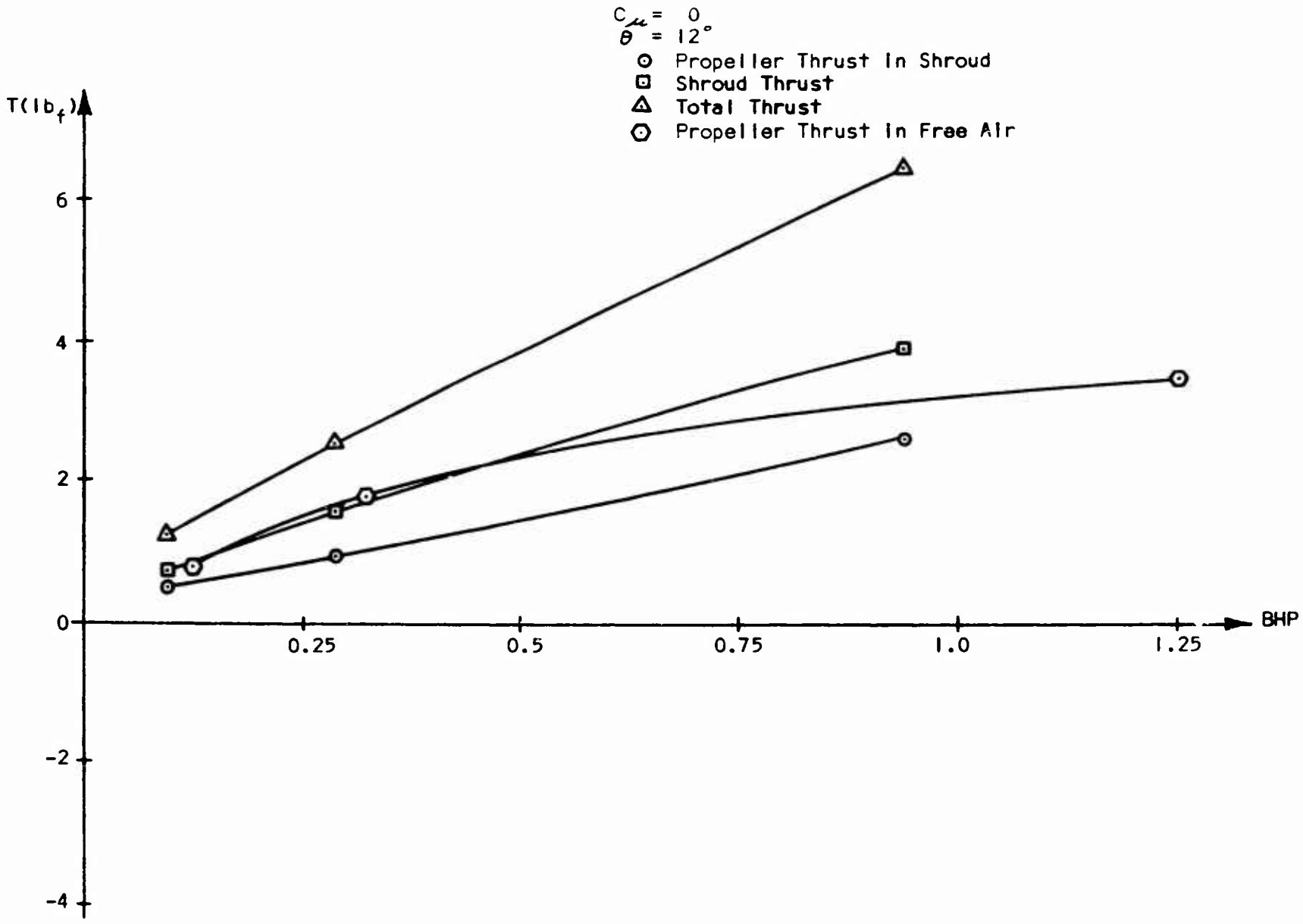

FIGURE 21. Thrust Versus Brake Horsepower

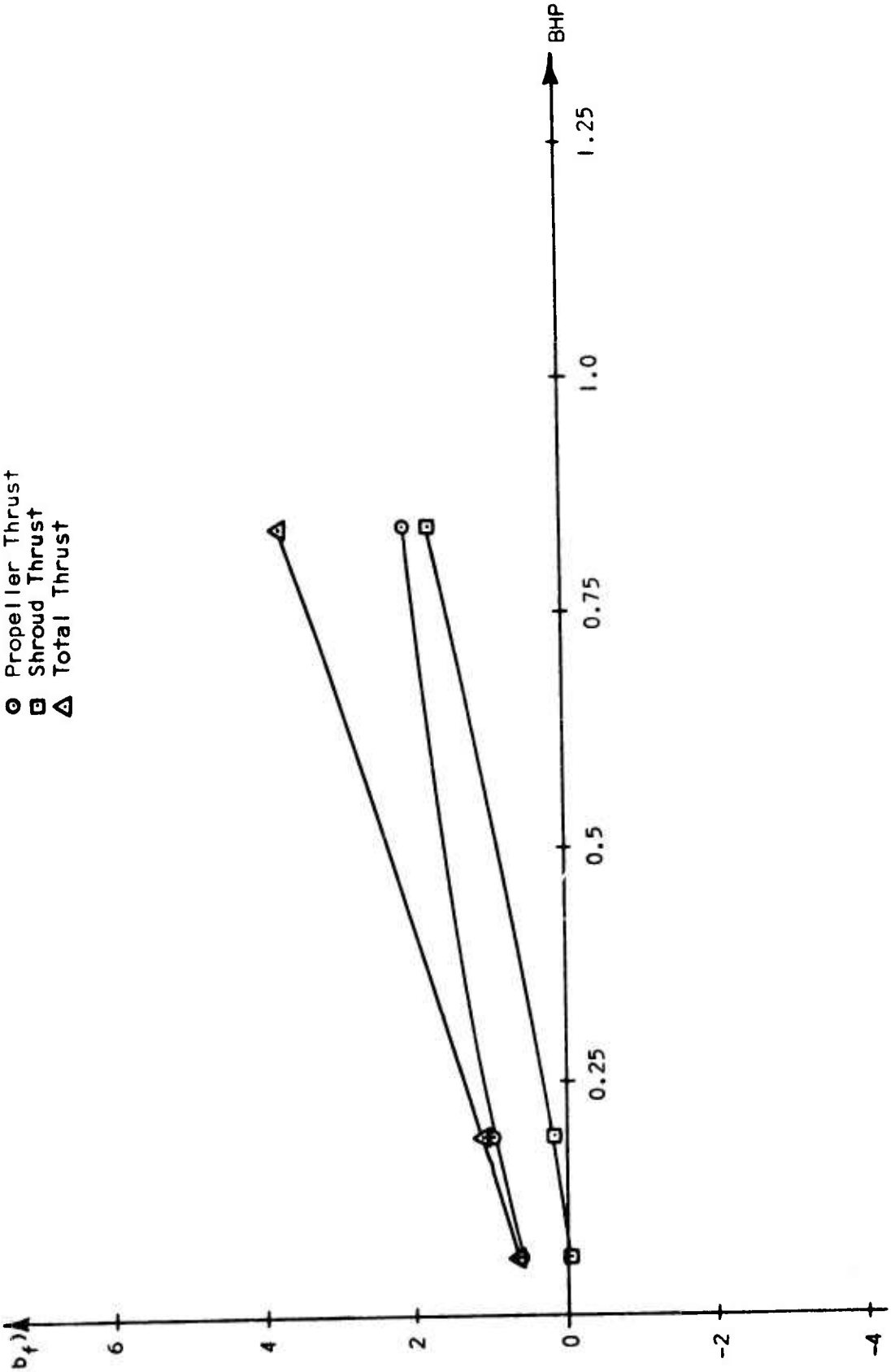

FIGURE 22. Thrust Versus Brake Horsepower

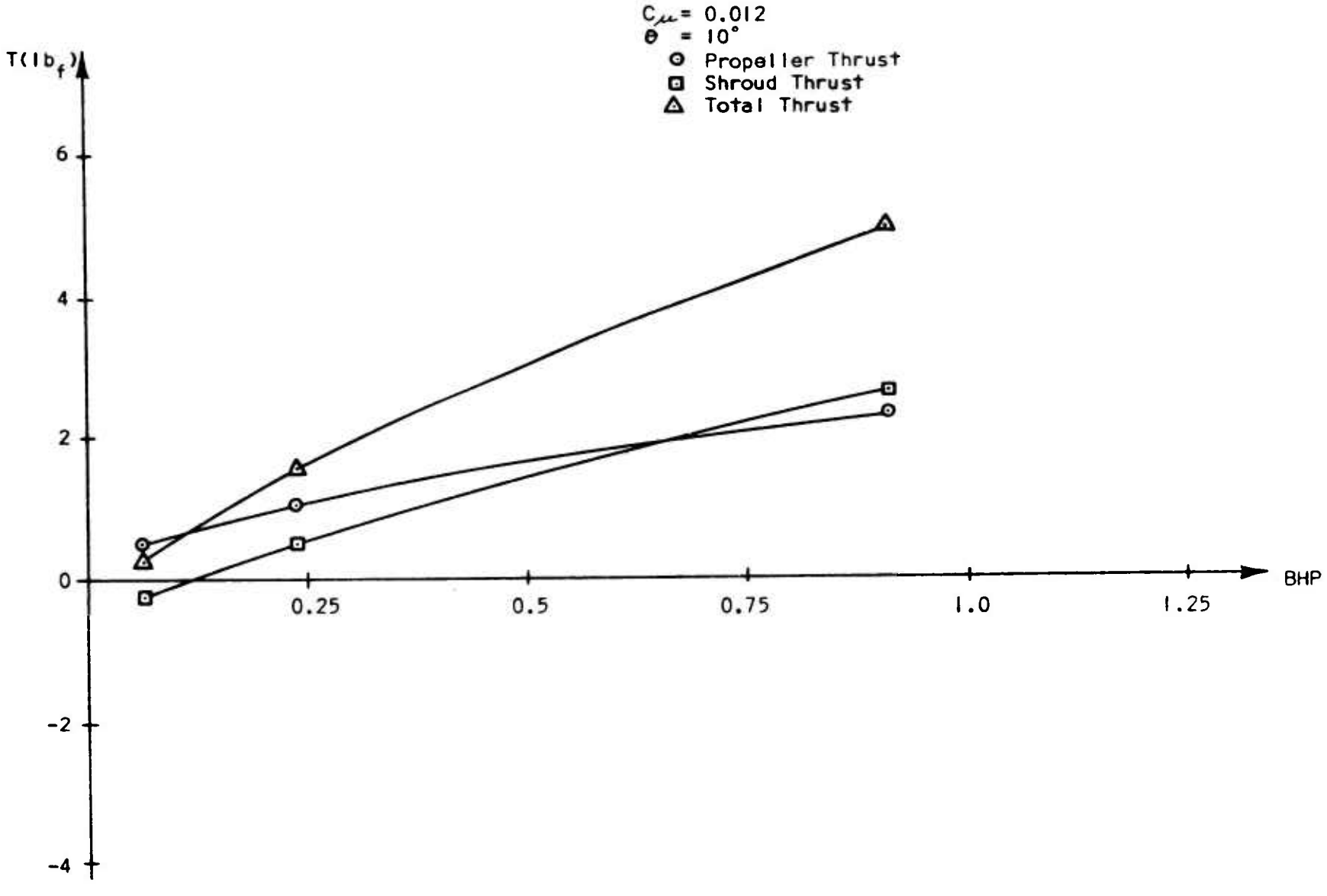

FIGURE 23. Thrust Versus Brake Horsepower

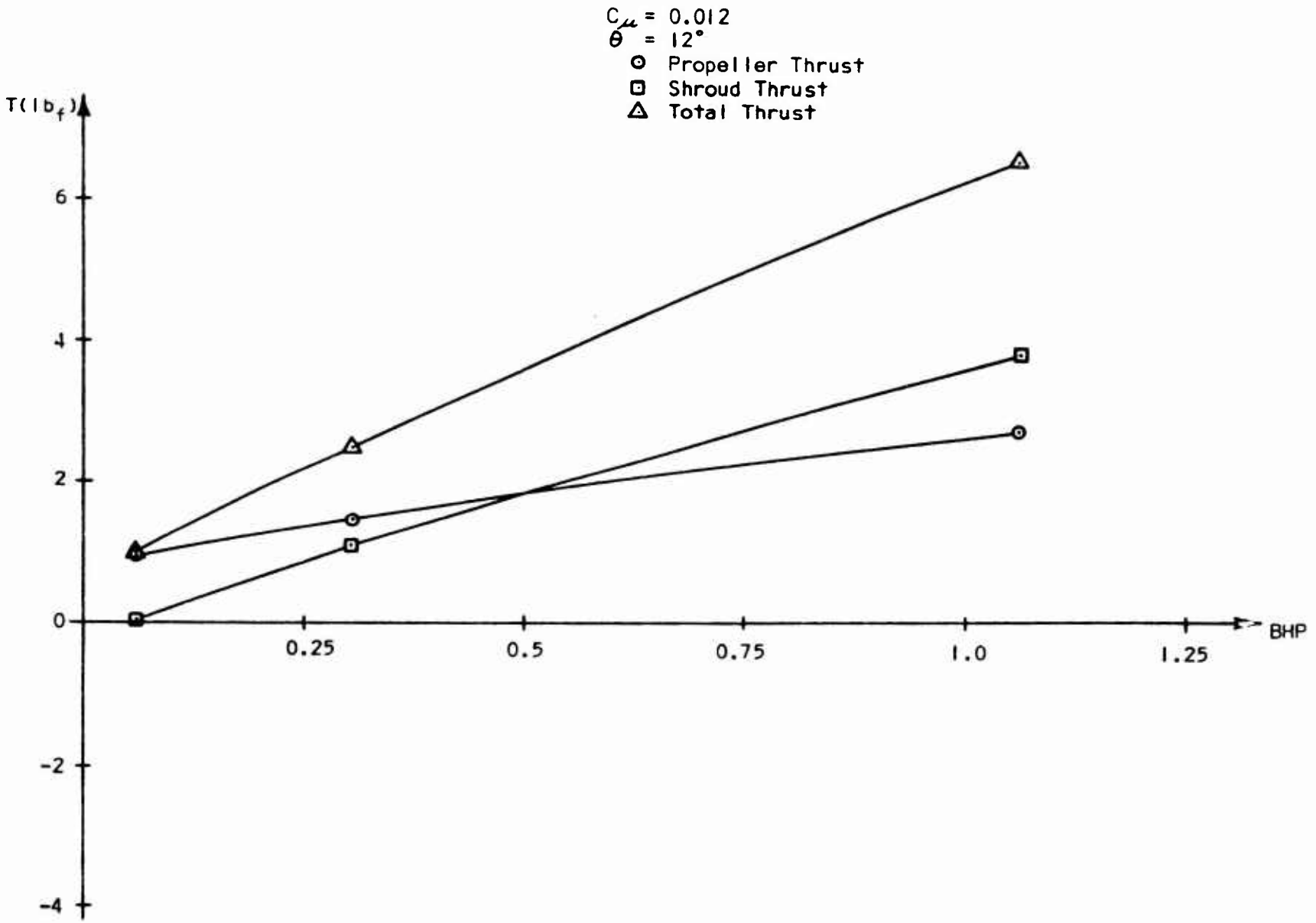

FIGURE 24. Thrust Versus Brake Horsepower

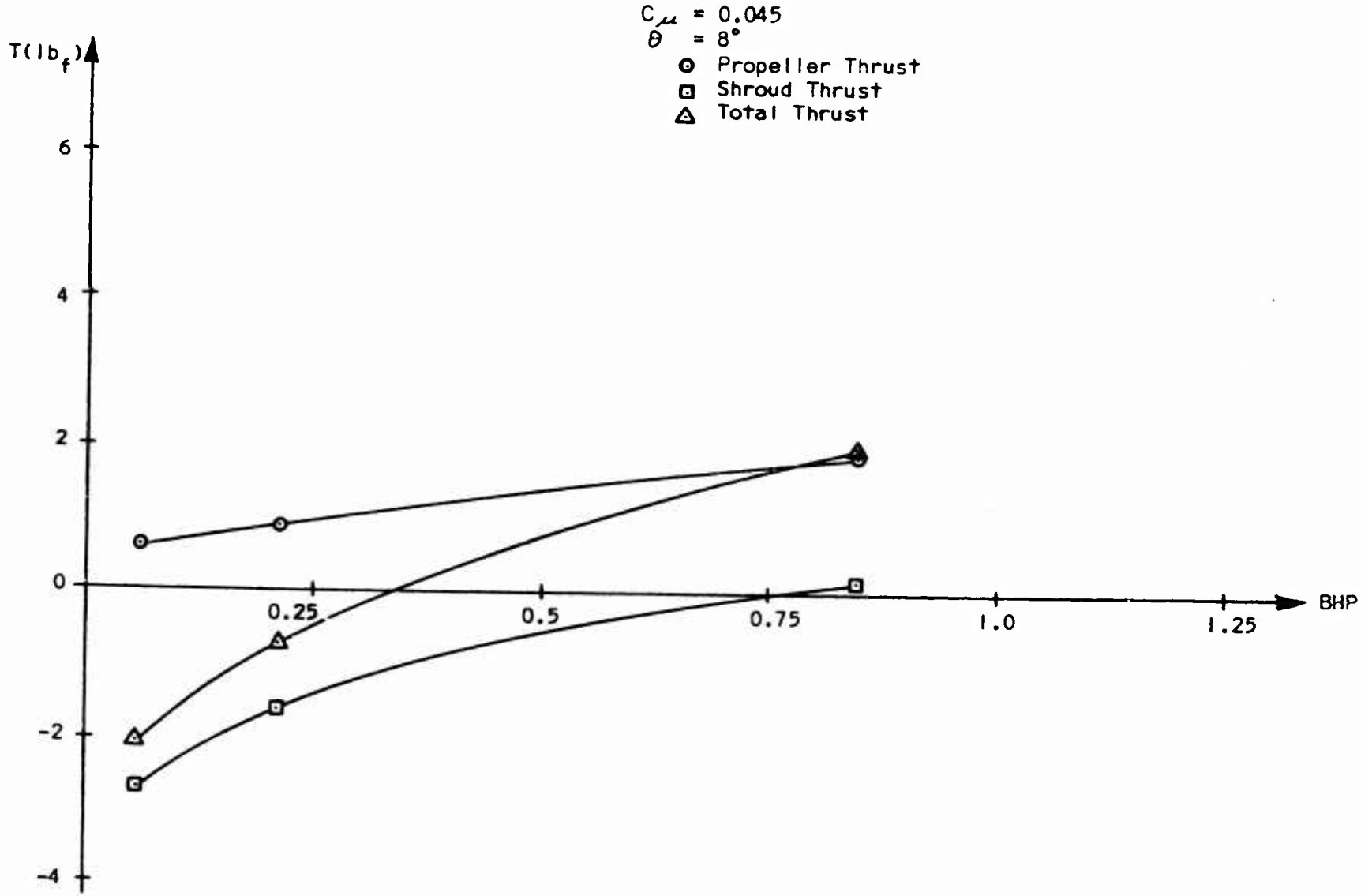

FIGURE 25. Thrust Versus Brake Horsepower

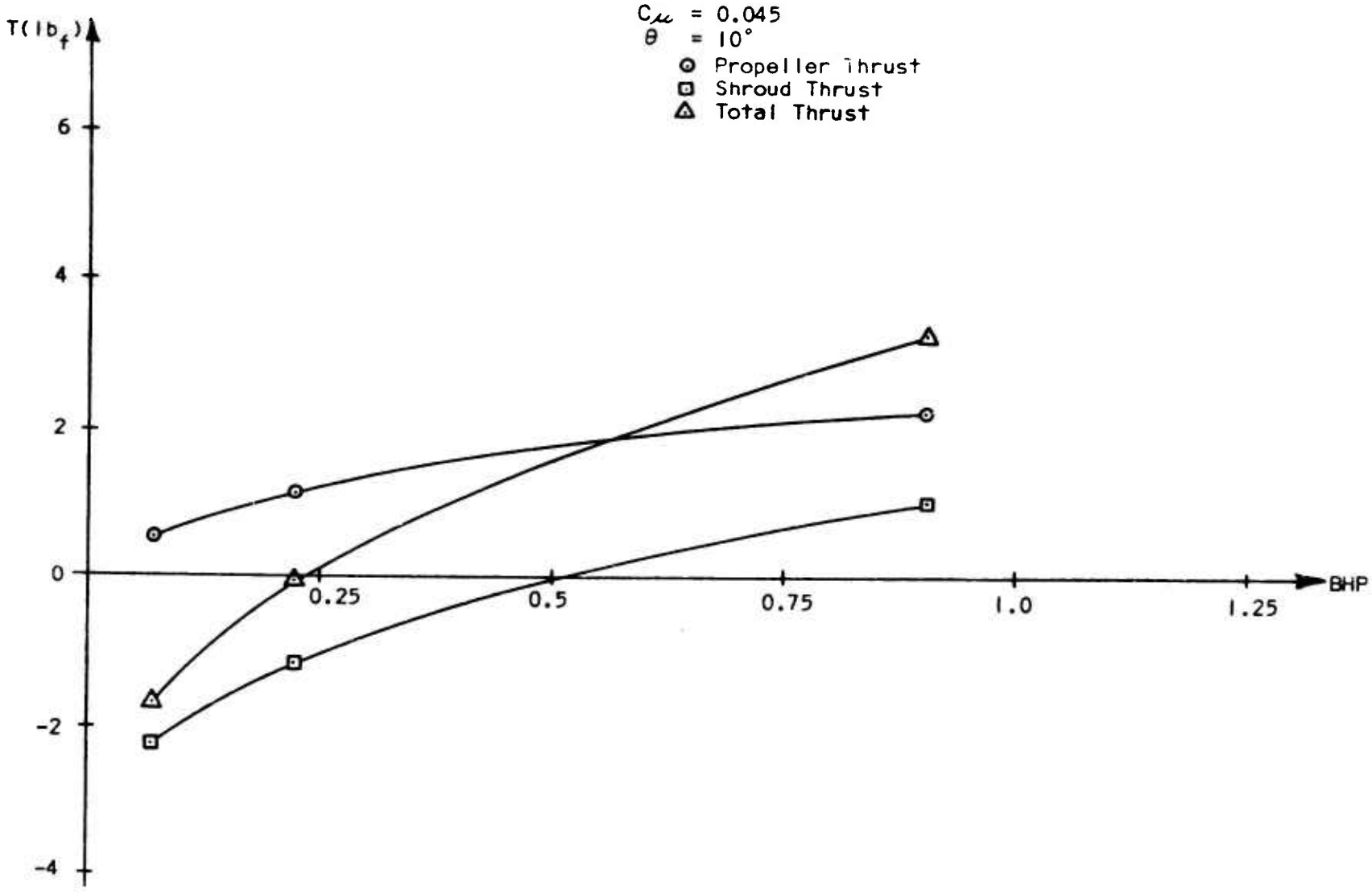

FIGURE 26. Thrust Versus Brake Horsepower

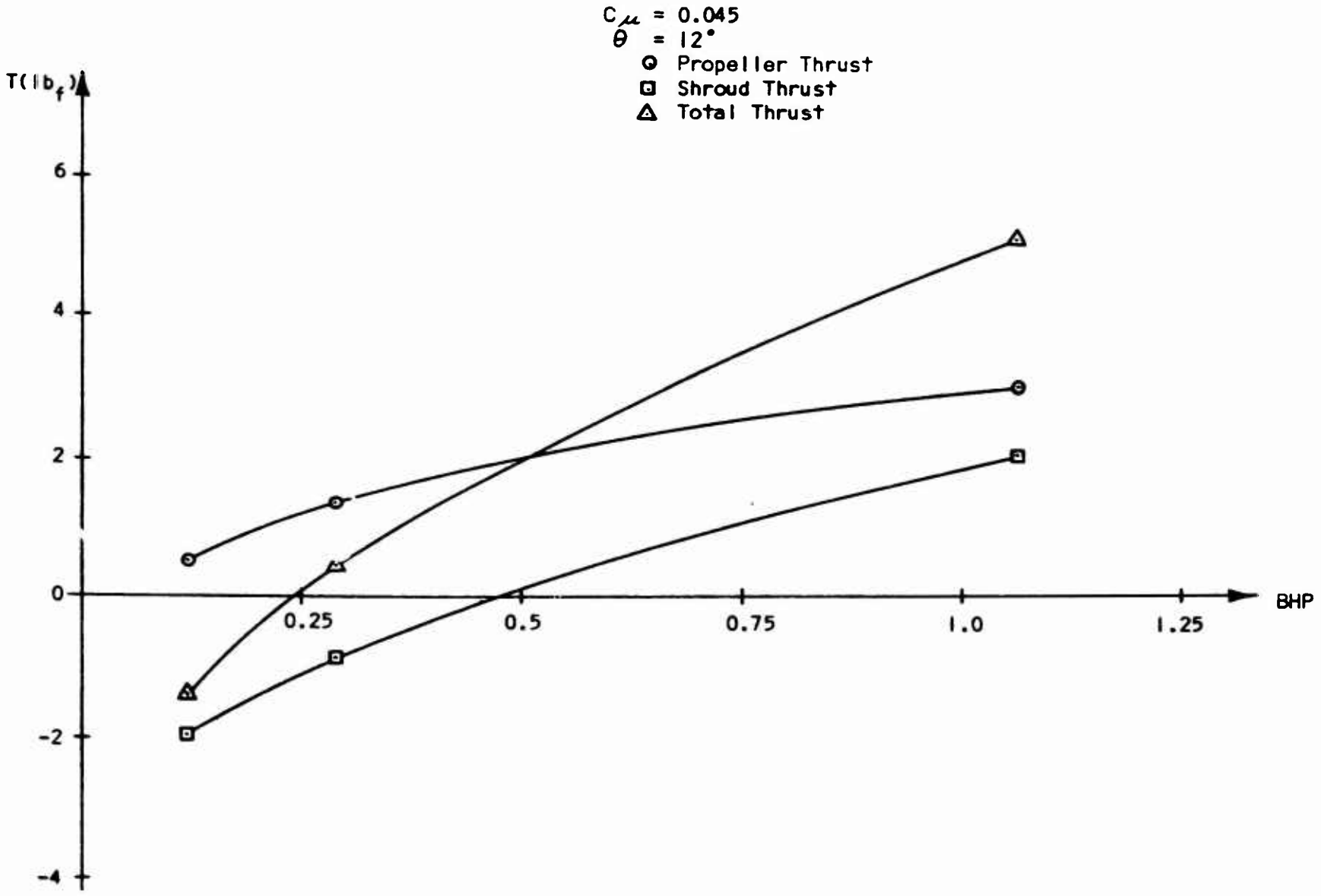

FIGURE 27. Thrust Versus Brake Horsepower

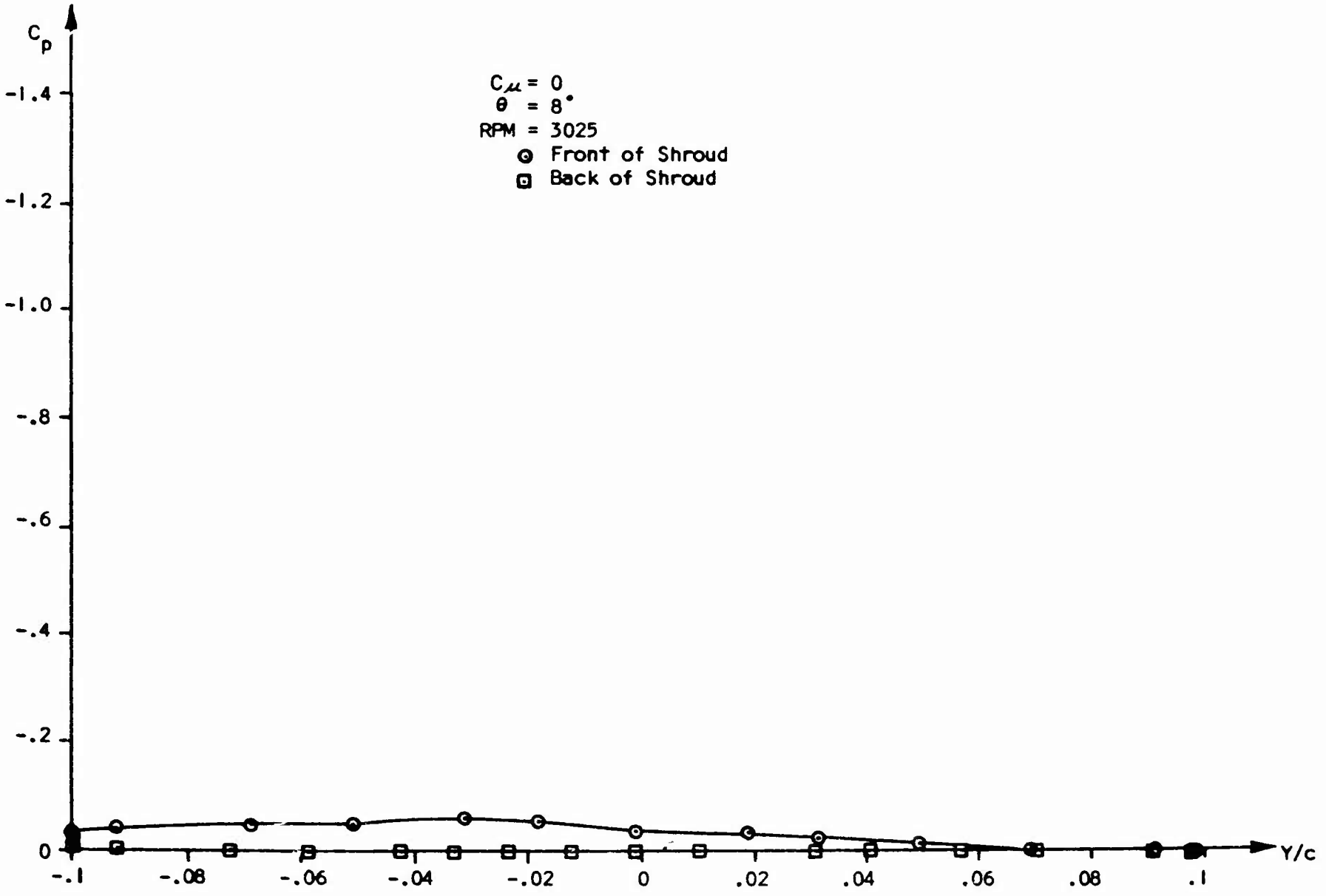

FIGURE 28. Pressure Coefficient Versus Vertical Ordinate

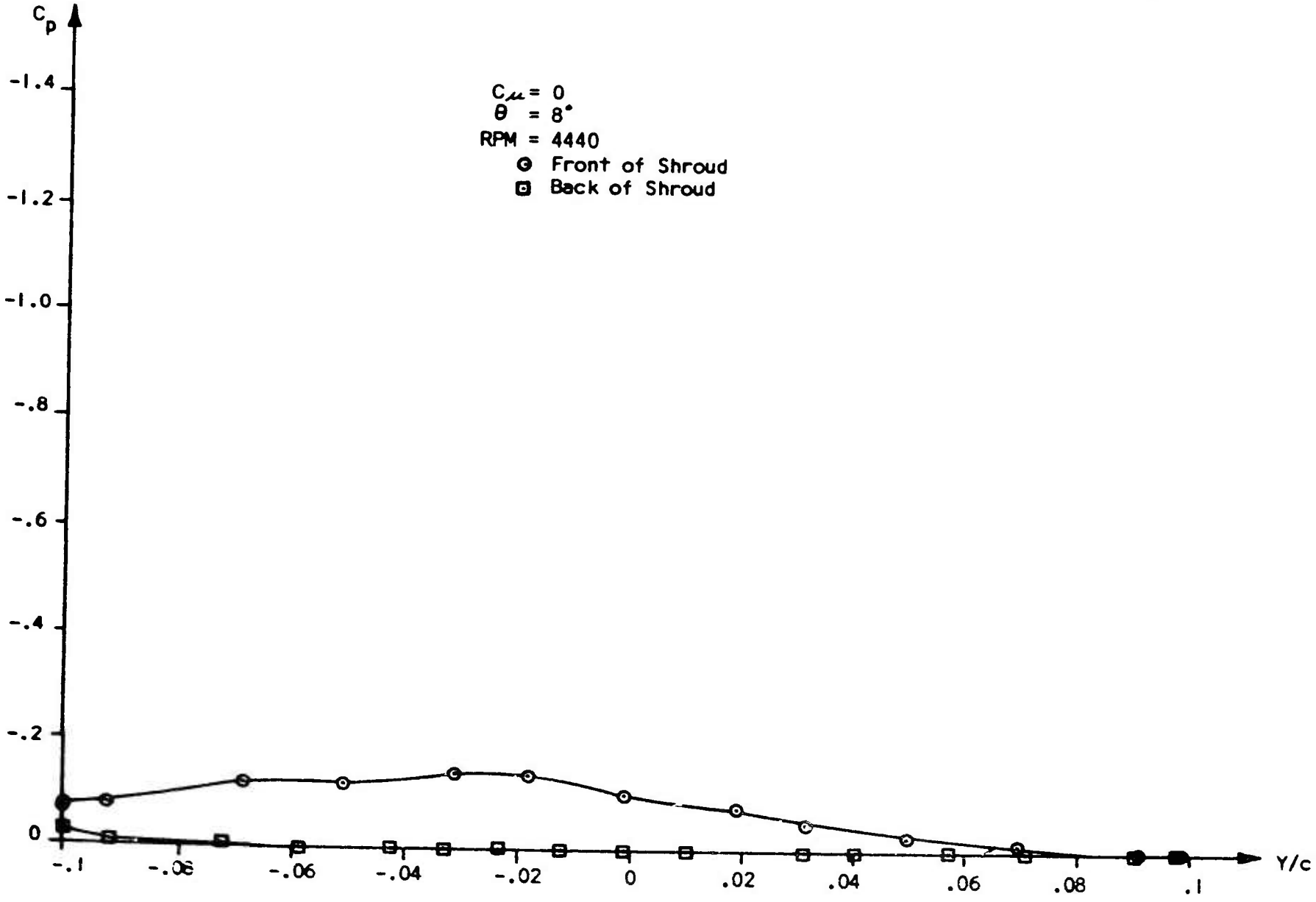

FIGURE 29. Pressure Coefficient Versus Vertical Ordinate

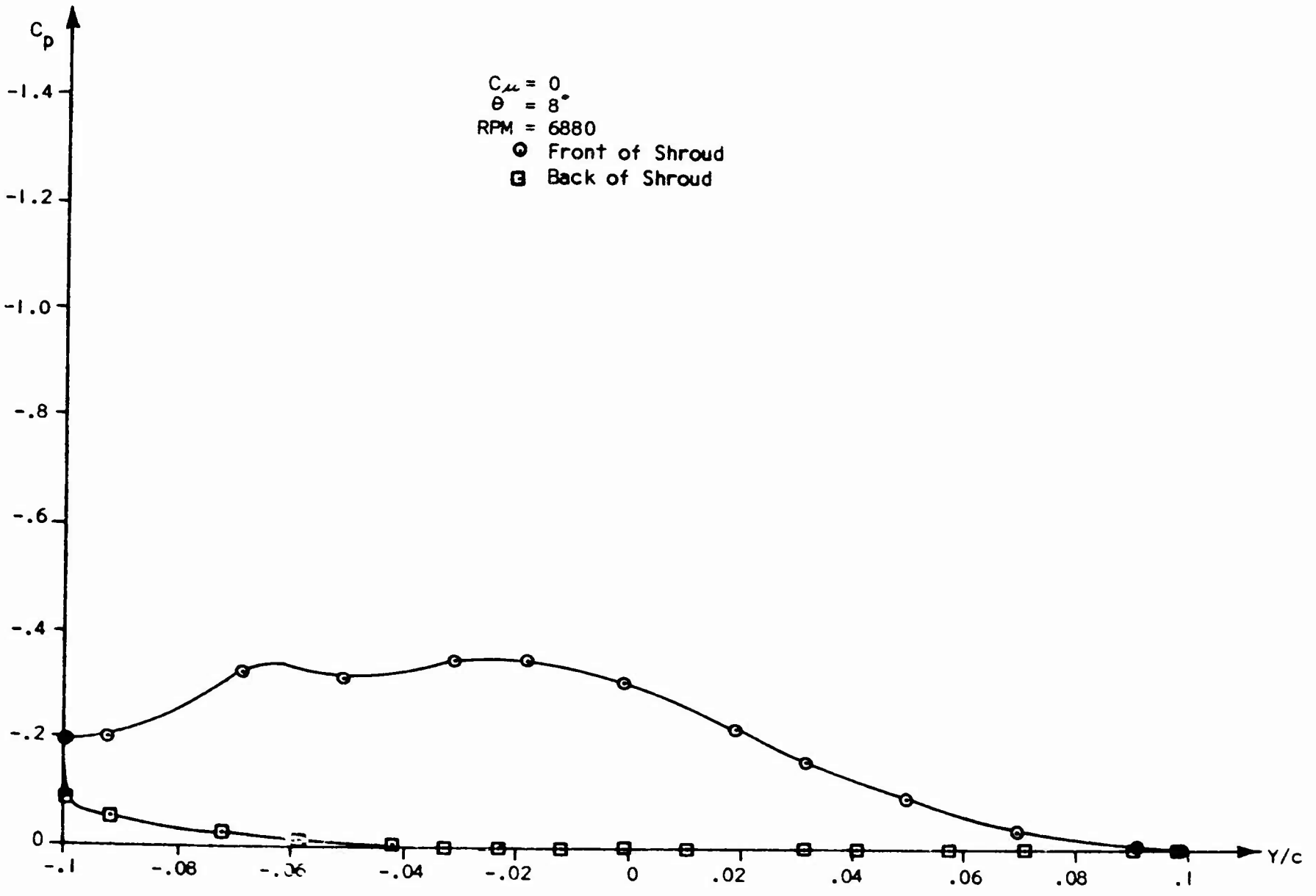

FIGURE 30. Pressure Coefficient Versus Vertical Ordinate

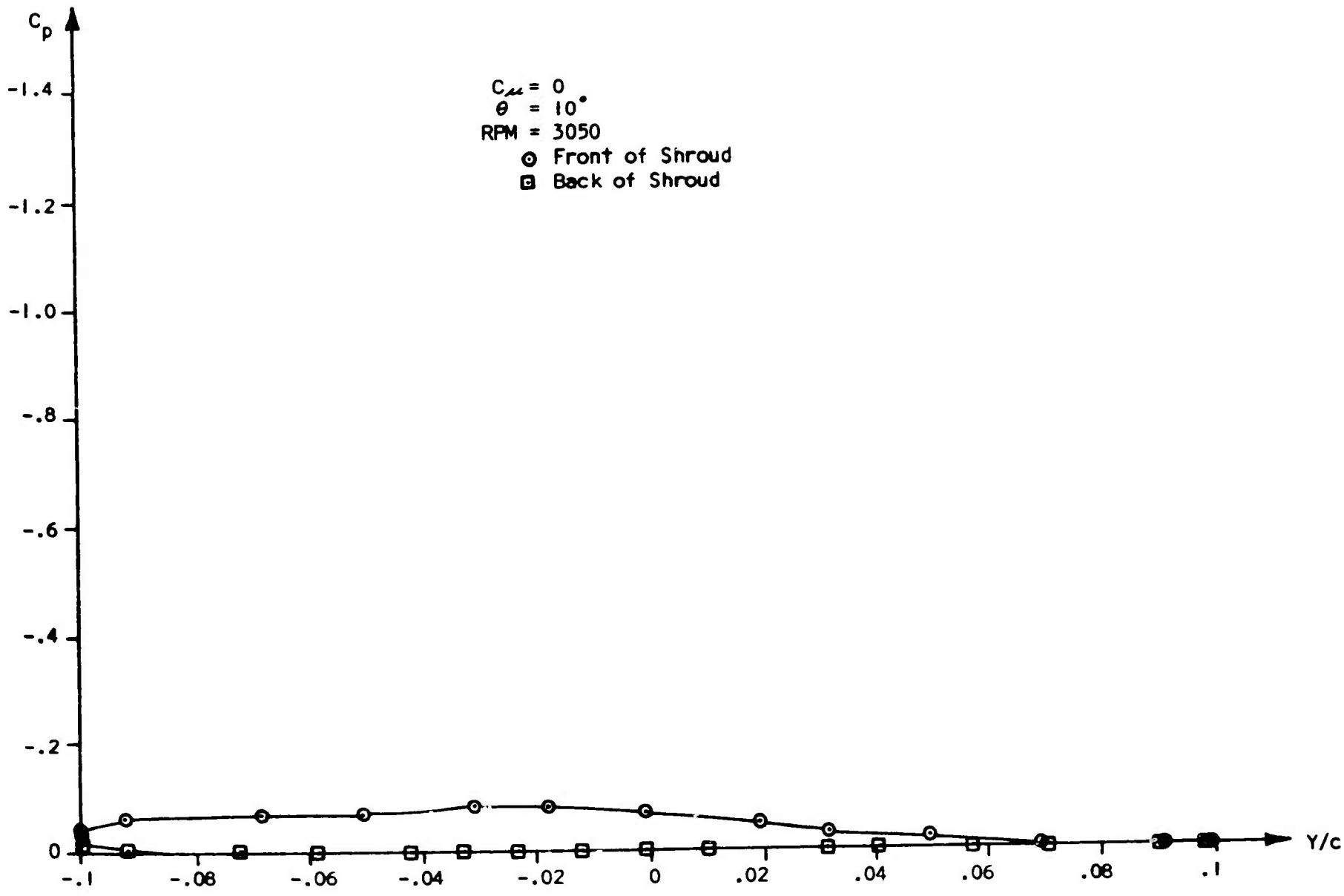

FIGURE 31. Pressure Coefficient Versus Vertical Ordinate

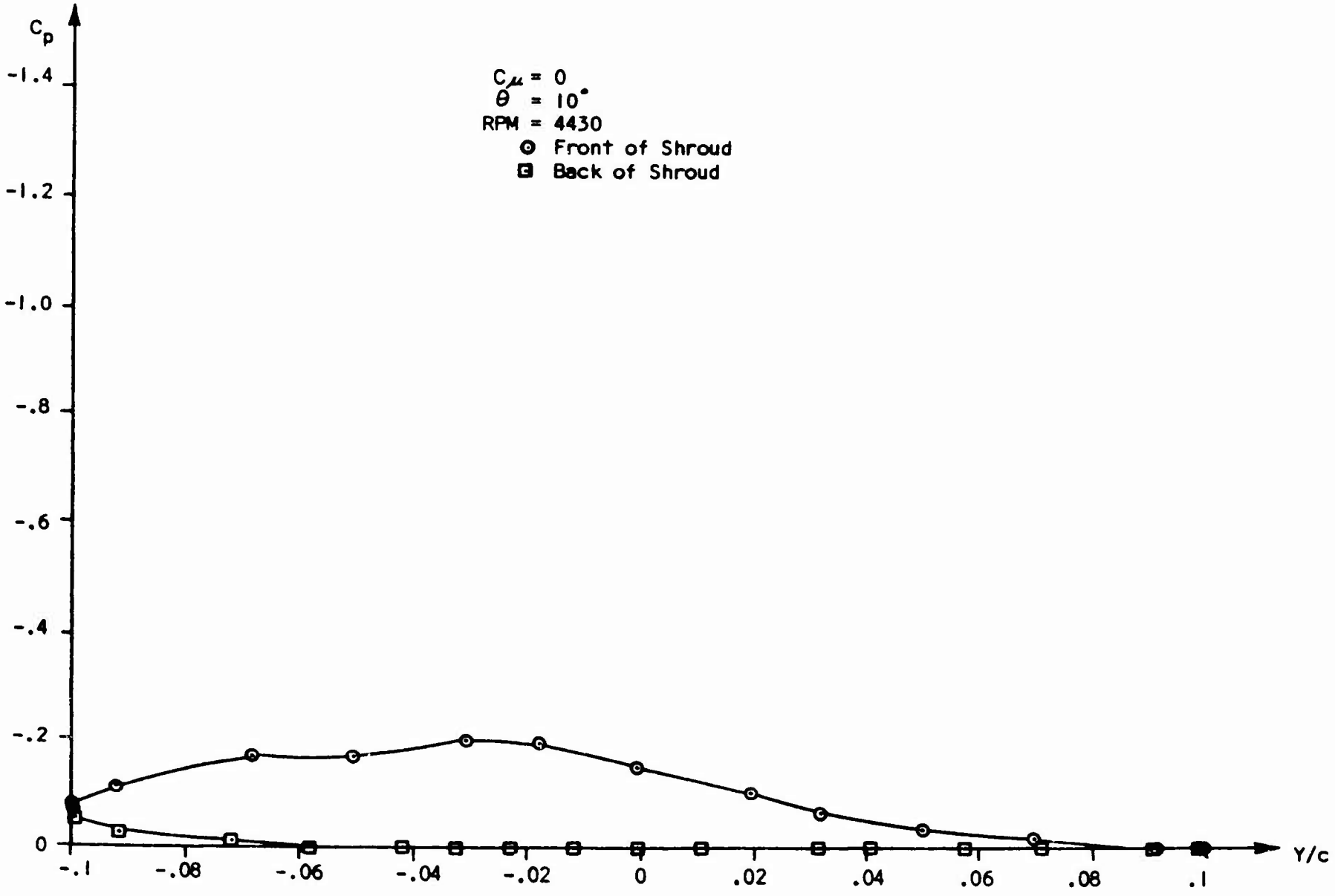

FIGURE 32. Pressure Coefficient Versus Vertical Ordinate

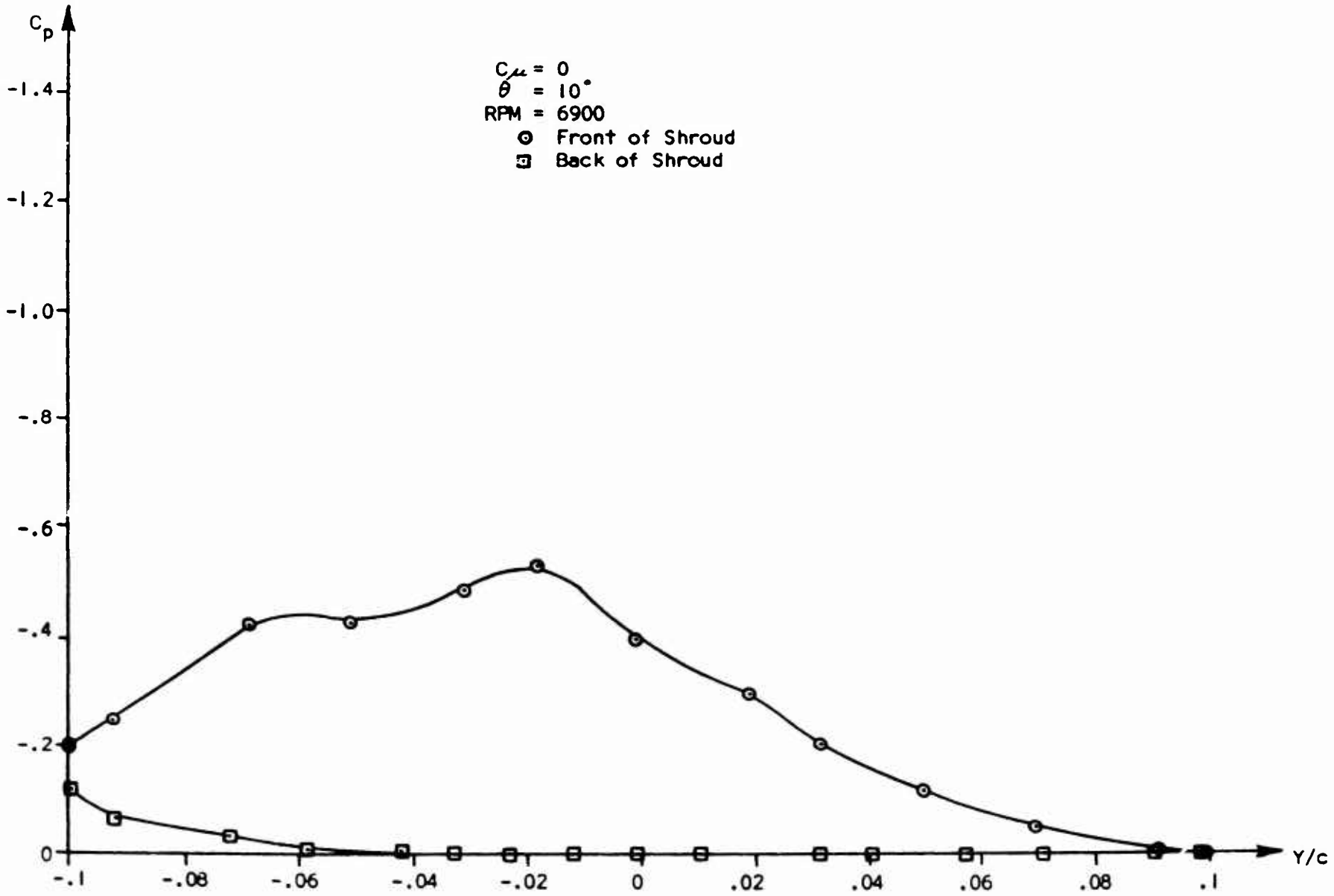

FIGURE 33. Pressure Coefficient Versus Vertical Ordinate

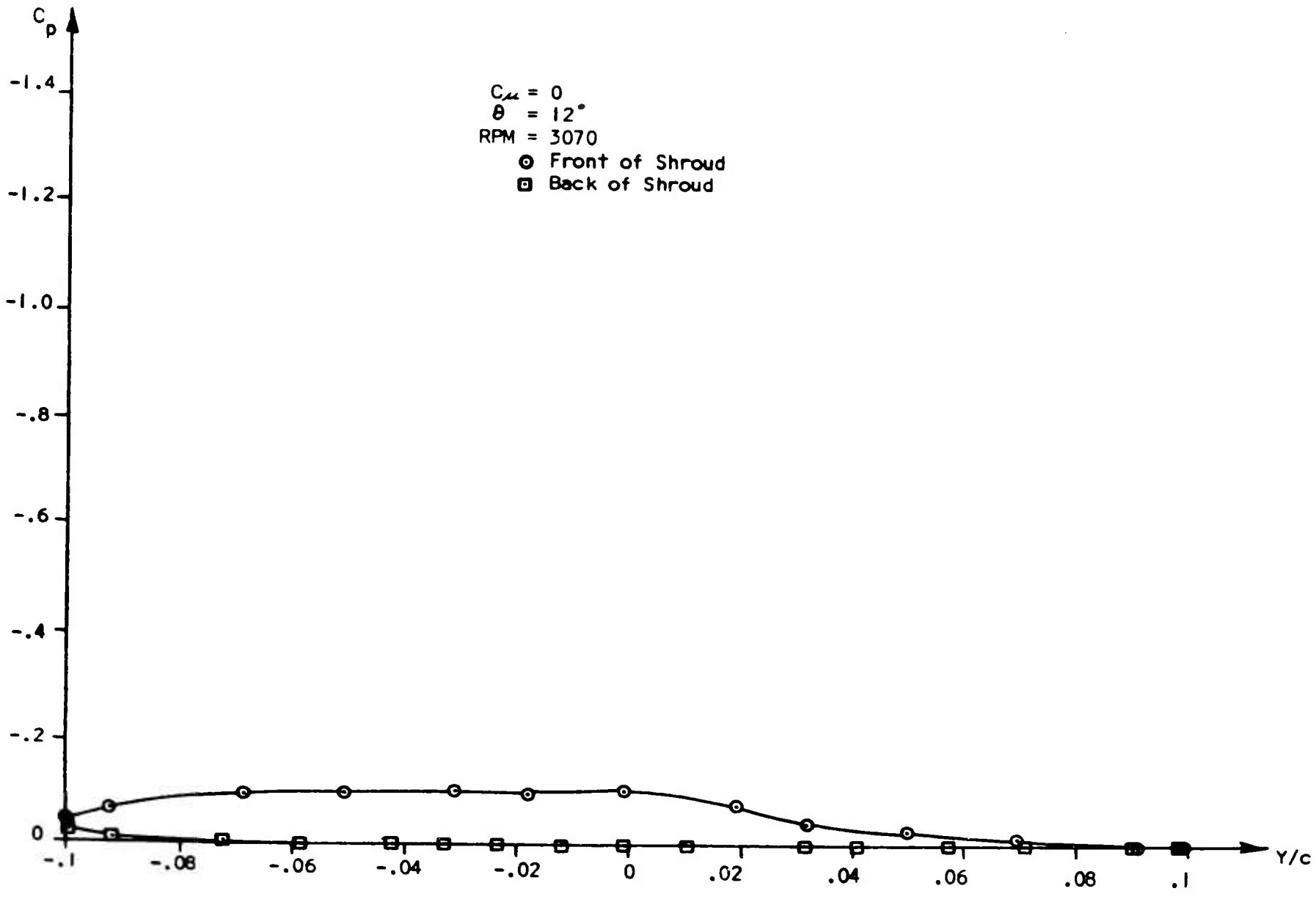

FIGURE 34. Pressure Coefficient Versus Vertical Ordinate

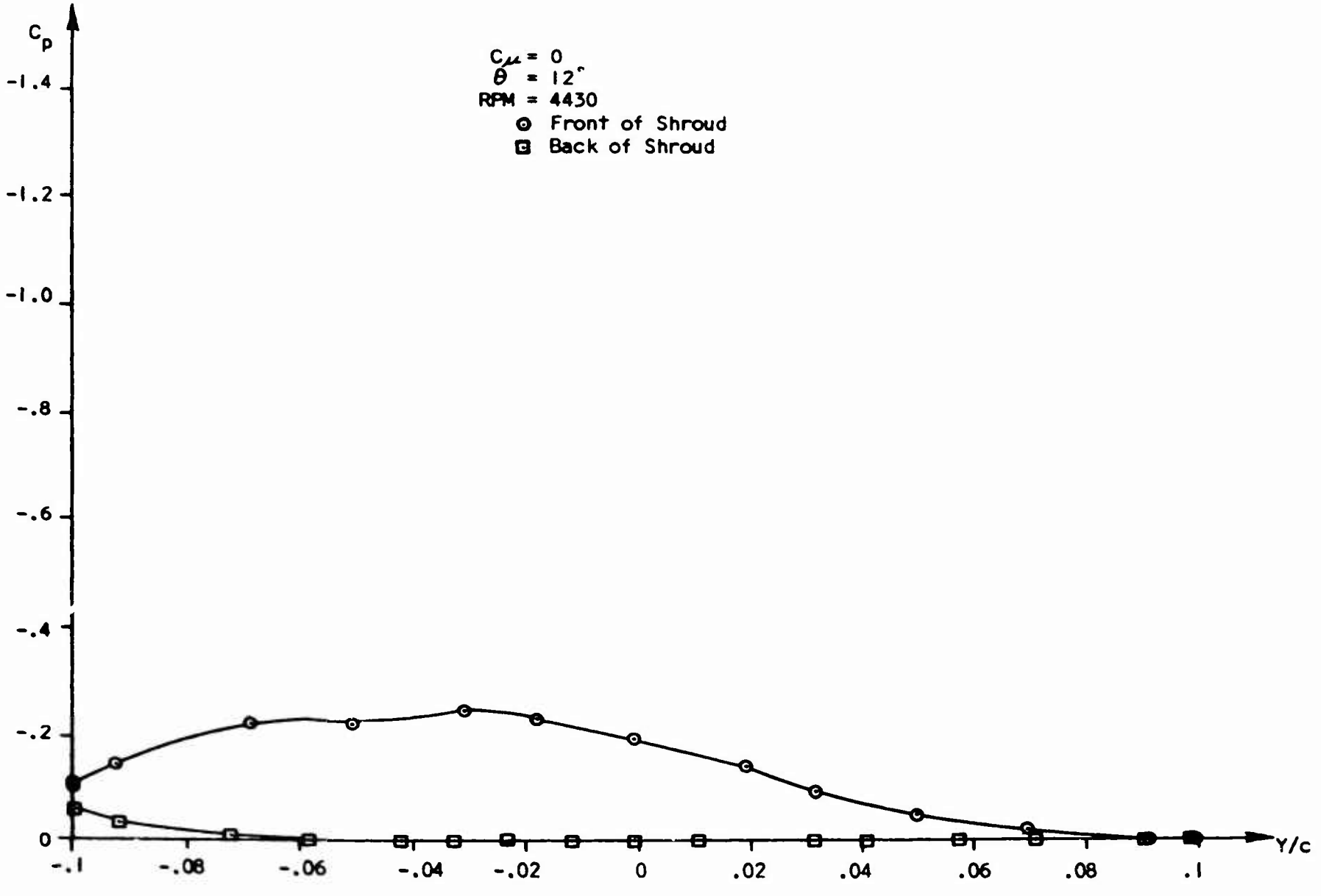

FIGURE 35. Pressure Coefficient Versus Vertical Ordinate

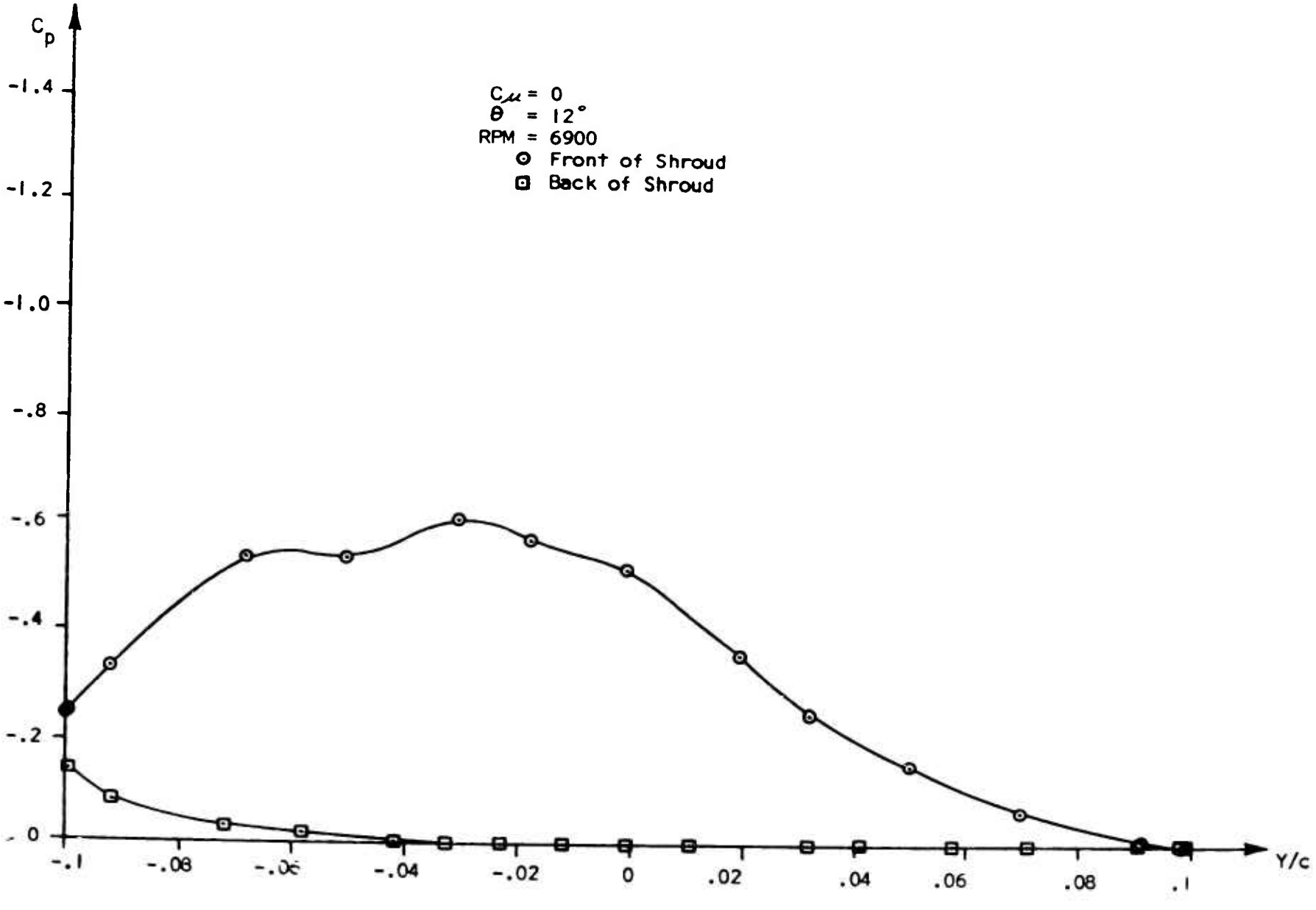

FIGURE 36. Pressure Coefficient Versus Vertical Ordinate

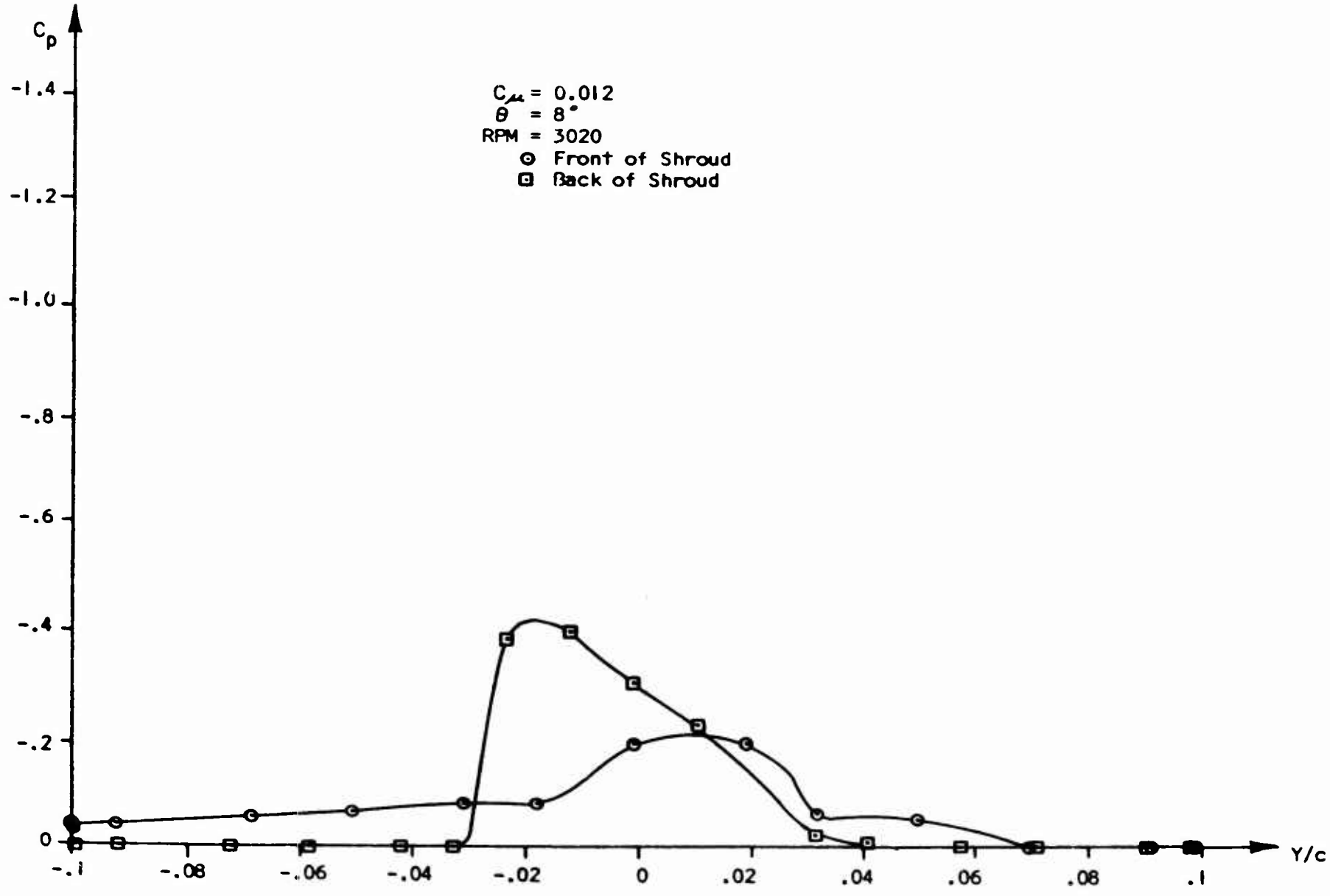

FIGURE 37. Pressure Coefficient Versus Vertical Ordinate

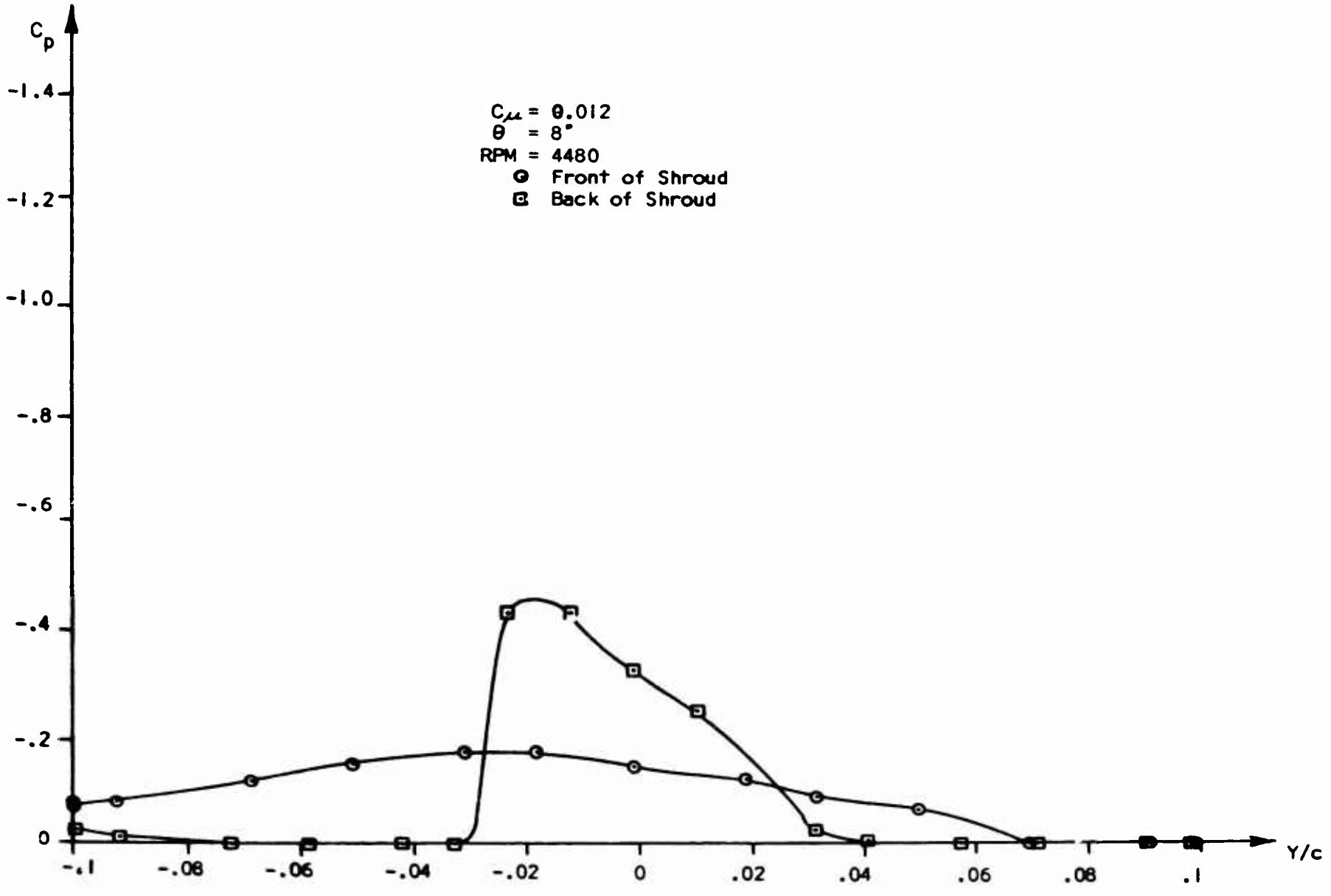

FIGURE 38. Pressure Coefficient Versus Vertical Ordinate

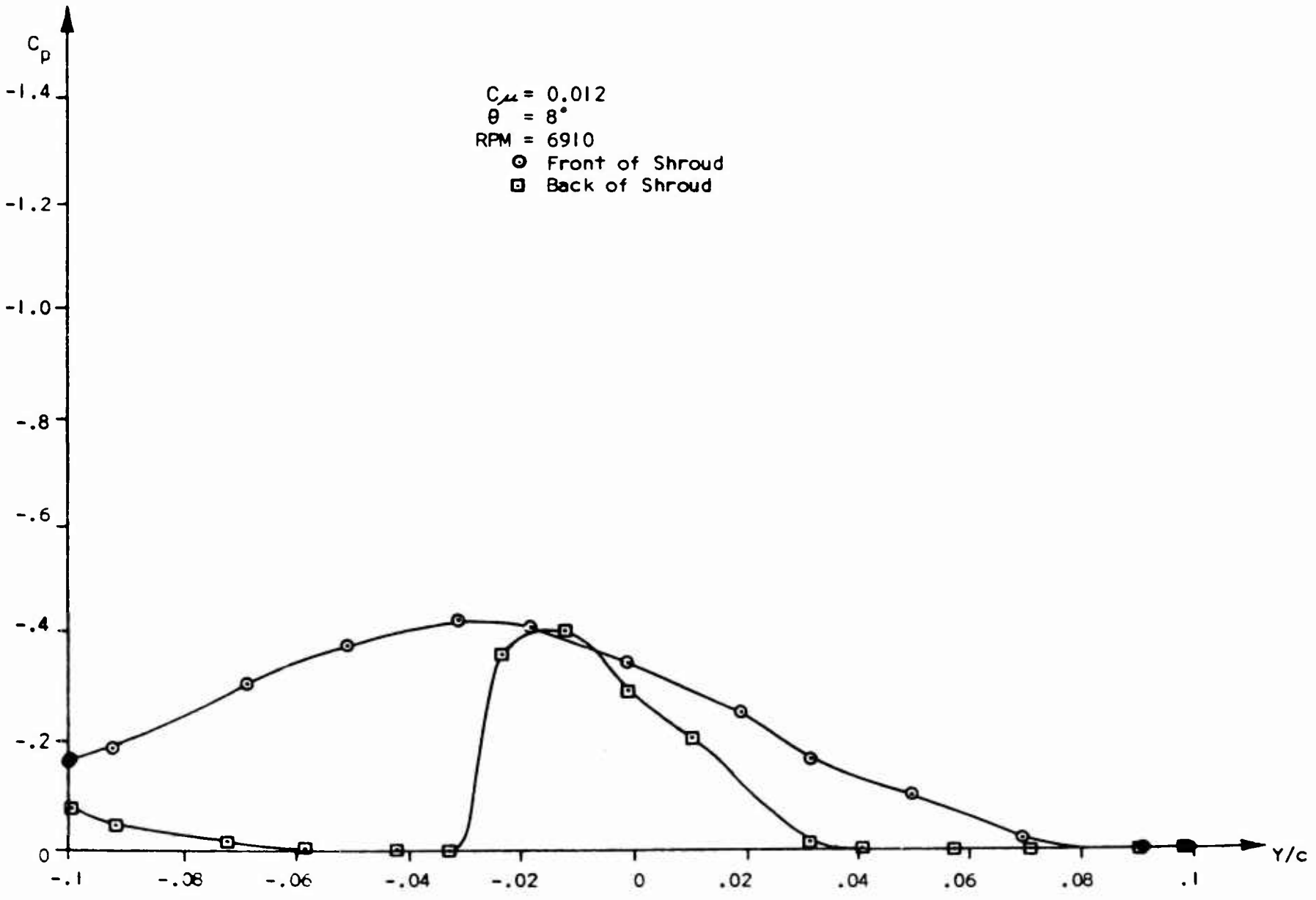

FIGURE 39. Pressure Coefficient Versus Vertical Ordinate

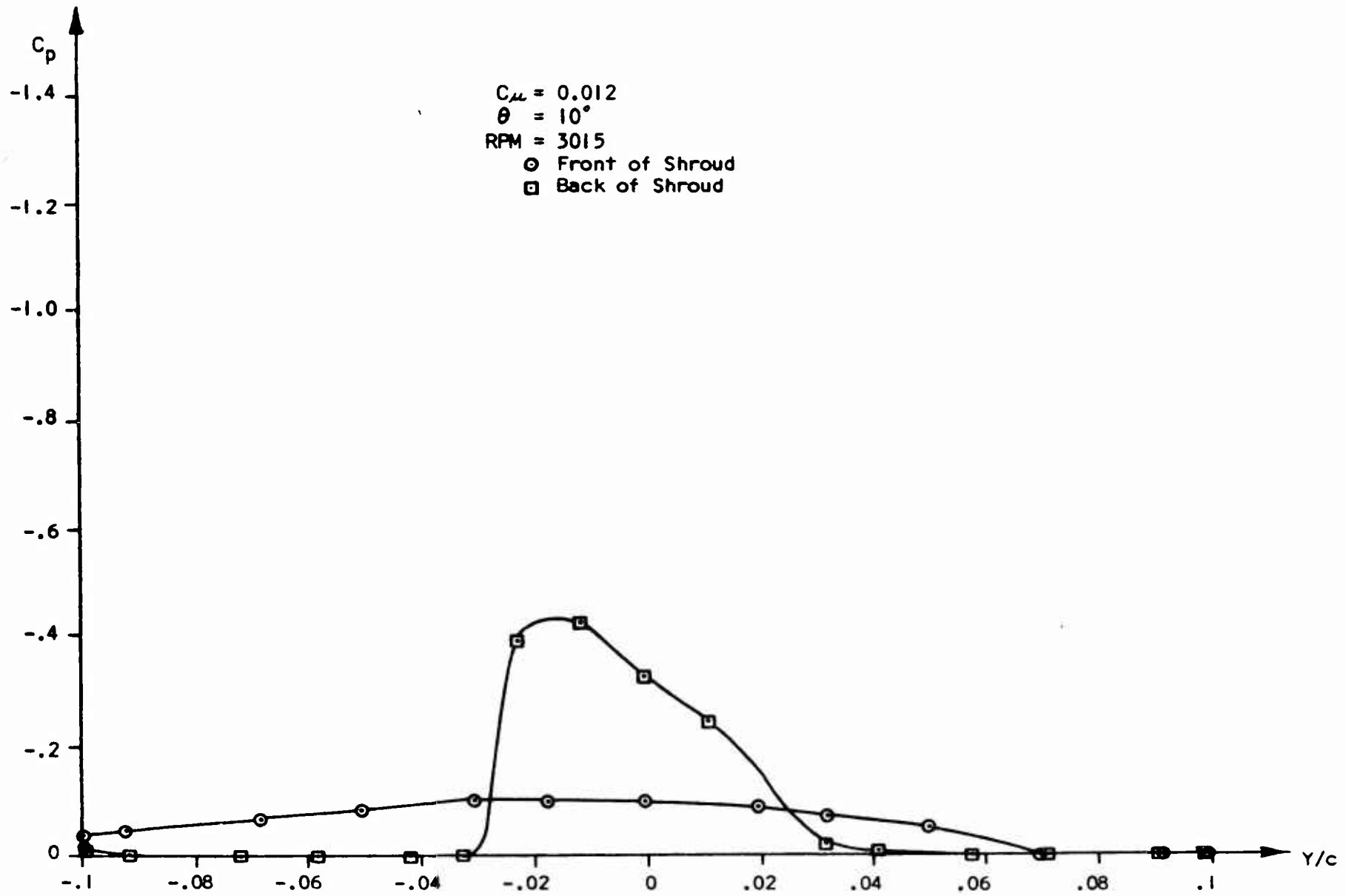

FIGURE 40. Pressure Coefficient Versus Vertical Ordinate

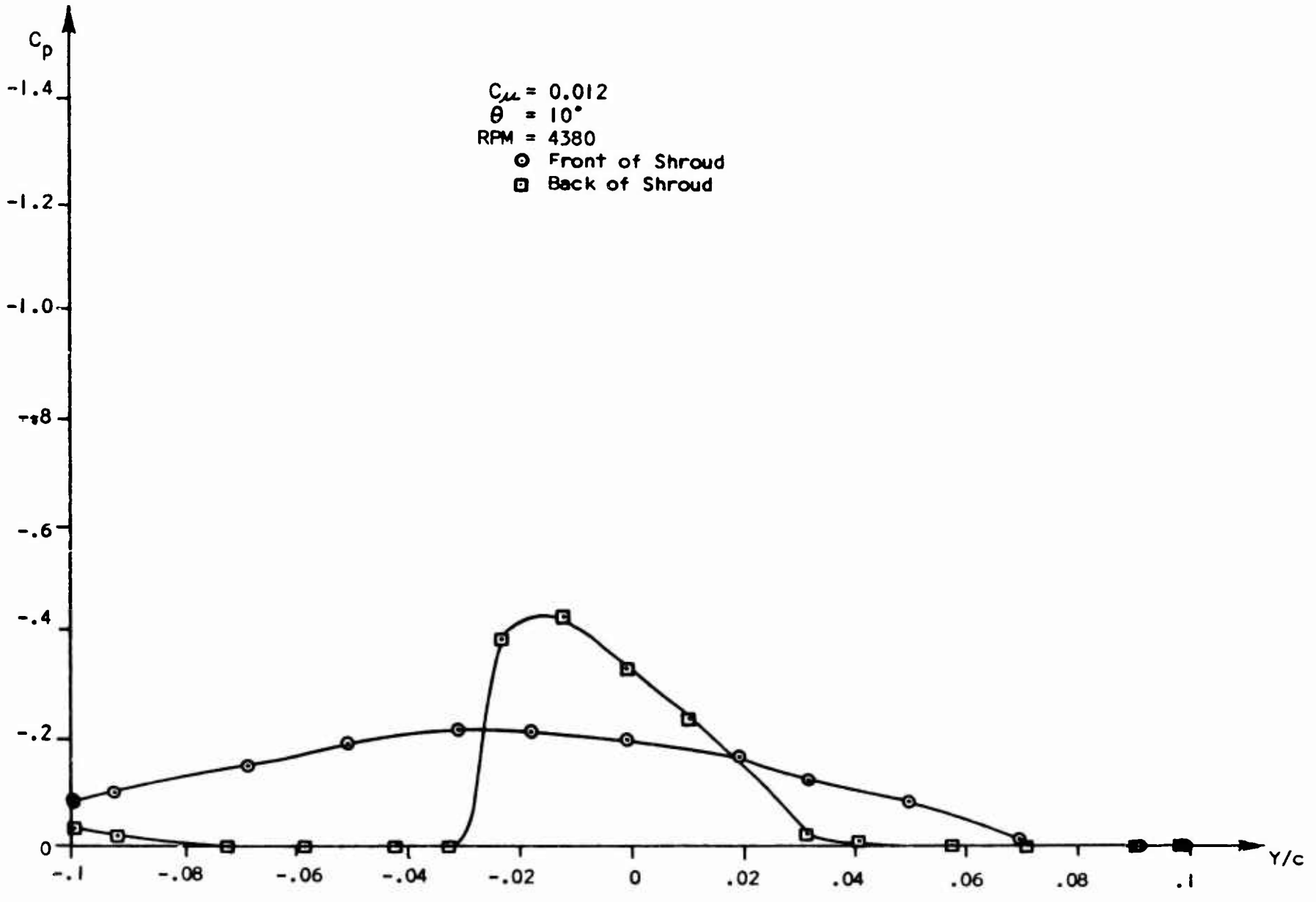

FIGURE 41. Pressure Coefficient Versus Vertical Ordinate

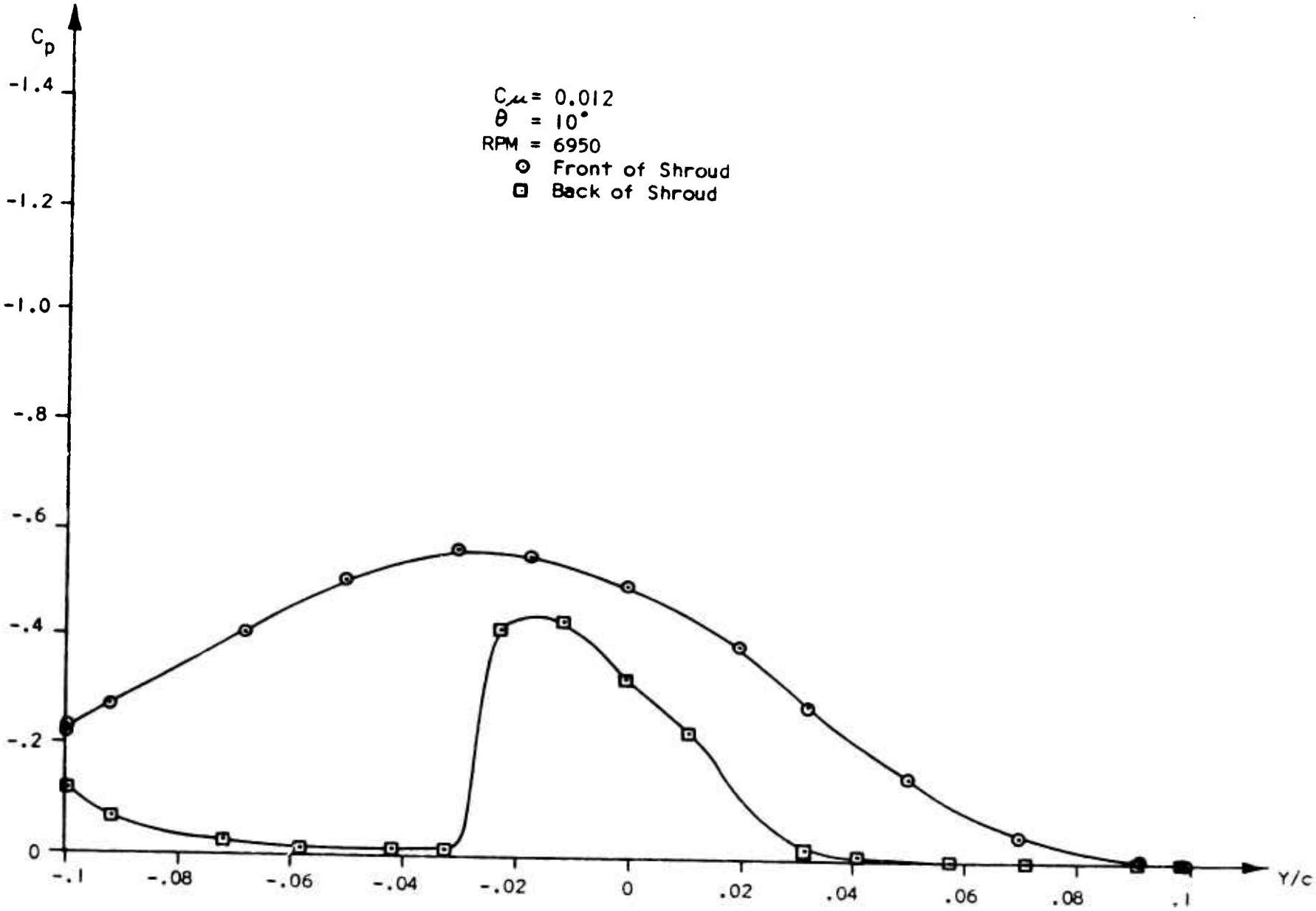

FIGURE 42. Pressure Coefficient Versus Vertical Ordinate

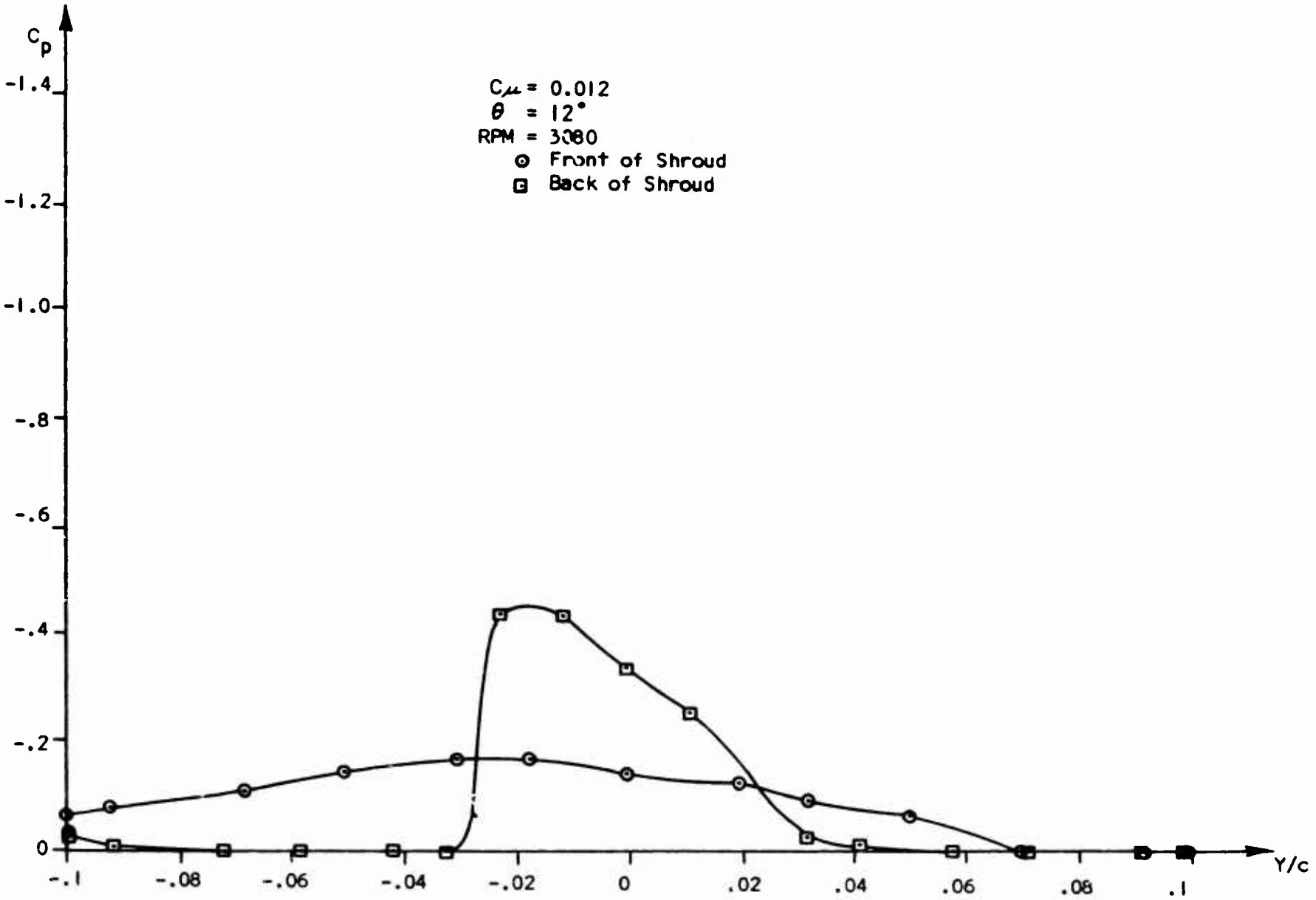

FIGURE 43. Pressure Coefficient Versus Vertical Ordinate

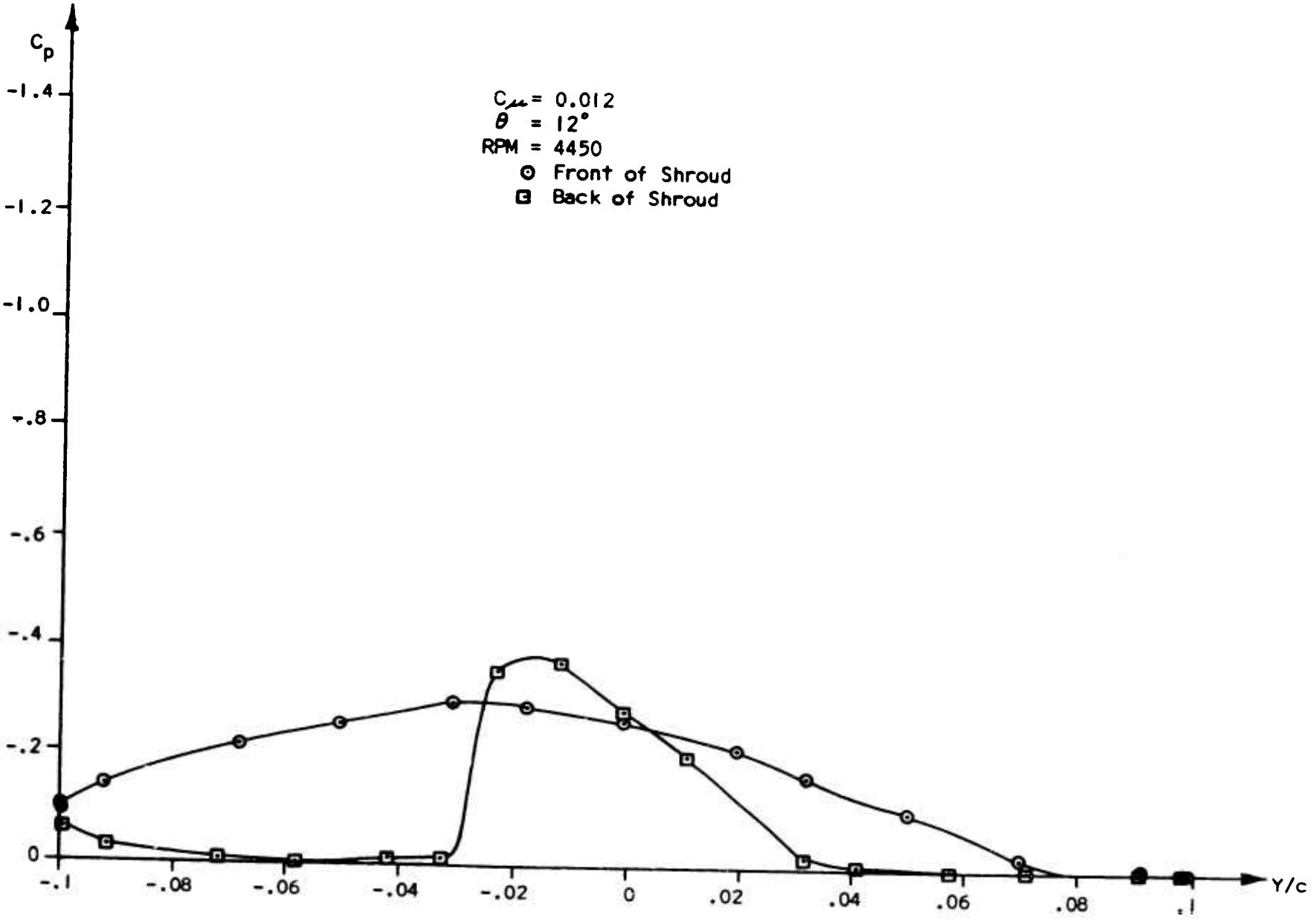

FIGURE 44. Pressure Coefficient Versus Vertical Ordinate

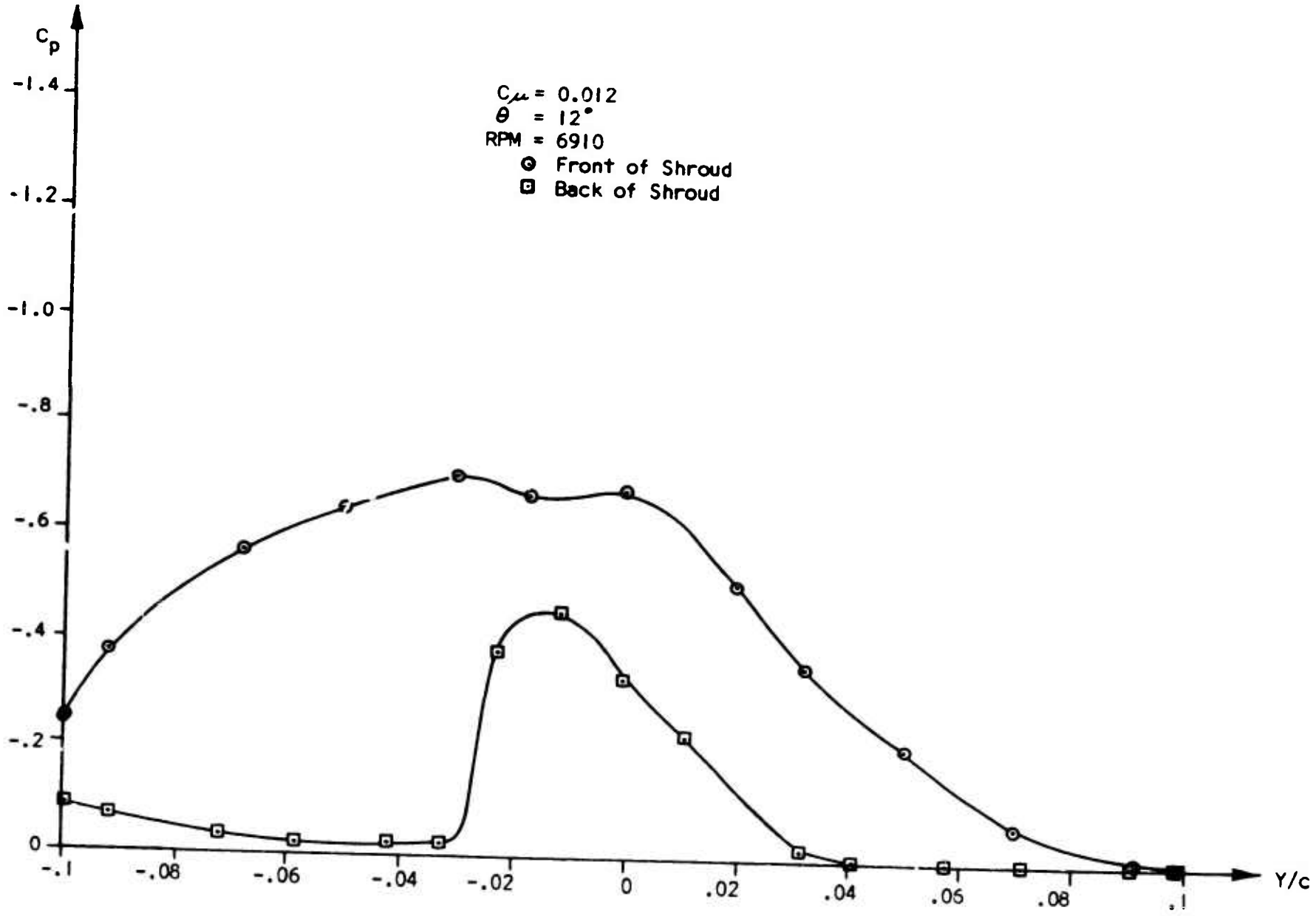

FIGURE 45. Pressure Coefficient Versus Vertical Ordinate

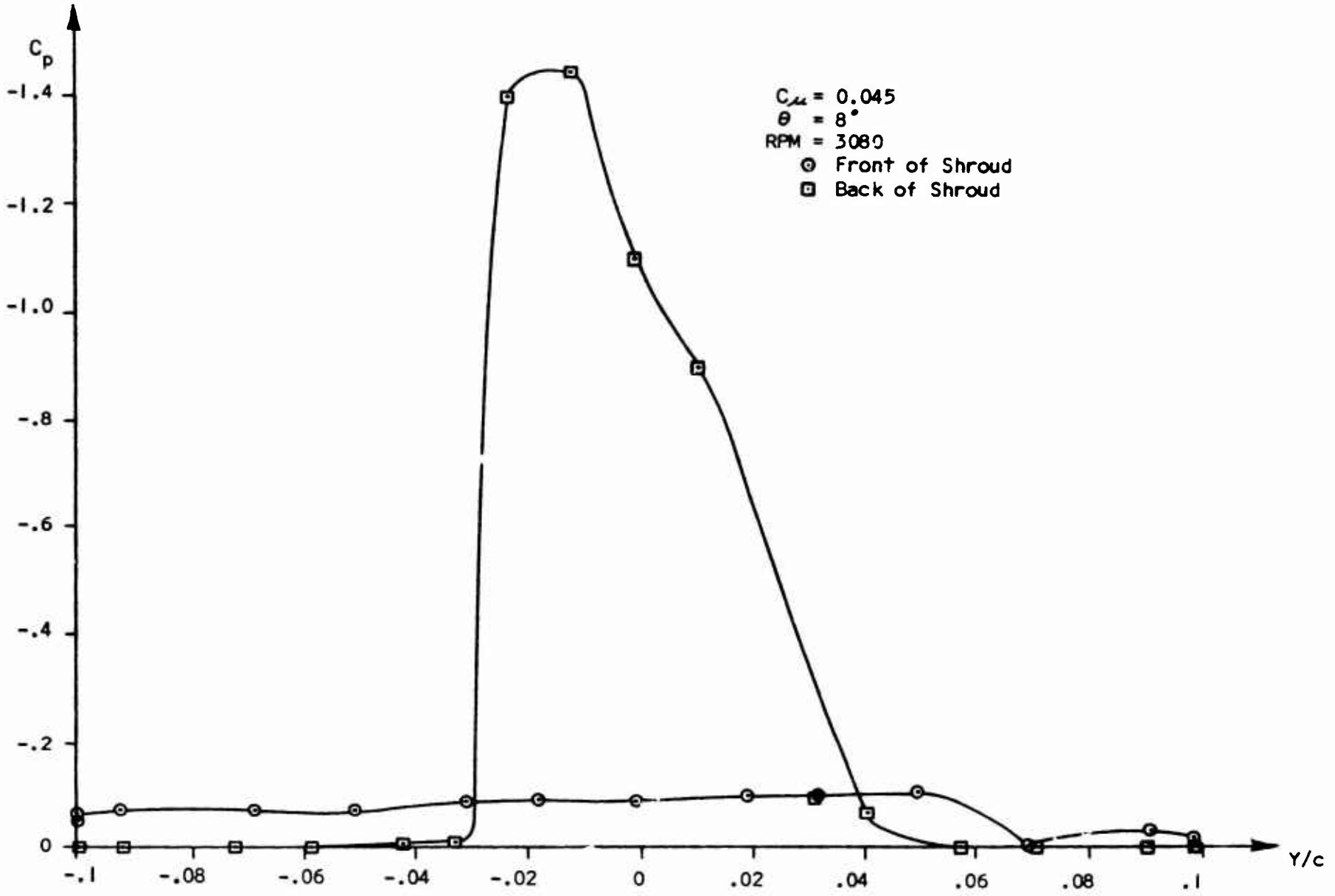

FIGURE 46. Pressure Coefficient Versus Vertical Ordinate

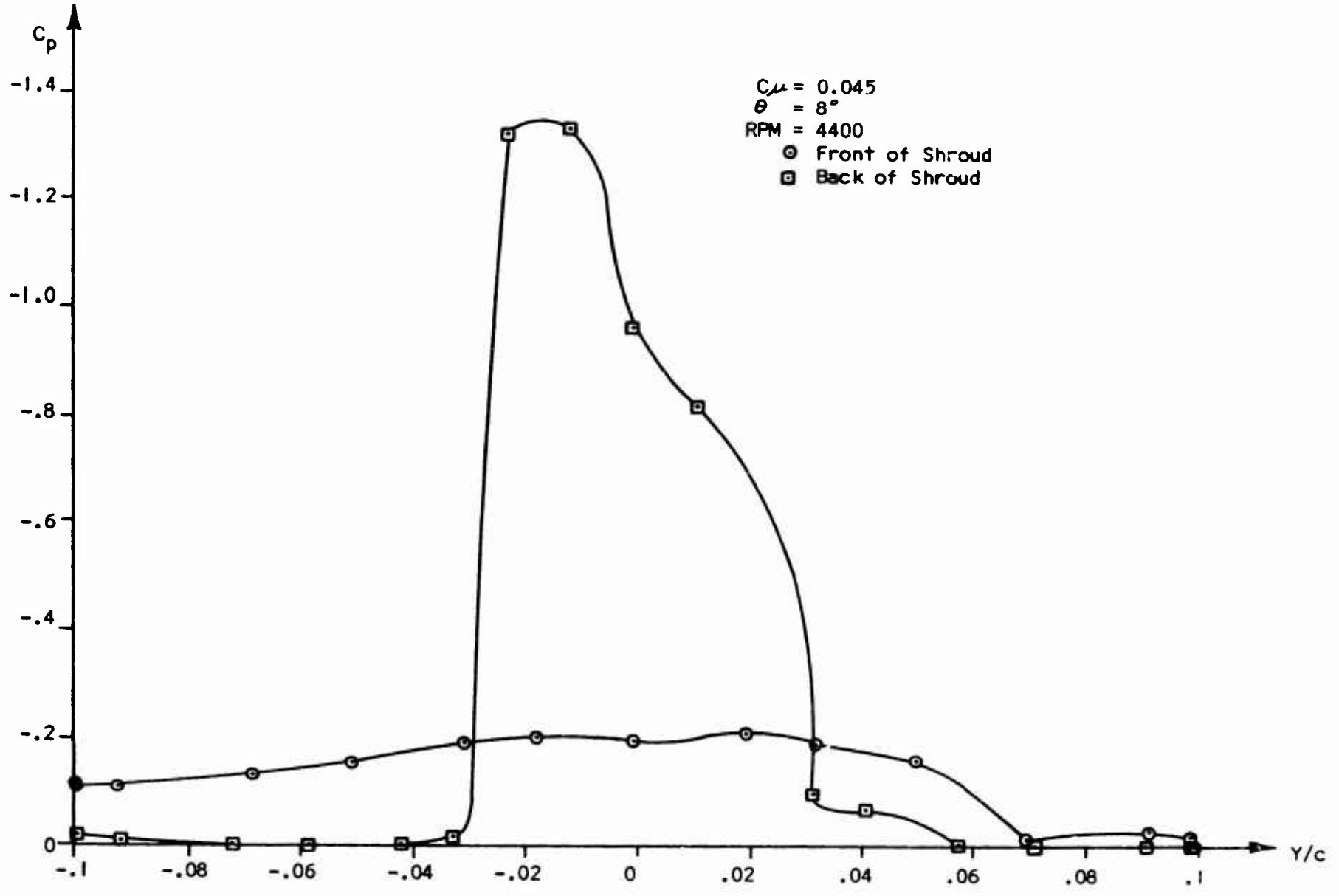

FIGURE 47. Pressure Coefficient Versus Vertical Ordinate

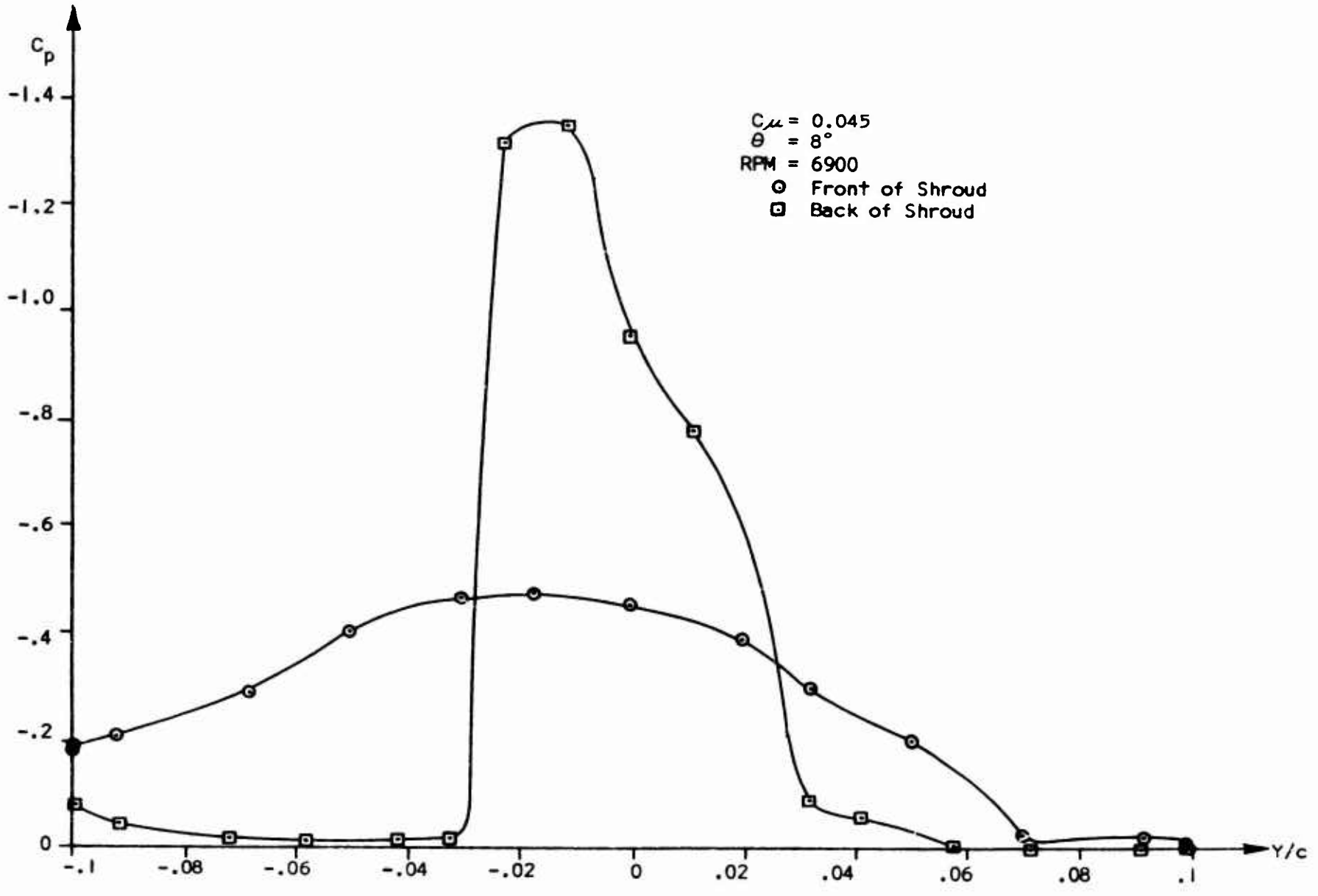

FIGURE 48. Pressure Coefficient Versus Vertical Ordinate

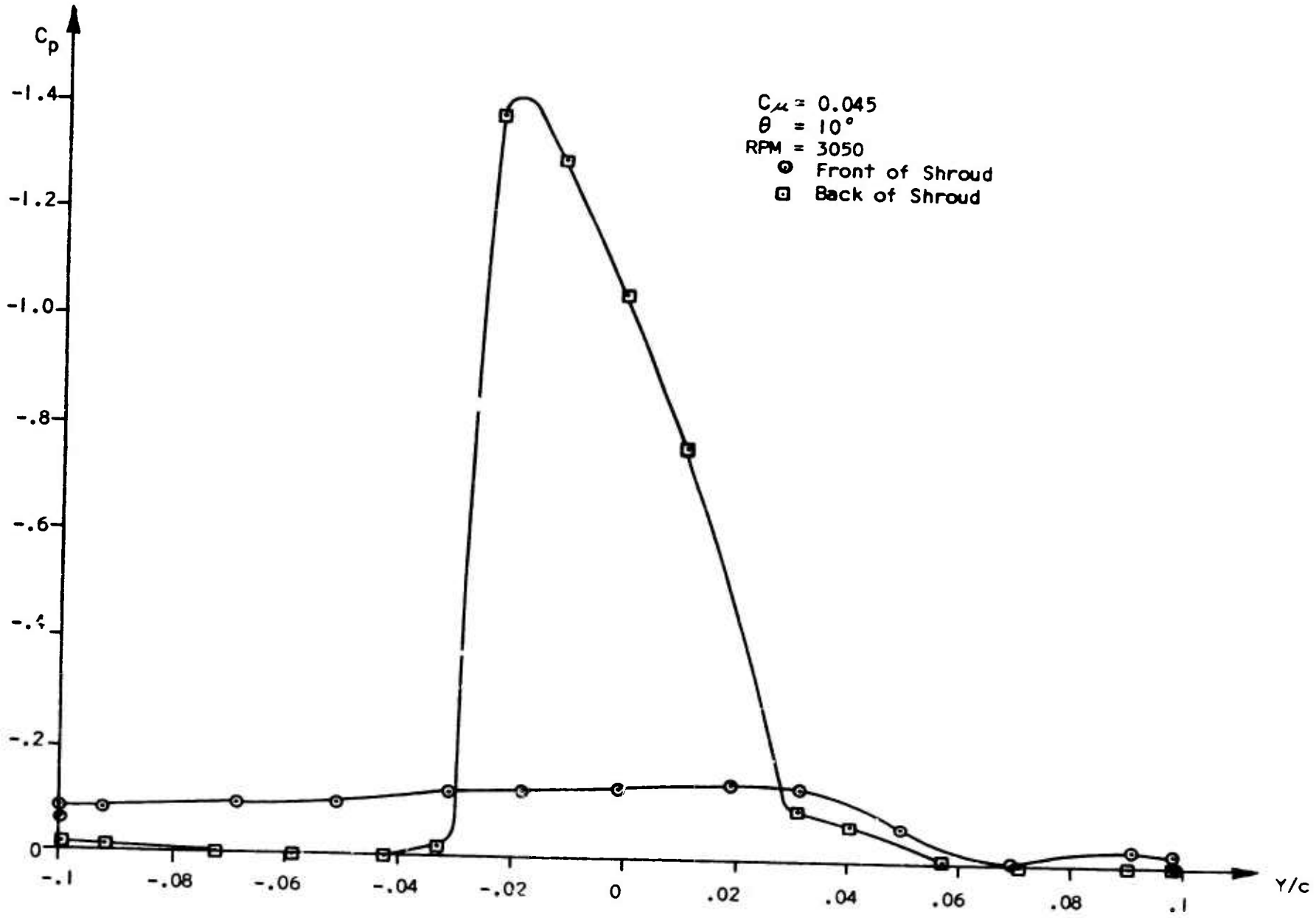

FIGURE 49. Pressure Coefficient Versus Vertical Ordinate

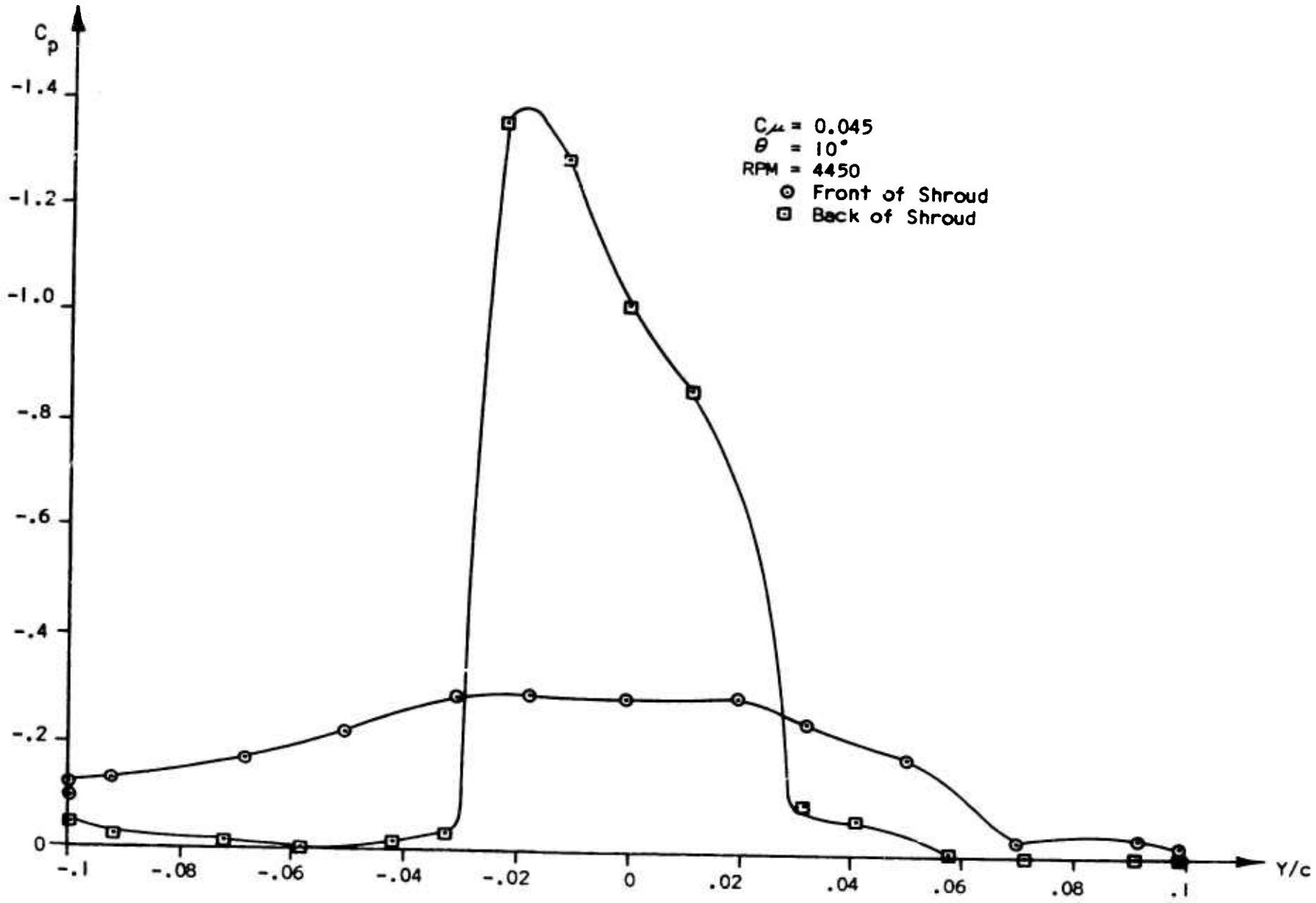

FIGURE 50. Pressure Coefficient Versus Vertical Ordinate

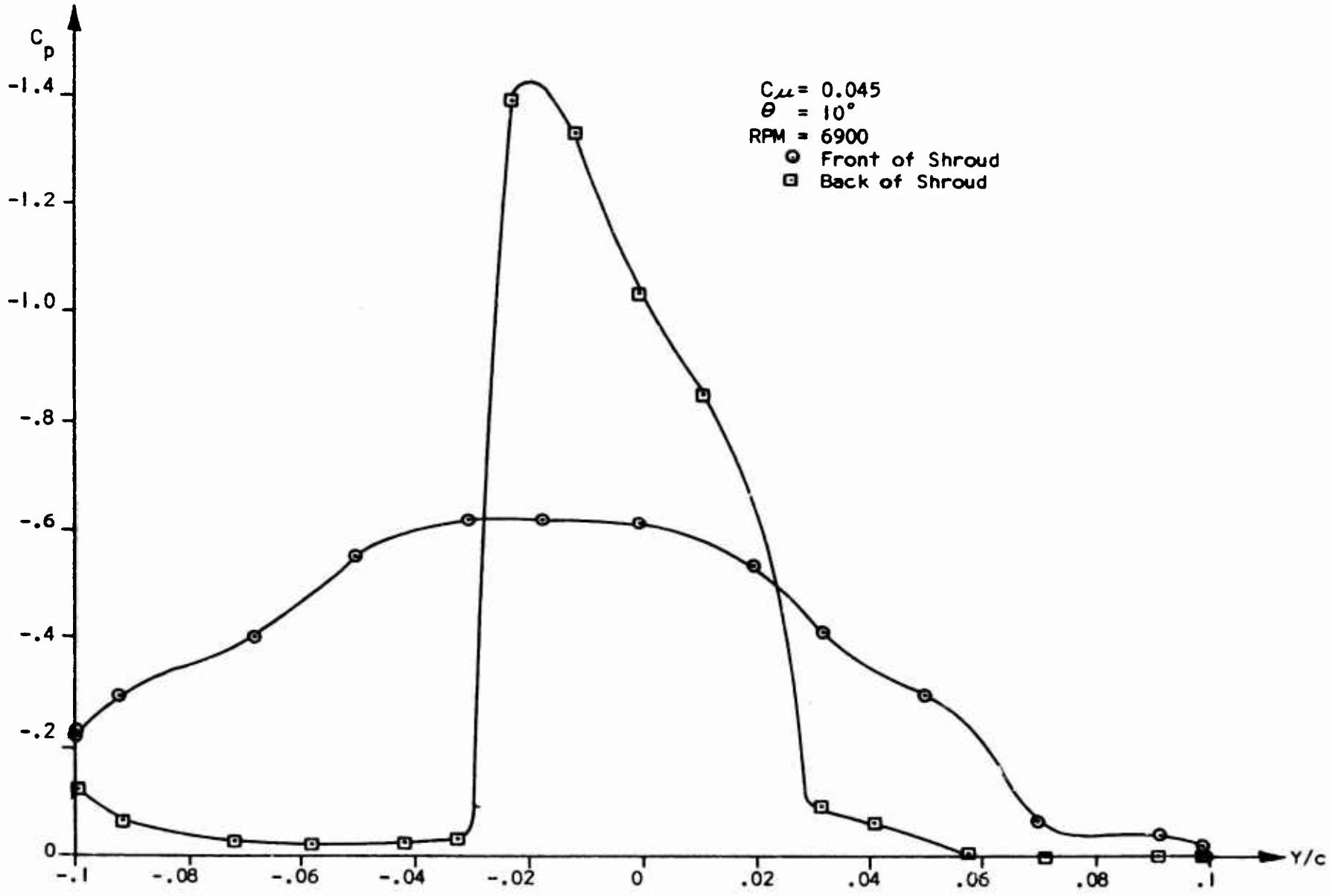

FIGURE 51. Pressure Coefficient Versus Vertical Ordinate

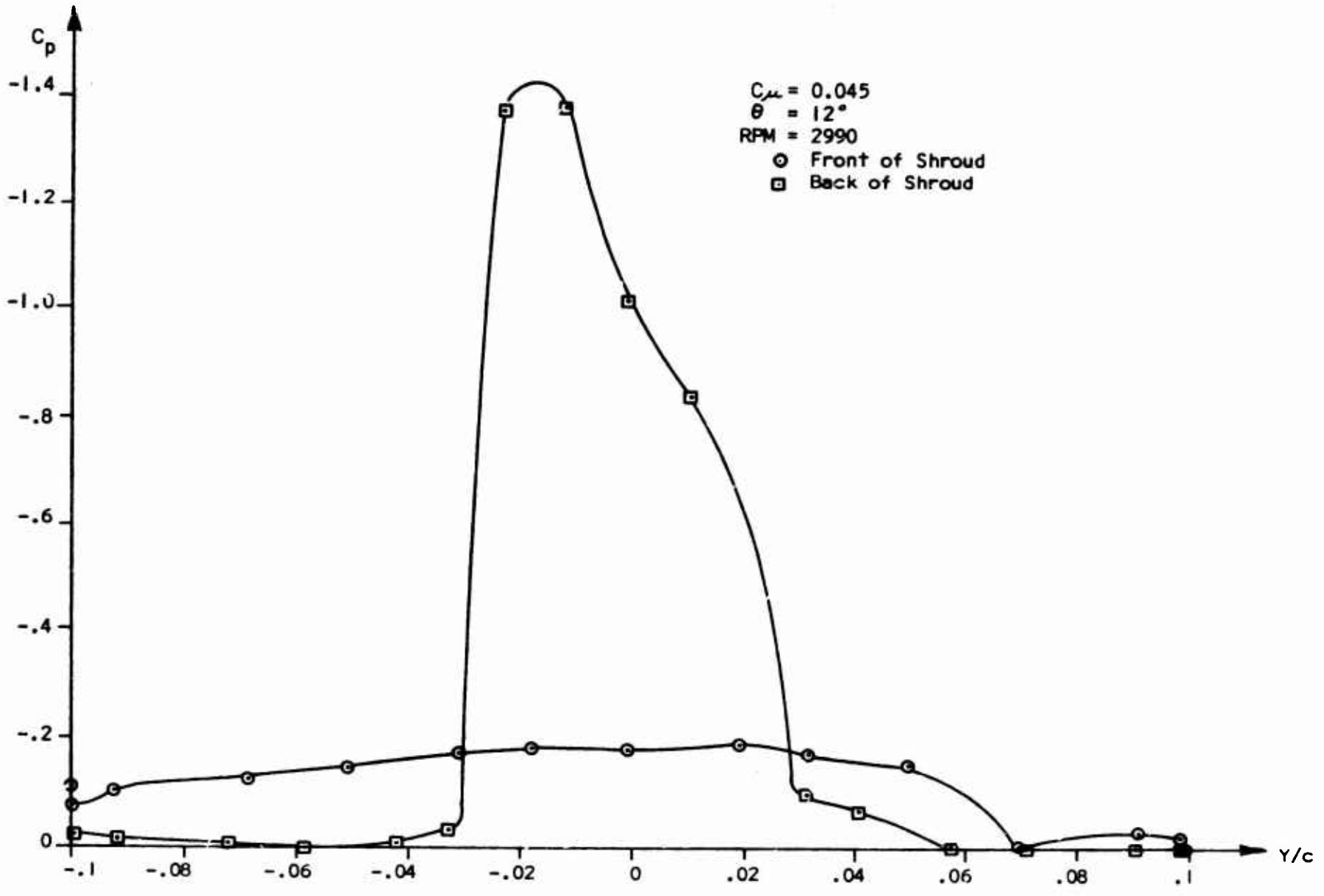

FIGURE 52. Pressure Coefficient Versus Vertical Ordinate

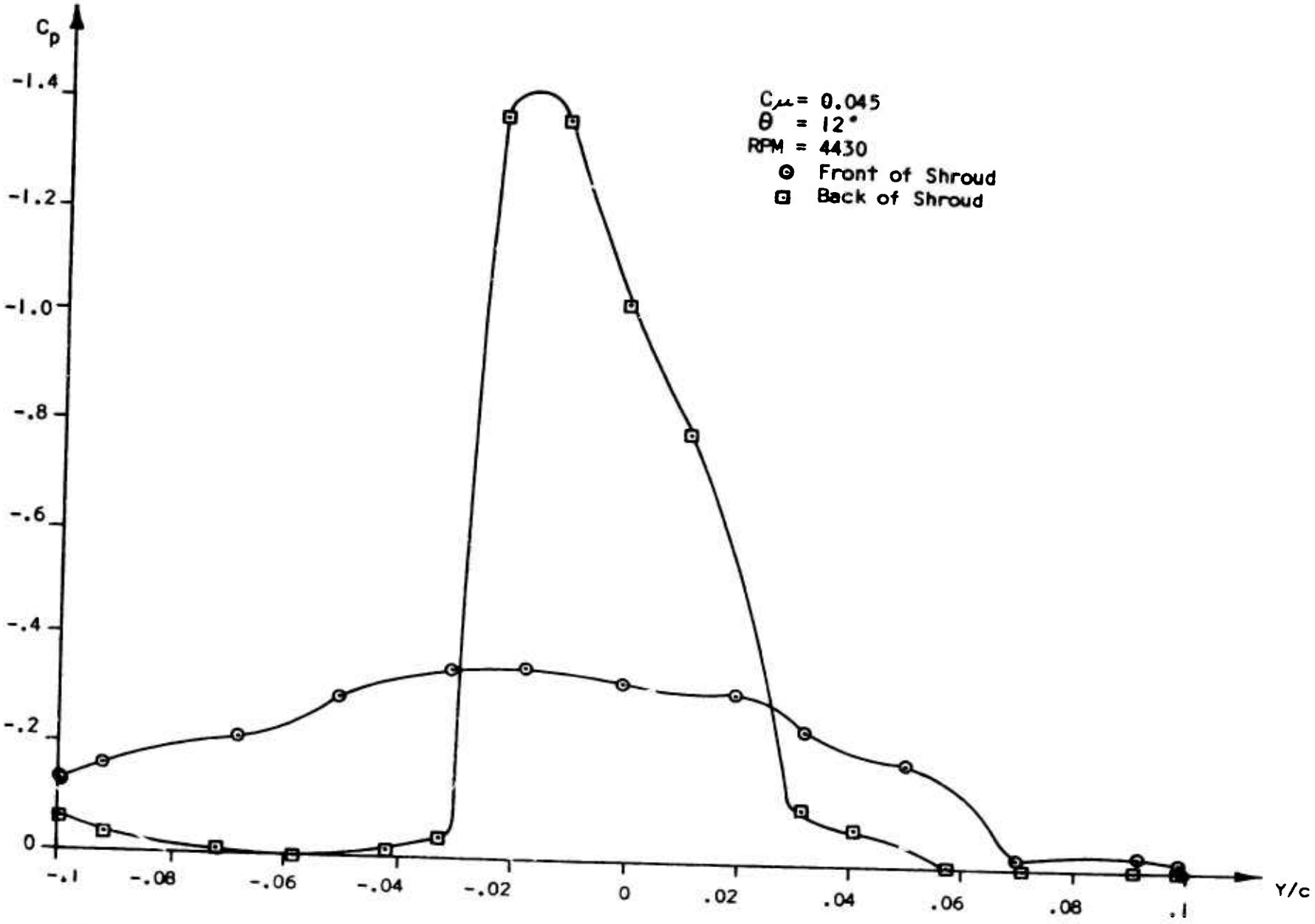

FIGURE 53. Pressure Coefficient Versus Vertical Ordinate

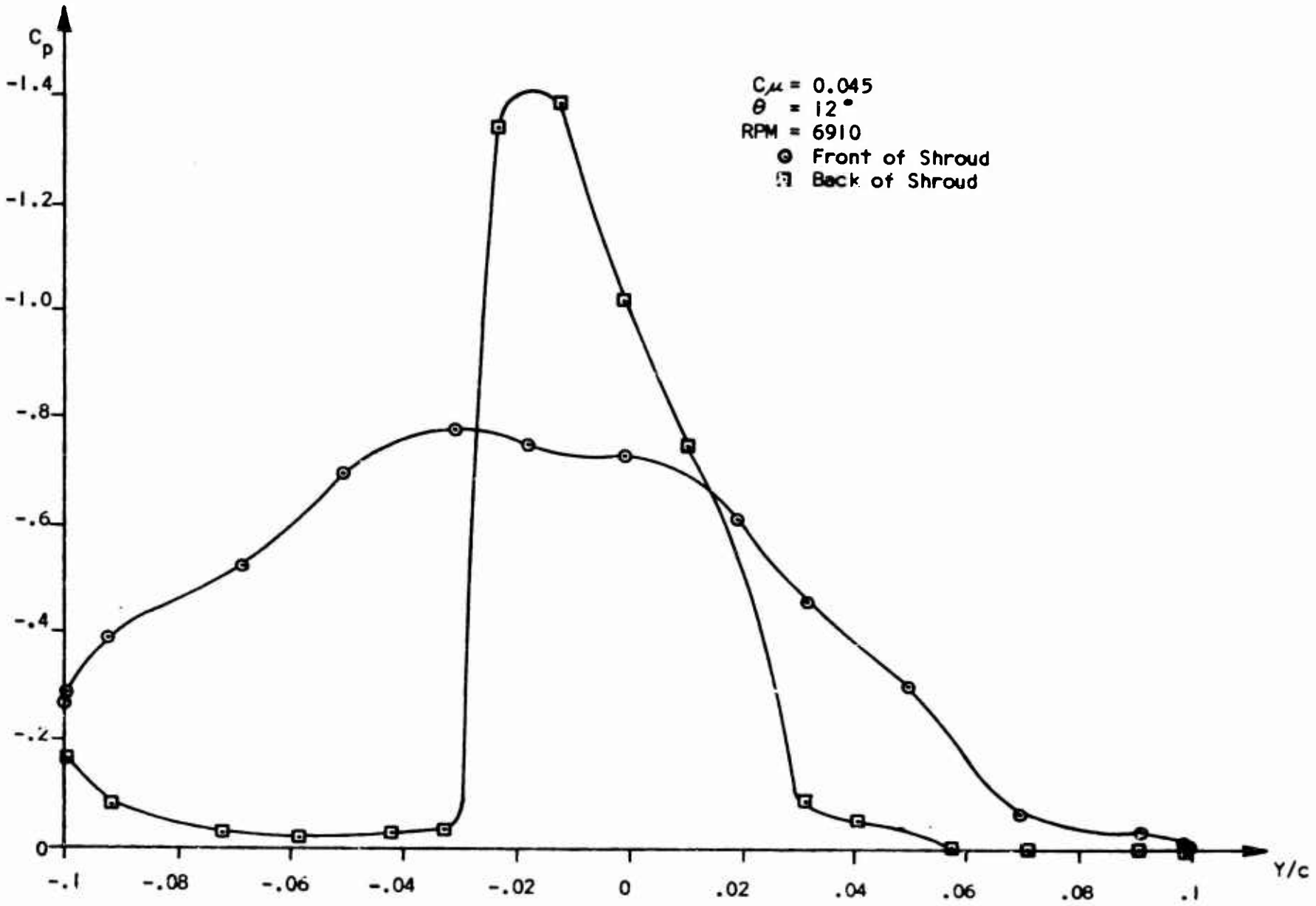

FIGURE 54. Pressure Coefficient Versus Vertical Ordinate

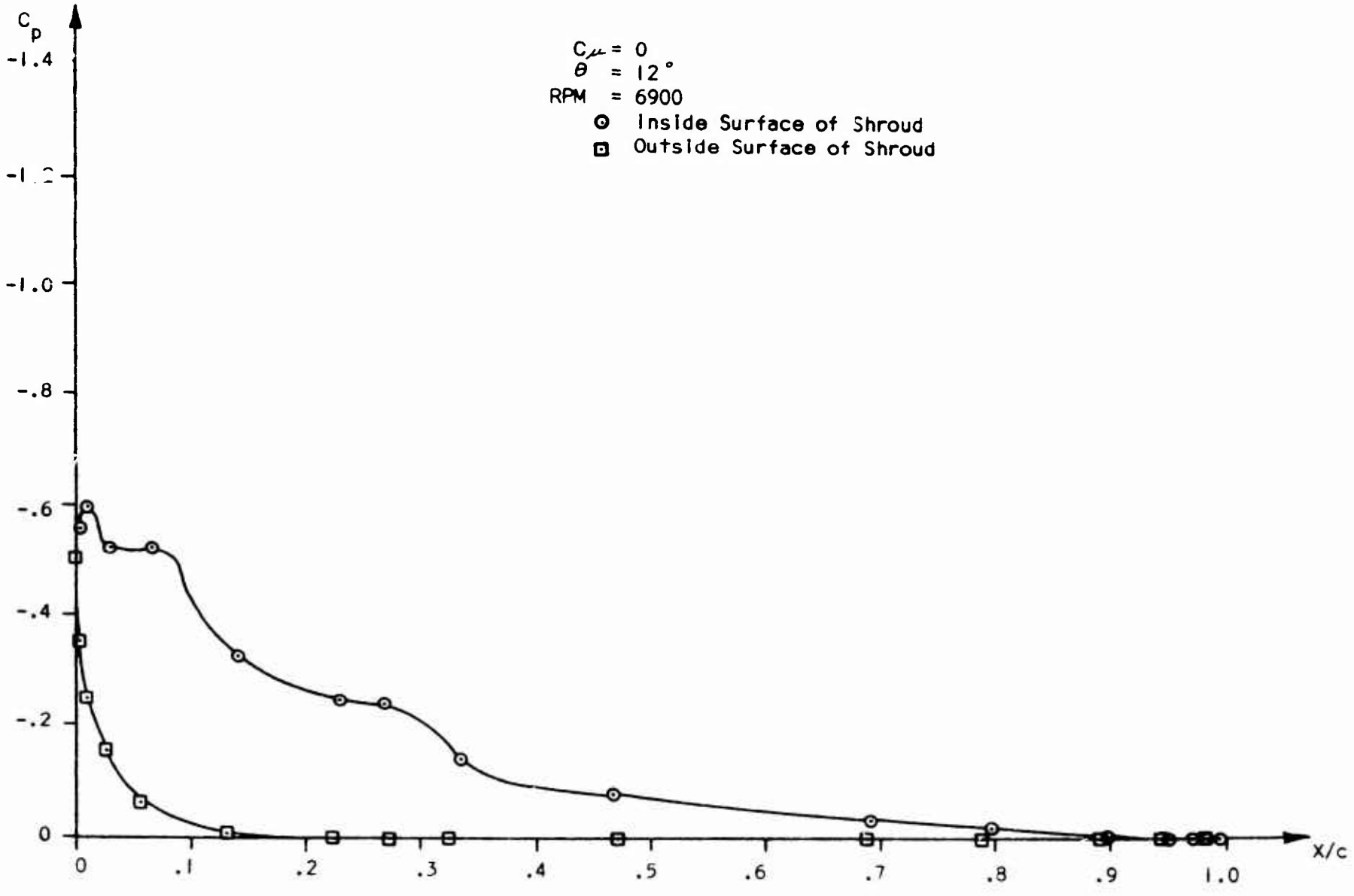

FIGURE 55. Pressure Coefficient Versus Chordwise Ordinate

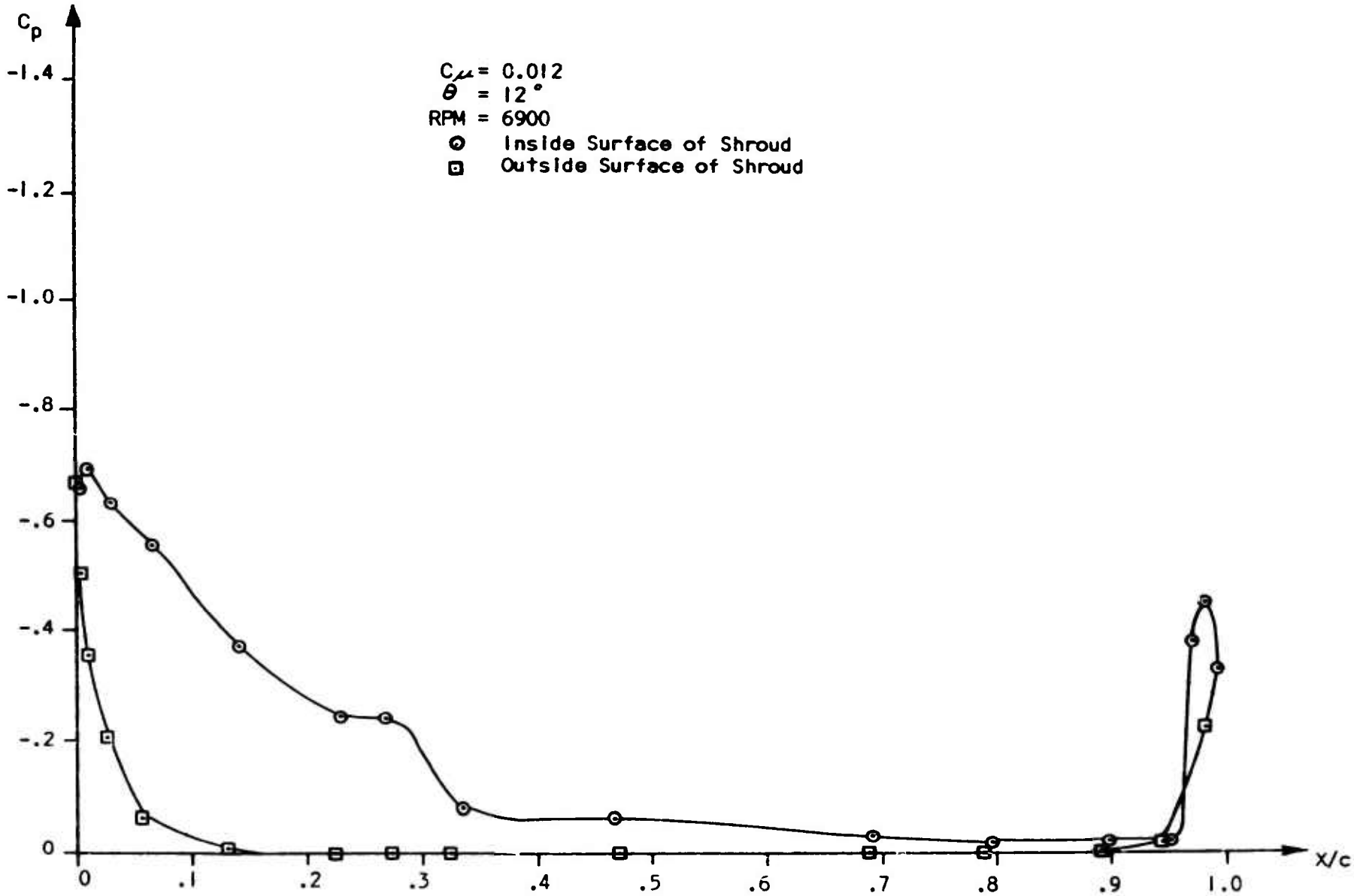

FIGURE 56. Pressure Coefficient Versus Chordwise Ordinate

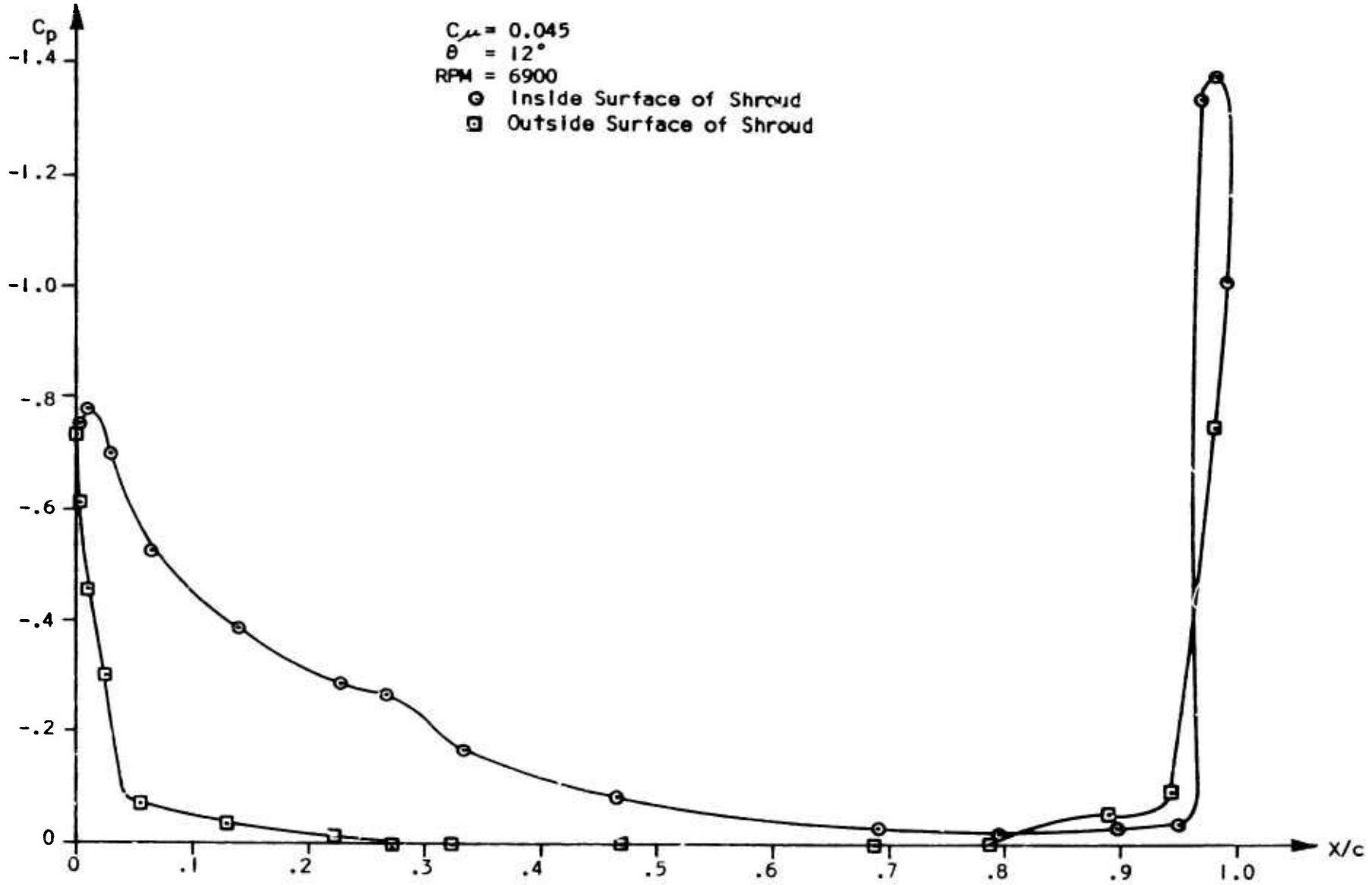

FIGURE 57. Pressure Coefficient Versus Chordwise Ordinate

APPENDIX B

TABLES

TABLE I

Pressure Tap Coordinates

	Left Side*		Right Side*	
Tap No.	X/c	Y/c	X/c	Y/c
1	0.0000	0.0000	0.0000	0.0000
2	0.0037	0.0201	0.0059	0.0157
3	0.0102	0.0326	0.0105	0.0308
4	0.0262	0.0507	0.0320	0.0457
5	0.0562	0.0705	0.0680	0.0656
6	0.1311	0.0922	0.1414	0.0922
7	0.2239	0.0997	0.2439	0.0997
8	0.2738	0.1000	0.2913	0.1000
9	0.3261	0.0995	0.3491	0.0995
10	0.4735	0.0917	0.4767	0.0917
11	0.6930	0.0719	0.6845	0.0719
12	0.7941	0.0583	0.7977	0.0583
13	0.8965	0.0417	0.9000	0.0417
14	0.9505	0.0323	0.9515	0.0323
inside slot	0.9775	0.0225	0.9775	0.0225
16	0.9886	0.0113	0.9886	0.0113
17	1.0000	0.0000	1.0000	0.0000
18	0.9886	-0.0113	0.9886	-0.0113
outside slot	0.9775	-0.0225	0.9775	-0.0225
20	0.9570	-0.0323	0.9527	-0.0323
21	0.9040	-0.0417	0.9035	-0.0417
22	0.8015	-0.0583	0.8000	-0.0583
23	0.6960	-0.0719	0.6990	-0.0719
24	0.4695	-0.0917	0.4750	-0.0917
25	0.3365	-0.0995	0.3385	-0.0995
26	0.2690	-0.1000	0.2675	-0.1000
27	0.2295	-0.0997	0.2350	-0.0997
28	0.1410	-0.0922	0.1325	-0.0922
29	0.0660	-0.0683	0.0599	-0.0769
30	0.0300	-0.0504	0.0250	-0.0565
31	0.0100	-0.0304	0.0075	-0.0370
32	0.0035	-0.0173	0.0019	-0.0173

*Right and Left side looking from rear of shroud

TABLE II

Slot Total Pressure Survey

Angle* (degrees)	Total Pressure (Inches Mercury)	
	$C_{\mu} = 0.012$	$C_{\mu} = 0.045$
22.5	1.10	3.25
45	1.30	4.90
67.5	1.25	4.50
90	1.25	4.90
112.5	1.20	4.20
135	1.33	4.80
157.5	1.30	4.75
180	0.95	2.60
202.5	1.30	4.85
225	1.30	4.90
247.5	1.25	4.90
270	1.30	4.65
292.5	1.33	4.60
315	1.25	4.30
337.5	1.30	4.50
360	0.95	2.70

*Angle measured clockwise from top of shroud

TABLE III

Data

Run No	θ (deg)	Motor Speed (volts)	Motor Speed (RPM)	Volume Flow (SCFM)	C_μ	T (cm)	T_q (cm)	T_f (cm)	T_{q_f} (cm)
1	8	21.64	3025	0	0	0.65	0.60	0.50	0.50
2	8	31.50	4440	0	0	1.05	0.85	1.40	1.15
3	8	48.90	6880	0	0	2.45	2.85	3.60	2.90
4	10	21.70	3050	0	0	0.50	0.60	0.60	0.65
5	10	31.50	4430	0	0	1.10	1.25	1.95	1.40
6	10	49.00	6900	0	0	2.30	3.10	3.80	3.70
7	12	21.80	3070	0	0	0.60	0.70	0.80	0.70
8	12	31.50	4430	0	0	1.10	1.50	2.00	1.60
9	12	49.00	6900	0	0	3.00	3.20	3.90	4.10
10	8	21.60	3020	60	0.012	0.70	0.50		
11	8	31.80	4480	60	0.012	1.10	1.00		
12	8	49.10	6910	60	0.012	2.60	2.60		
13	10	21.50	3015	60	0.012	0.60	0.50		
14	10	31.10	4380	60	0.012	1.20	1.30		
15	10	49.30	6950	60	0.012	2.70	3.00		
16	12	21.90	3080	60	0.012	1.10	0.50		
17	12	31.60	4450	60	0.012	1.70	1.50		
18	12	49.10	6910	60	0.012	3.20	3.60		
19	8	21.90	3080	120	0.045	0.70	0.40		
20	8	31.30	4400	120	0.045	1.00	1.10		
21	8	49.00	6900	120	0.045	2.20	2.60		
22	10	21.70	3050	120	0.045	0.60	0.60		
23	10	31.60	4450	120	0.045	1.30	1.20		
24	10	49.00	6900	120	0.045	2.60	3.00		
25	12	21.30	2990	120	0.045	0.60	0.70		
26	12	31.50	4430	120	0.045	1.60	1.50		
27	12	49.10	6910	120	0.045	3.50	3.60		

TABLE IV

Results

Run No	Thrust C_T	Inward Force C_F	Propeller Torque (ft-lb$_f$)	Propeller Thrust (lb$_f$)	Shroud Thrust (lb$_f$)	Strut Drag (lb$_f$)
1	0.0061	0.0153	0.128	0.563	0.3566	0.0027
2	0.0147	0.0296	0.190	0.900	0.8593	0.0065
3	0.0401	0.0890	0.557	2.105	2.3441	0.0136
4	0.0089	0.0184	0.128	0.425	0.5203	0.0027
5	0.0203	0.0440	0.310	0.950	1.1867	0.0065
6	0.0547	0.1102	0.700	1.984	3.1975	0.0136
7	0.0121	0.0226	0.163	0.510	0.7073	0.0027
8	0.0270	0.0563	0.338	0.950	1.5783	0.0065
9	0.0669	0.1351	0.715	2.588	3.9107	0.0136
10	-0.0012	0.0147	0.113	0.600	-0.0702	0.0027
11	0.0026	0.0357	0.225	0.950	0.1520	0.0065
12	0.0293	0.0888	0.645	2.040	1.7127	0.0136
13	-0.0044	0.0181	0.113	0.510	-0.2572	0.0027
14	0.0085	0.0409	0.290	1.030	0.4969	0.0065
15	0.0454	0.1183	0.688	2.325	2.6539	0.0136
16	0.0009	0.0302	0.113	0.950	0.0526	0.0027
17	0.0184	0.0582	0.363	1.465	1.0756	0.0065
18	0.0652	0.1411	0.813	2.765	3.8113	0.0136
19	-0.0461	0.0208	0.100	0.600	-2.6948	0.0027
20	-0.0275	0.0384	0.250	0.863	-1.6075	0.0065
21	0.0003	0.0917	0.645	1.900	0.0175	0.0136
22	-0.0378	0.0309	0.128	0.510	-2.2096	0.0027
23	-0.0203	0.0510	0.270	1.120	-1.1866	0.0065
24	0.0176	0.1177	0.538	2.244	1.0230	0.0136
25	-0.0329	0.0382	0.163	0.520	-1.9232	0.0027
26	-0.0151	0.0649	0.338	1.375	-0.8827	0.0065
27	0.0355	0.1566	0.813	3.025	2.0752	0.0136

TABLE IV
(continued)

Results

Run No	Total Thrust (lb_f)	Propeller Thrust In Free-Air (lb_f)	Propeller Torque Free-Air ($ft\text{-}lb_f$)	Shrouded Propeller BHP (HP)	Free-Air Propeller BHP (HP)	Slot BHP
1	0.9169	0.425	0.112	0.0734	0.0646	0
2	1.7528	1.025	0.285	0.1606	0.2388	0
3	4.4355	3.100	0.650	0.7297	0.8539	0
4	0.9426	0.475	0.150	0.0741	0.0865	0
5	2.1302	1.700	0.313	0.2615	0.2622	0
6	5.1679	3.367	0.825	0.9196	1.0838	0
7	1.2146	0.775	0.160	0.0950	0.0923	0
8	2.5218	1.725	0.383	0.2847	0.3209	0
9	6.4851	3.410	0.920	0.9393	1.2087	0
10	0.5271			0.0647		0.0804
11	1.0955			0.1919		0.0804
12	3.7391			0.8486		0.0804
13	0.2528			0.0646		0.0804
14	1.5204			0.2419		0.0804
15	4.9653			0.9098		0.0804
16	0.9999			0.0660		0.0804
17	2.5341			0.3072		0.0804
18	6.5627			1.0690		0.0804
19	-2.0975			0.0587		0.2230
20	-0.7510			0.2095		0.2230
21	1.9039			0.8474		0.2230
22	-1.7023			0.0741		0.2230
23	-0.0731			0.2288		0.2230
24	3.2534			0.9032		0.2230
25	-1.4059			0.0925		0.2230
26	0.4858			0.2847		0.2230
27	5.0866			1.0690		0.2230